ANL-7073

Argonne National Laboratory

SELF-SUSTAINED HYDRODYNAMIC OSCILLATIONS IN A NATURAL-CIRCULATION TWO-PHASE-FLOW BOILING LOOP

by

Kamal C. Jain

Printed in USA. Price $4.00. Available from the Clearinghouse for Federal Scientific and Technical Information, National Bureau of Standards, U. S. Department of Commerce, Springfield, Virginia

ANL-7073
Engineering and Equipment
(TID-4500, 47th Ed.)
AEC Research and
Development Report

ARGONNE NATIONAL LABORATORY
9700 South Cass Avenue
Argonne, Illinois 60439

SELF-SUSTAINED HYDRODYNAMIC OSCILLATIONS IN A NATURAL-CIRCULATION TWO-PHASE-FLOW BOILING LOOP

by

Kamal C. Jain

Reactor Engineering Division, ANL

and

Associated Midwest Universities

August 1965

Based on a thesis
Submitted to the Graduate School
of Northwestern University
in partial fulfillment of the requirements
for the degree of
Doctor of Philosophy

Operated by The University of Chicago
under
Contract W-31-109-eng-38
with the
U. S. Atomic Energy Commission

FOREWORD

This report is one of a series that describes heat-transfer and fluid-flow studies performed at Argonne under a program sponsored jointly by the Associated Midwest Universities and the Argonne National Laboratory.

The earlier reports in this series are:

ANL-6625 Local Parameters in Cocurrent Mercury-Nitrogen Flow
L. G. Neal

ANL-6667 A Study of the Flow of Saturated Freon-11 through Apertures and Short Tubes
Hans K. Fauske and Tony C. Min

ANL-6674 Reduction of Vapor Carryunder in Simulated Boiling
P. L. Miller and C. P. Armstrong

ANL-6710 Transient Behavior of a Natural-Circulation Loop Operating Near the Thermodynamic Critical Point
Darrel G. Harden

ANL-6734 Two-phase (Gas-liquid) System: Heat Transfer and Hydraulics. An Annotated Bibliography
Robert R. Kepple and Thomas V. Tung

ANL-6738 Development of an Electrical Resistivity Probe for Void-fraction Measurements in Air-Water Flow
George P. Nassos

ANL-6754 An Experimental Investigation of Two-phase, Two-component Flow in a Horizontal, Converging-diverging Nozzle
Joseph A. Vogrin, Jr.

ANL-6755 Two-component Two-phase Flow Parameters for Low Circulation Rates
Georges E. Smissaert

ANL-6779 Two-phase Critical Flow with Application to Liquid-Metal Systems (Mercury, Cesium, Rubidium, Potassium, Sodium, and Lithium)
Hans K. Fauske

ANL-6796 The Slug-annular Flow Regime Transition at Elevated Pressure
Peter Griffith

ANL-6854 Effect of a Transverse Magnetic Field on Vertical Two-phase Flow through a Rectangular Channel
Richard J. Thome

ANL-6862 Two-phase Heat Transfer with Gas Injection through a Porous Boundary Surface
A. A. Kudirka

ANL-6948 Condensation of Metal Vapors: Mercury and the Kinetic Theory of Condensation
Donald J. Wilhelm

ANL-7032 An Investigation of Instabilities Encountered during Heat Transfer to a Supercritical Fluid
Archie Junior Cornelius

ANL-7041 Frequency-response Analysis of Steam Voids to a Sinusoidal Power Modulation in a Thin-walled Boiling Water Coolant Channel
Carl C. St. Pierre

ANL-7053 Propagation of Density Disturbances in Air-Water Flow
George P. Nassos

TABLE OF CONTENTS

TABLE OF CONTENTS

TABLE OF CONTENTS

LIST OF FIGURES

LIST OF FIGURES

LIST OF TABLES

NOMENCLATURE

a_1, a_2	Constants, defined by Eq. (6.17)
a_k^1	Defined by Eq. (6.15)
A	Area
A_w	Cross-sectional area of test-section wall
B	Defined by Eq. (6.11)
c_1	Parameter, defined by Eq. (7.18)
c_2	Parameter, defined by Eq. (7.19)
c_1'	Parameter, defined by Eq. (7.25)
c_2'	Parameter, defined by Eq. (7.26)
C	Defined by Eq. (4.7)
C_p	Specific heat of saturated liquid
C_w	Specific heat of test-section wall
d	Diameter
E	Internal energy
f	Friction factor, defined by Eq. (6.17)
F	Defined by Eq. (6.18b)
F_b	Frictional pressure drop, defined by Eq. (7.2)
g	Acceleration due to gravity
g_1, g_2	Constants, defined by Eq. (6.52)
G	Mass velocity
h	Heat-transfer coefficient
H	Saturation enthalpy
H_{lg}	Latent heat of vaporization
J	Mechanical equivalent of heat
k	Constant
K	Flow parameter, defined by Eq. (6.6)
K_e'	Defined by Eq. (6.62)
K_f	Correction factor, defined by Eq. (8.1)
K_{fb}	Friction-factor multiplier
K_h	Constant, defined by Eq. (6.52)
L	Length
L_d	Downcomer driving height, defined by Eq. (7.23)
m	Number of nodes in subcooled region
n	Number of nodes in boiling region
p	Perimeter
P	Pressure
P_f	Frictional pressure drop
Pr	Prandtl number
q	Heat flux
Q	Total heat input per unit length
Q'	Heat input to the fluid per unit length
Q_{sc}	Heat input required to bring the liquid to saturation
Re	Reynolds number
r	Defined by Eq. (6.8)
s	Laplace transform variable
S	Slip ratio
t	Time
T	Temperature
T'	Defined by Eq. (7.39)
ΔT_{in}	Inlet subcooling
u	Velocity
v	Specific volume
V	Velocity
W	Mass flow rate
X	Steam quality
z	Axial position
z_1	Axial position of boiling boundary

Superscripts

*	Dimensionless form
~	Transformed variable, Chapter VI
−	Cross-sectional average, Chapters V and VII

Subscripts

a	Average within a node
b	Bulk boiling
c	Test section
d	Downcomer
ex	Test-section exit
f	Friction
ℓ	Liquid
g	Vapor
i	For ith node
in	Test-section inlet
nb	Subcooled nonboiling
r	Riser
re	Riser exit
sat	Saturation
sc	Subcooled boiling
w	Test-section wall
zl	Boiling boundary
0	Steady-state value
n+1	Defined by Eq. (6.61)
1	At inlet end of node
2	At exit end of node

Greek Symbols

α	Void fraction
β	Defined by Eq. (4.8)
ξ	Defined by Eq. (6.26)
δ	First-order perturbation term
ζ	Position variable
η	Defined by Eq. (6.4)
ϕ^2	Martinelli-Nelson frictional-pressure-drop parameter, defined by Eq. (6.16)
λ	Thermal conductivity
μ	Dynamic viscosity
ν	Defined by Eq. (6.29)
ω	Frequency of oscillation
Ω	Correction term for two-phase frictional pressure gradient
ρ	Density
ρ'	Defined by Eq. (7.4)
σ_e	Area ratio
τ	Time
τ_{fsc}	Defined by Eq. (6.59)

SELF-SUSTAINED HYDRODYNAMIC OSCILLATIONS IN A NATURAL-CIRCULATION TWO-PHASE-FLOW BOILING LOOP

by

Kamal C. Jain

ABSTRACT

The effects of geometry, subcooling, and pressure on the inception and development of oscillatory behavior in a natural-circulation boiling-water loop were studied. The following range of parameters was covered by the experimental study:

Heat flux, Btu/hr-ft^2:	0.2-3.1 x 10^5
Pressure, psia:	200-1500
Inlet subcooling, °F:	0-62
Test section, length, in.:	48, 72, 96
ID, in.:	0.364, 0.625, 0.8125
Riser, length, in.:	48, 60
ID, in.:	0.3125, 0.625, 1.049

The critical power density was determined by an arbitrary criterion, since the steady-oscillation amplitude increases continuously with power. For large oscillations, periodic inlet-flow reversals were found, which could be large compared to the steady inlet-flow velocities. These phenomena are emphasized by lower system pressure and small-diameter test section and riser. Other parameters did not affect these phenomena in a distinct fashion. The frequencies of the oscillations varied from 0.24 to 0.76 cps and, in general, increased with increasing power, as did the flow amplitudes.

Two theoretical models were investigated, one linear and one nonlinear. The linear analysis in frequency domain due to Jones showed good ability to predict the oscillation threshold and the frequency associated with the initial oscillations. The predictions of the threshold power were correct within ±5% for over 60%, and within ±10% for over 80%, of the tested cases.

The nonlinear model of Jahnberg had to be modified to provide a satisfactory prediction of the steady inlet-flow velocities. However, this modification and the original model failed to give reasonable predictions of the oscillation thresholds and frequencies. Neither form of the model provided a satisfactory prediction of the amplitudes. It is thought that the one-dimensional formulation fails to take into account vaporization, which

acts as a periodic forcing function, of superheated liquid near the leading edge of the two-phase region. The introduction of such a forcing function allows the computation of periodic bounded oscillations similar to those observed experimentally, and also explains qualitatively the observed trends with parameter variation.

I. INTRODUCTION

The proper design of many systems of technological importance requires the understanding of the behavior of heat-transfer systems in which the circulation is provided by the density difference caused by boiling in the heated section. Such systems include the evaporators for the process of desalinization of seawater, natural-circulation boilers, natural-circulation boiling-water reactors, and similar devices. The behavior of these natural-circulation systems is characterized by oscillatory conditions in the system parameters, such as flow rate, pressure, inlet temperature, wall temperature, etc. Some consequences of this oscillatory behavior are the difficulty of providing adequate control of system, thermal and mechanical stress cycles which will lead to a decrease in the durability of equipment,[41, 42] and a possibility of premature burnout (wall-temperature excursion resulting in the melting of the heating-section wall). An additional consequence of this oscillatory condition lies in the potential for instability, either by itself, or coupled with other phenomena such as the power level and reactivity of a nuclear reactor.

The main objective of this work is to obtain a well-documented consistent set of experimental data over a wide range of pertinent variables to provide a test of any mathematical descriptions. On the analytical side, the problem represents a sensitive application of the equations of conservation of mass, momentum, and energy in two-phase-flow systems. Since understanding of two-phase-flow phenomena is rather insufficient, resort is made to empiricisms in order to provide adequate descriptions for engineering practice. The present study is aimed at testing some of the mathematical models to find out whether, among other things, the existing empirical correlations are satisfactory for representing the oscillatory characteristic of the system. An additional purpose of this work is to analyze the system oscillations with the help of the available mathematical tools, so as to be able to find a reasonable explanation of the origin of the oscillatory phenomena and the forces causing them.

II. LITERATURE SURVEY

Because of the technological importance of the subject, the literature is widespread, depicting the experimental and theoretical efforts of many investigators. In this chapter, most of the pertinent literature is

divided into several general classes and reviewed critically. A general review of this subject is given in several reports.[1,2,3]

The description that follows is not intended to include all published information related to instabilities in boiling systems. Instead, it emphasizes only studies that are believed particularly pertinent to this investigation.

A. Flow Excursion

The criterion of instability first suggested by Ledinegg[4] in 1938 was later identified with the "flow-excursion" phenomenon. Figure 2.1 shows the qualitative behavior of steady-state channel pressure drop as a function of flow rate for a boiling system. In forced convection, if the operating point is in the region of negative slopes of the curve (point B), and if the characteristic curve of the pump has multiple intersections with the curve for the channel pressure drop, then a small flow disturbance in the system can lead to another common point (A or C). This spontaneous shift of flow rate is known as a flow excursion.

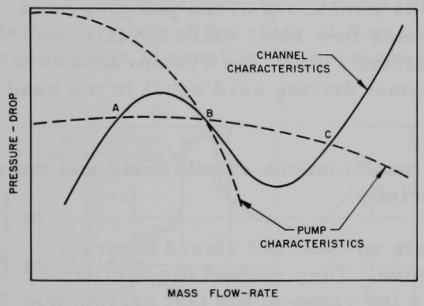

Fig. 2.1. Pressure-drop Characteristics against Flow Rate

Ledinegg analyzed this behavior for a boiler tube. He assumed buoyancy effects and entrance losses to be negligible and suggested that the point of initiation of unstable behavior was the power at which pressure drop decreased with increase in flow rate. Mathematically, this condition can be put as

$$\frac{d\Delta P}{dW} = 0, \tag{2.1}$$

where ΔP is the total pressure drop, consisting of sum of friction and momentum pressure drop, and W is the mass flow rate. Ledinegg obtained an analytical expression for a forced-circulation system and predicted the regions of instability by using the above condition. However, this analysis must be modified for a natural-circulation system since the buoyancy terms can no longer be neglected.

Chilton,[5] following the approach of Ledinegg, obtained a criterion for flow excursion by assuming a homogeneous flow. Levy and Beckjord[8] observed that the presence of two-valued flow, as formulated in Chilton's

model, was insufficient to result in undamped cyclic flow variations. The system should also be dynamically unstable at two points from energy or force considerations.

B. Flow-oscillation Experiments

Several in-pile as well as out-of-pile test results are available on the oscillatory behavior of natural- and forced-circulation boiling systems. A comparison of the test results, as to the effect of the mode of circulation, shows that both systems may display similar trends in oscillatory behavior.

Anderson and Lottes[1] suggested that "the reason for this is not firmly established, but it may be argued that in the regions of instability, the change in the buoyancy term which is a measure of the pumping head is not greatly affected by a change in mass flow rate, while the friction and momentum changes are greatly affected. Thus, the system acts as a forced circulation system with the constant driving head equal to the head of water in the downcomer."

In this section, some natural-circulation out-of-pile tests and their important conclusions are described briefly.

Wissler et al.[6,7] made some tests on open and closed natural-circulation loops at atmospheric pressure. They studied the oscillatory behavior of the loop under single-phase (no vapor in the test section due to low power inputs), as well as two-phase, flow conditions, but no data were obtained to study instability thresholds. Flow-rate and temperature oscillations were recorded which were of nonharmonic character and whose amplitudes and frequencies were found to be functions of the power input. The oscillation periods measured were of the order of 50-200 sec, whereas test results from other loops[1,8] showed two shorter periods (a short period of the order of 5 sec, and a long period of the order of 50-100 sec).

Zivi and group[13,14] at Space Technology Laboratories (STL) studied the oscillatory behavior of a natural-circulation loop at atmospheric pressure by using a variety of rectangular test sections. They observed spontaneous flow oscillations in a channel believed to have a scarcity of nucleating centers (a welded channel), as contrasted to the different flow oscillations arising in a channel with an abundance of nucleating centers (a soldered channel). Another interesting experiment was performed during these tests wherein power modulation at 1 cps was imposed on the system at a mean power level slightly below the threshold of instability. They observed no instability. Before the power was modulated, the power level had first been raised to the point at which spontaneous flow oscillations at approximately 1 cps were observed. The oscillations were allowed to persist long enough until they became steady; then the power level was

reduced just enough to make the system stable. The flow oscillations could not be triggered by superimposing sinusoidal modulation of amplitudes up to 20% of mean power on this threshold power. The authors observed that the flow instability results from a very specific (but as yet undetermined) power-influenced flow condition. When this flow condition does not exist, the system is stable even in the presence of disturbances of the critical frequency.

The range of periods of the flow oscillations in these tests made at STL was from 0.8 to 2.5 sec. Figure 2.2 shows a typical envelope of flow oscillations of the welded channel (which was chosen to simulate SPERT IA Reactor Geometry) plotted against power input.[14]

The experimental work by Quandt[17] at Bettis Atomic Power Laboratory consisted of the study of flow oscillations in a uniformly-heated rectangular channel in the pressure range of 600-1000 psia. He observed that the exit steam quality at which flow oscillations occurred was a function of absolute pressure and subcooling, and that the inception and cessation of oscillations were reversible.

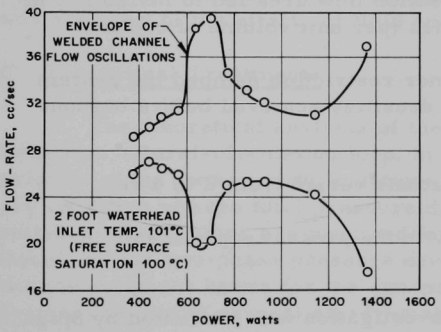

Fig. 2.2 Flow-oscillation Envelope[14]

At Argonne National Laboratory, a series of tests was conducted[1] on the "Armadilla" loop[9] (a 600-psi natural-circulation test facility) as well as on the high-pressure natural-circulation test loop (2000 psia). For the tests on the Armadilla loop, nonrandom fluctuations in the steam void fraction, which were measured by the one-shot gamma-attenuation technique,[10] were used as a primary indication of instability. For the high-pressure loop tests, the continuously-recorded output of a differential pressure transducer, connected across a venturi located in the downcomer, was used to determine instability. The information was mostly of qualitative nature and may be summarized as follows:

1. Stability increased with pressure (possibly a linear relationship).

2. Stability was influenced by the geometries of the test section, riser, and downcomer. The general trend seemed to be that an increase in the pressure drop in the two-phase region of the flow loop decreased stability, while an increase in the pressure drop in the single-phase region increased stability.

3. Over the limited range of variation in the geometry of the loop, the stability was independent of the liquid level above the riser.

The results from other experimental tests show similar behavior, except for the effect of liquid level on stability. It has been shown that the liquid level influences the oscillatory behavior of a boiling system.

Similar tests were made by Levy and Beckjord[8] at General Electric on a 1000-psi natural-circulation loop. They used an annular test section and examined the effect of inlet subcooling, heater-rod geometry, and flow restrictions. An arbitrary criterion of ±10% variation in the pressure drop across the test section was used for the instability threshold. The following observations were made:

1. Instability occurred at lower steam qualities and higher flows as the inlet subcooling was increased.

2. An increase in the test-section flow area led to instability at lower exit qualities and power densities (per unit volume of coolant).

3. Operation with a downcomer restriction damped the system oscillations, but the maximum power densities achieved before burnout were relatively unchanged.

4. The periods of the oscillations varied from 2 to 4 sec.

Their results are compared with the present experiments in Chapter IV.

An interesting experimental investigation was presented by Spigt, Dijkman, and Bogaardt,[11] Eindhoven University, Netherlands. They obtained autocorrelation functions and power-density spectra for the pressure-drop signal at the test-section inlet. The rms values of the inlet pressure drop at the instability frequency were then derived from the power-density curves and plotted as a function of power. An annular test-section geometry was used for these tests. The results showed a flow reversal at low pressure (approximately 29 psia). At high pressures (approximately 337 and 435 psia), this phenomenon was not seen at either low or high inlet subcoolings (approximately 3 and 27°F).

The results from low-pressure tests (approximately 15 and 115 psia) by Fabrega[12] at Grenoble, France, indicate boundaries at which oscillations occur under given conditions of geometry and pressure. The following phenomena were observed in the tests at atmospheric pressure:

1. Slug flow with considerable coalescence in the riser was noted under unstable conditions.

2. Recurrence of stability took place when the inlet subcooling was reduced or the power was increased.

Becker and his associates[15,16] at AB Atomenergi, Sweden, varied a wide range of parameters in studying the inception of instability of a natural-circulation loop. For these tests, a throttling valve was located at the test-section inlet, and a variable sharp-edged area reduction was mounted in a chamber at the test-section exit. Inlet throttling showed a stabilizing trend; exit throttling had the opposite effect. In these tests, the inlet temperature (not the inlet subcooling) was kept constant, so that the subcooling varied with pressure. Inlet subcooling as high as 430°F and a pressure of 150-1000 psia were covered. The following operating characteristics were noted: (1) diverging oscillations causing burnout, (2) stable oscillations, and (3) burnout without oscillations.

In these tests, the flow rates were measured with a differential pressure cell connected across a venturi. It was indicated that these flow rates might be erroneous after the onset of instability. The reason for this was ascribed to the effects of fluid acceleration on the venturi readings.

C. Theoretical Treatments

The theoretical analysis of the prediction of hydrodynamic oscillations in a natural-circulation loop, in general, consists of some type of solution of the conservation equations of the boiling channel with the boundary condition of zero total pressure drop around the system. In addition, suitable relationships are required for the slip ratio between steam and liquid and for two-phase pressure drops. Since these two-phase flow relationships are not known for the dynamic conditions, a general trend has been to use one of several steady-state empirical models.

A few of these analyses are satisfactory in the sense that they predict the frequency of oscillation in the range observed experimentally, and some have also been shown to predict the point of inception of oscillation with reasonable accuracy. Some questions remain unresolved, such as whether the use of the two-phase, steady-state flow models is justified and, if so, which of these models is most accurate. Whether these analyses can predict the experimentally observed amplitude of oscillation at a given power, also remains unresolved. It is intended here to indicate briefly a general description of the principal features used in most of these analyses.

A few analyses utilize the simulation of the boiling loop on the analog computer. Garlid *et al.*[18] used a lumped parameter model without linearization of the basic equations and simulated the low-pressure test facility at the University of Minnesota. Negligible heat capacity of the test-section wall was assumed, and the slip ratio was taken to be either constant or

linearly variable. In the conclusions, it is observed that, "the mechanism by which oscillations are initiated and sustained at high pressure appears to be essentially the same as that at low pressure despite the fact that in one case the oscillations appear to be relaxation oscillations and in the other case nearly harmonic."

In another analog-simulation study of the dynamic behavior of natural-circulation systems, Anderson et al.[19] claim that the predictions from their model compared well with the oscillatory behavior observed experimentally. Several slip-ratio models were tested, and a comparison with the analog model indicated that the oscillation threshold was sensitive to the magnitude of the slip ratio, but insensitive to the rate of change of slip ratio with power.

Levy and Beckjord[8] developed a mathematical expression for the instability thresholds, based on the following hypothesis:

At equilibrium, a certain fraction of the test-section volume is occupied by steam. Any change in heat flux or inlet flow rate should result in the change of the steam-volume fraction. This does not happen instantaneously, but changes with average flow velocity. The driving head in natural-circulation system is a function of the steam-volume fraction and therefore changes after a delay caused by the transit time of the signal up to the two-phase region.

The above considerations led to the following mathematical expression:

$$\frac{dV}{dt} + aV^2 + bV - c + \int_0^T f'[Q, V(t-\tau)]\, d\tau = 0 \qquad (2.2)$$

where

V = inlet water velocity,

t = fluid transit time across riser,

f' = function of void fraction dependent upon inlet velocity and heat input,

Q = heat input,

and

a,b,c = loop-friction loss and heat parameters.

In the discussion, Levy and Beckjord show that the measured oscillation period compared satisfactorily with the values predicted by this model. They point out, however, that unless the precise nature of the function, f', is known, the onset of instability with respect to heat input, loop pressure and inlet velocity cannot be predicted.

Levy and Beckjord also discuss another viewpoint concerned with flow mechanics and flow-pattern instability. The model deals basically with the causes of instability rather than the quantitative aspects of the behavior of a system. They examined the energy transmitted by shear forces at the steam-water interface and at the fluid channel interface and suggested that when the shearing energy received by one fluid exceeds its ability to dissipate that energy at the channel wall, the excess energy appears in the form of eddies or slugs causing oscillations. If this is the cause of instability, at threshold a discontinuity should exist in the pressure drop in the two-phase region. But the experimental data[1] do not show this discontinuity. The model also fails to predict the frequency of oscillation.

Wallis and Heasley[20] employed a Lagrangian coordinate model which permits an exact solution of the conservation equations for a channel subjected to cyclic variation in inlet flow. The authors made a mathematical analysis of three modes of oscillation of a simple two-phase-flow, natural-circulation system: (1) oscillations due to changes in riser buoyancy, (2) oscillations excited by the heated section, and (3) parallel-channel oscillations. They assumed zero slip and made a qualitative check with a small, natural-circulation, pentane loop. A general mathematical criterion for inception of oscillation was not developed.

Boure[21] initiated a different approach. He considered two models, the "Density Effect Model" and the "Delay Effect Model." In the first model, he considered a characteristic time, which is a function of power density and the slope of the curve of specific volume versus enthalpy. This enabled the period of oscillation to be predicted. The second model, also known as the "Propagation Model," is based upon the propagation signal of small disturbances in two-phase flow. Boure suggests that continuity and dynamic waves are associated and that the mass transfer between two phases plays an important role.

Fleck[22] analyzed the dynamic behavior of boiling-water reactors by using the laws of mass, momentum, and energy. Several simplifying assumptions, such as zero slip and zero subcooling, weaken the analysis, and the equations are solved by considering the heated section as one lumped region. The analysis does not predict oscillations but consists of convergent or divergent values of the flow rate. In the interpretation of the instability in the coolant cycles of the BORAX and SPERT I nuclear reactor experiments, Fleck points out that the unstable behavior displayed by these reactors was more likely a hydraulic phenomenon and not a conventional feedback instability arising from time delays inherent in these systems.

Quandt[17] applied small-perturbation theory to the linearized conservation equations and obtained the transfer functions by Laplace

transformation of these equations. He utilized these transfer functions as the criterion for the flow oscillations. Homogeneous flow and monotonic spatial variation of enthalpy and mass flow rate were assumed. The transfer function that results, shows that the flow response to change in power is oscillatory when a certain coefficient becomes zero. This gives a necessary condition for flow oscillations in terms of the exit quality:[3]

$$X_{ex} = \frac{[1 + \overline{X}\, v_\ell/(v_g - v_\ell)]\,(1 + fL/D)}{1 - 2v_\ell/(v_g - v_\ell)} \qquad (2.3)$$

where $\overline{X}$ is the quality at the midpoint of the channel. Other terms are defined in the Nomenclature and have their usual meanings.

A check of the above criterion showed that the experimental data fell considerably below the prediction and that the slope of the X_{ex}-versus-fL/D line was less than that of the data.

Jones,[23] in a similar linearized mathematical treatment, considered the effect of a moving boiling boundary and applied the Nyquist criterion for the prediction of instability. His analysis shows that the moving boundary effects due to presence of a subcooled region play an important role in determining flow stability and should not be ignored. The model checked well[26,27] with other experimental data; hence, this was one of the models that was used to compare its predictions with the experimental data of the present study. Further details are presented in Chapter VI.

The momentum-integral model of Meyer and Rose[28] used a digital computer to obtain a numerical solution of difference equations representing partial differential equations of hydrodynamics and energy. The model neglects compressibility effects and considers the heat capacity of the channel, and the effect of proper time-space energy-transport relationship is illustrated. A separate digital-computer program[29] contains provision for two-dimensional flow. The predictions show good agreement with the experimental data of Blubaugh and Quandt,[30] though somewhat more damped than indicated by experiment.

Meyer also considered the effect of compressibility in another analysis and developed a "sectionalized compressible model."[31] The analysis was, however, limited because of the numerical stability problems. Also, the required time-step size was of the order of time for a sonic wave to pass through one differential step, in the sinusoidal direction, which required a prohibitively large time for digital computation.

Jahnberg[16,32] used a difference approximation to solve a one-dimensional form of the nonlinear equations of mass, momentum, and energy written for a natural-circulation loop. The steady-state flow rate

is approximated by an iteration procedure, and a step increment in power (momentary or otherwise) is made to study dynamic behavior of the system. The model checked reasonably well with experimental data (see References 15, 17, 26, and 27) and, therefore, was used to compare with the present results, as discussed in Chapter VII.

Nahavandi and von Hollen[33,34] obtained a generalized theoretical model to predict the dynamic behavior of forced- or natural-circulation boiling-water reactor systems. The space-dependent neutron kinetics equations for the reactor core and the space- and time-dependent flow-conservation equations for the coolant system were expressed spatially in finite-difference form and then integrated in the time domain. The results were verified with the experimental data of Levy and Beckjord.[8] Analytical predictions of the instability thresholds and frequency of oscillations are shown to be in good agreement with the test data.

D. Closure

Some of the experimental and theoretical investigations were analyzed comprehensively by Neal and Zivi.[26,27] Some of their conclusions are summarized below:

1. Most of the data on boiling-water loop oscillations are explainable as a result of feedback between the flow rate and the steam voids.

2. The linearized model of Jones[23] predicted threshold of instability and oscillation frequencies quite well for about 70% of the cases. Thus, the oscillations can be considered to be a linear phenomenon for small amplitudes.

3. The nonlinear analysis by Jahnberg[32] provided a fairly reasonable prediction of the steady-state values. The prediction of threshold and frequency of hydrodynamic oscillations was somewhat less reliable than Jones's model.

In Chapter IV, some of the published experimental results are compared with the observations of the present experimental investigation. In Chapter VIII, the predictions from two of the theoretical models[23,32] are compared with the data obtained in this study.

III. EXPERIMENTAL APPARATUS AND PROCEDURE

In keeping with the main objective, a series of experiments was planned to cover a wide range of parameters, taking special care to obtain information about the effects of the test-section and riser geometry on the oscillatory behavior of the system. The design of the experimental facility was kept simple, and appropriate arrangements were made for a control on each parameter. Sudden expansion and contraction of the flow path were avoided as far as possible, and other constrictions in the loop were kept to a minimum.

A. Description of Equipment

A schematic diagram of the loop is shown in Fig. 3.1. All components of the loop were designed to withstand pressures greater than 2000 psi.

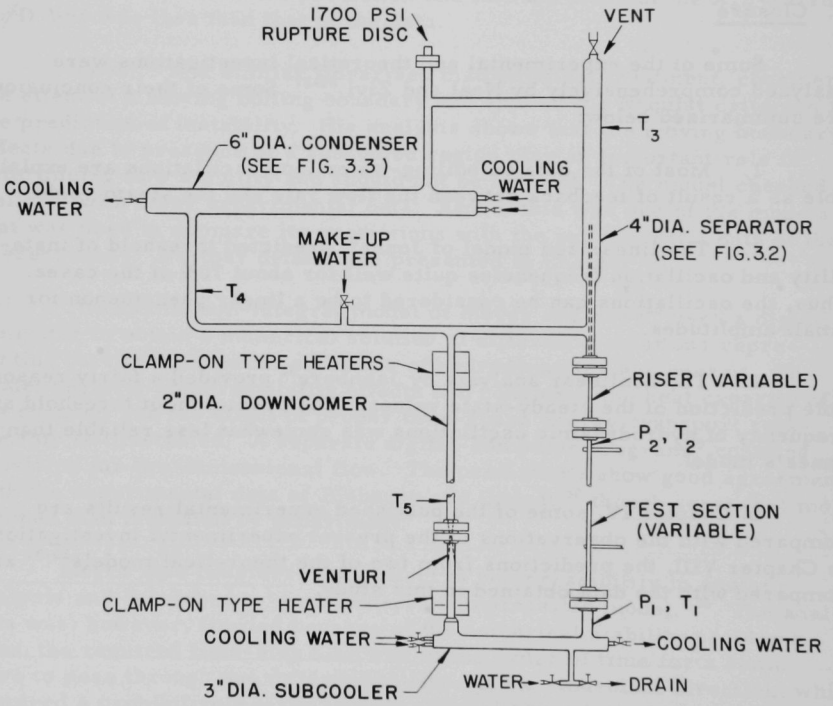

Fig. 3.1. Schematic Diagram of Test Loop

A general description of some components follows:

1. Power Supply

A 300-kW, 60-cps, alternating-current power supply provided heat to the test section. The maximum output voltage of this supply was 100 V at 3000 Amp, and an ignitron circuit provided a continuously-variable manual adjustment in the range of 5-100 V. The unit was designed to have negligible current fluctuations and was capable of maintaining a constant rms power level to within ±1%. As an emergency feature, the system included a relay contactor for tripping the power.

2. Test Section and Riser

Variations in the test-section and riser geometries were made possible by using three pairs of flanges to join them to the rest of the loop. The lower end of the test section was connected to a 2-in. pipe section by means of a pair of 2-in. flanges. The flow path to the test section was tapered to minimize any disturbance in the system due to change in cross-section area. In addition, a calming length equivalent to several diameters of the tube was allowed between the tube inlet and the lower bus bar. A pair of 1-in. flanges joined the test section and riser; the top end of the riser was held into the steam separator by means of a pair of 2-in. flanges. Durabla gaskets sealed the flange joints and provided electrical insulation between the test section and the rest of the loop.

All the test sections were designed to have uniform power distribution. The wall thickness of each test section was chosen to withstand a bursting pressure greater than 3500 psi and to provide electrical resistance for a maximum power input of more than 200 kW. The dimensions of test sections and risers used in different geometrical combinations are listed in Table I. Except for one riser, which was a 1-in., Schedule 40, steel pipe section, all the test sections and risers were standard, seamless, stainless-steel tubes.

TABLE I. Test-section and Riser Geometry

Geometry No.	Test Section			Riser		
	Length, in.	ID, in.	OD, in.	Length, in.	ID, in.	OD, in.
1	96	0.8125	0.875	48	1.049	1.315
2	96	0.364	0.54	48	0.3125	0.375
3	96	0.625	0.75	48	0.625	0.75
4	72	0.625	0.75	48	0.625	0.75
5	48	0.625	0.75	48	0.625	0.75
6	96	0.625	0.75	60	0.625	0.75

3. Steam Separator

The two-phase mixture from the riser was separated in the steam separator. As shown in Fig. 3.2, this was a 4-in.-diam pipe section, the top end of which was welded to a 4-in. cap. The lower end was attached to the riser by means of a 2-in. flange welded to a reducer. A 2-in.-diam steam outlet near the upper end joined the line leading to the condenser, and another 2-in.-diam line near the lower end joined the crossover. A 1/4-in. vent was provided in the center of the cap.

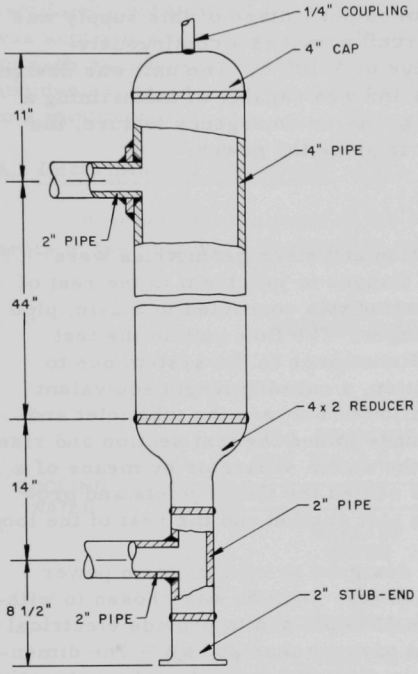

Fig. 3.2. Steam Separator

4. Steam Condenser

This parallel-flow heat exchanger had been used previously in other experimental work[43] and was designed for heat dissipation of approximately 230 kW. However, its heat-removal capacity was found to be considerably reduced, most likely because of scale formation on the cooling tubes. A drawing of the steam condenser is shown in Fig. 3.3. The shell of the cooler was a 6-in. steel pipe, the ends of which were enclosed by two 6-in. caps. Cooling water entered through four 7/16-in. pipes, each of which had a separate regulating valve. This water was then discharged through a 1-in. pipe after passing through a manifold inside the condenser, where the four streams were combined.

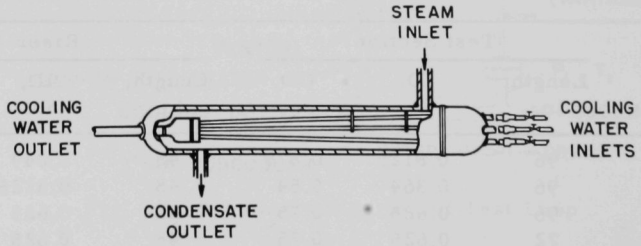

Fig. 3.3. Steam Condenser

Such an arrangement provided flexibility of operation, and single readings of exit temperature and flow-rate measurement sufficed. Steam entered the condenser through a 2-in. line at the top, and the condensate discharged through another 2-in. opening at the bottom.

5. Subcooler

Before the inlet to the test section, another cocurrent heat exchanger provided a cooling capacity of up to 50 kW, whenever additional cooling was necessary for the temperature control of the water at the inlet to the test section. The lower horizontal section of the loop was used as the heat-exchanger shell (3-in. diam) in which the loop water entered from the 2-in.-diam downcomer and discharged through the 2-in. line joining the test section. The cooling water entered through three individually-regulated 1/2-in.-diam pipes and discharged through a 3/4-in.-diam pipe after combining in a manifold.

6. Preheaters

Three clamp-on resistance heaters, each of 3-kW capacity, were located on the downcomer line to provide additional heat input whenever necessary to raise the inlet temperature of the water entering the test section. Two of these heaters were operated by on-off-type switches, and the third was connected through a variable voltage supply for finer control of the heat input.

B. Instrumentation

This experiment provided a wide choice of variables for studying the system behavior. The final selection was based upon ease of measurement, equipment availability, and freedom from excessive noise and drift. A differential pressure transducer connected across a venturi located in the downcomer was used to measure the inlet flow rate. Other variables measured were pressure drop across test section, wall temperature, and bulk-fluid temperatures, in addition to the power input and loop pressure.

A study of the oscillatory behavior of these variables required an accurate and fast-responding recorder, with a possibility of varying the chart speed. At first an FM tape recorder was used; this was later replaced by an oscillograph. Their use required auxiliary instrumentation, which included a bucking-voltage system, amplifiers, and a calibration unit. The instrument panels are shown in Figs. 3.4 and 3.5, and a general description of the instruments follows.

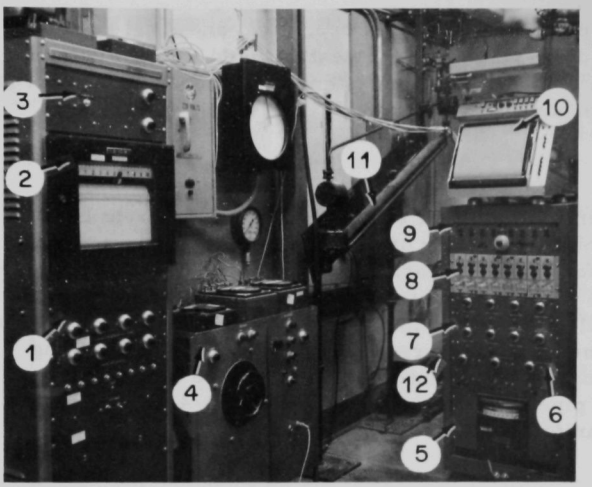

1. Burnout Detector
2. Brown Recorder
3. Integrating Circuit
4. Control Panel--Power Supply
5. Pyrovane
6. Power Supply--Transducers
7. Bucking Voltage System
8. Amplifiers
9. Voltage Supply--Calibration
10. Oscillograph--Visicorder
11. Manometer--Venturi
12. Voltage Regulator

Fig. 3.4. Some Instrument Panels

1. Variable Transformer
2. Regulating Valves--Subcooler
3. Regulating Valve--Make-up
4. Barton Gauge (Liquid Level)
5. Ammeters--Preheaters
6. Switches--Preheaters
7. Manometer--Subcooler Coolant
8. Manometer--Make-up
9. Manometer--Condenser Coolant
10. Pressure Gauge--T.S. Exit
11. Pressure Gauge--T.S. Inlet
12. Emergency Power Switch
13. Regulating Valves--Condenser
14. Regulating Valves--Steam Vent
15. Regulating Valve--Water Inlet
16. Regulating Valve--Water Drain

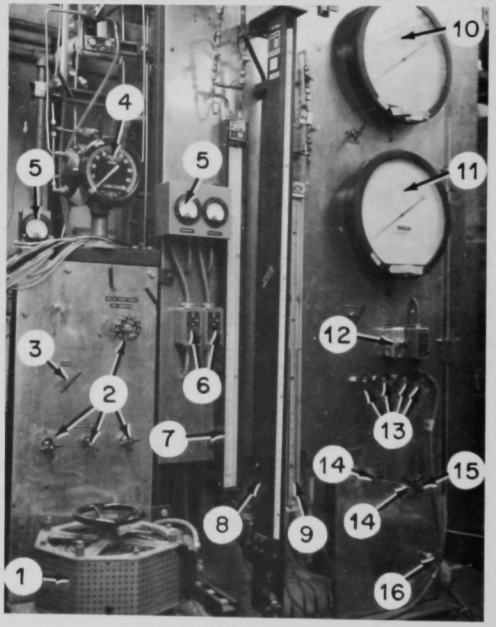

Fig. 3.5. Additional Instrument Panels

1. Power Measurements

The electrical power input to the test section was measured by a Westinghouse Model 310 a.c.-d.c. wattmeter. Its range was 500 W at 100 V, and the accuracy rating was 0.25% full-scale. The power input was also determined by the product of the voltage drop across the test section and the current flowing through it. The voltage drop was read on a Westinghouse type PA-5 portable a.c. voltmeter, whose rated accuracy was 0.25% at a full-scale reading of 150 V. The current input was reduced with a transformer by a ratio of 500:1 before reading on a Weston Model 370 ammeter of 5 or 10 Amp full-scale. The accuracy of this instrument was specified to be 0.17% full-scale over the first half of the scale, and 0.25% over the second half.

2. Pressure Gauges

Two, 0-1500-psig, pressure gauges (Heise Bourdon Tube Company) were connected at the test-section inlet and exit. These gauges had 1-psi subdivisions. A dead-weight pressure tester was used for calibration.

3. Liquid-level Gauge

A liquid-level gauge, 0-50-in. range, manufactured by Barton Instrument, Inc., was used. Its two lines were connected to the condenser bottom and the downcomer inlet.

4. Manometers

A high-pressure inclined manometer, 20-in. full-scale range, was connected across the venturi (0.707-in. throat diameter) in the downcomer. Another high-pressure manometer was connected in the make-up water line across a 0.2916-in.-diam orifice. Ordinary manometers were used to measure the cooling-water flow rates through the condenser and subcooler.

5. Pressure Transducers

Two differential-pressure transducers (Statham Instruments, Inc.) measured the pressure drops across the venturi in the downcomer and across the test section. The ranges of the transducers were 1 and 15 psi, respectively. In the preliminary tests, an additional differential-pressure transducer, 0-15-psi range, was installed across the riser, but had to be removed because of faulty performance.

An absolute-pressure transducer (Statham) of 0-2000-psi range was connected at the test-section exit to record the local pressure variations. It was found that, in most cases, this pressure variation was quite low (rarely exceeded 5 psi), and the recorder was unable to indicate it because of the low sensitivity of the transducer (12 μV/psi); also the instrument noise obscured these small changes. The use of this transducer was discontinued after tests were completed with the first geometry.

Regulated d.c. power supplies from Harrison Laboratories, Inc., were used for the excitation voltage to the transducer bridge circuits. These transformed a 95-135-V a.c. input power to a regulated output of 0-15 V (0-0.2 Amp). The noise characteristics of these power supplies were rated to be less than 100 μV rms for any combination (within rating) of line voltage, output voltage, and load current; the total drift for 8 hr at a constant ambient temperature was less than 0.1% plus 5 mV.

6. Thermocouples

The fluid temperatures were measured at various locations in the loop with 0.011-in.-diam Chromel-Alumel sheathed thermocouples (0.061-in. OD). The tips of the thermocouples were positioned approximately in the center of the flow cross section. The thermocouples, calibrated in a hypsometer over 50-500°F, were located at the test-section inlet and exit, in the steam separator, at the condenser exit, and in the downcomer. The time constant of these thermocouples was estimated[44] to be 50-150 msec.

Several 30-gauge Chromel-Alumel thermocouples, insulated by thin mica sheets to minimize electrical pickup, were held securely against the test-section wall with glass tape. Some of these thermocouples were used as burnout detectors. The time constant of these thermocouples was estimated to be about 25 msec,[44] but the heat capacity of the test-section wall and the mica sheet added considerable time lag, reducing the overall temperature response of these thermocouples to the order of a few cycles per second.

Chromel-Alumel thermocouples were also placed in the cooling-water discharge of the condenser and subcooler.

7. Bucking-voltage System

Eight units were used, each consisting of a voltage-dividing circuit connected to a 1.35-V mercury cell. The range was 0-20 mV, and linear tolerance was within ±0.25%. The voltage-dividing circuit was sized so that the effect of loading would not cause the bucking voltage to vary by more than 1/2%.

The system limited the amplifier output to a desired range, so as not to overload the galvanometers. It also allowed adjustment of the position of the galvanometer signal on the oscillograph chart.

8. Amplifiers

Eight, Model A-12, Electro Instruments, Inc., d.c. amplifiers were used. These amplifiers had a continuously-variable gain in the range of 0-1000. Some important features of these amplifiers were:

D.C. gain accuracy	±0.1% at gain setting
D.C. gain stability	±0.01% at gain setting
Drift	<4 μV in 200 V at constant ambient temperature <0.45 μV/°F
Noise (referred to input)	0-3 cps: 10 μV peak-to-peak 0-750 cps: 7 μV rms 0-50 kc: 14 μV rms
Frequency response	±3 dB to 50 kc; ±1.0% to 2 kc
Linearity	±0.1% to 2 kc

9. Brown Recording Potentiometer

An eight-channel 0-10-mV Brown Recording Potentiometer was used for measuring signals from the thermocouples located in the flow stream at the condenser exit, in the downcomer, and in the discharge of cooling water from the condenser and the subcooler.

10. Tape Recorder

At the start of this investigation, the data were recorded on magnetic tapes by means of a Honeywell Portable Model 8100 FM tape recorder equipped with seven data channels. The information on the tape could be recorded and played back at tape speeds of $1\frac{7}{8}$, $3\frac{3}{4}$, 15, and 30 in./sec for frequency-response ranges of 0 to 0.625, 1.25, 5, and 10 kc, respectively. The noise was specified to be a maximum of ±2% rms at full scale. The specifications required the input signals to be in the 2- to 10-V range, which the instrument played back in the 0- to 2-V range. The information from the tapes was digitized on a six-channel, Packard-Bell Analog-to-Digital Converter capable of digitizing at a sampling rate of 0.5 to 768 msec.

The tape recorder provided the possibility of fast and convenient data processing. It was intended to be used for statistical correlation of the system variables, which required a large number of samples

for digital calculations. Unfortunately, its use was unsatisfactory in this work because of the requirement that the input signal be amplified to be close to 10 V for the best results. This required an amplification of the order of 10^3 with the d.c. component of the signal in, and of the order of 10^5 without the d.c. component (bucked out) of the signals from the thermocouples and transducers. The noise level associated with the available amplifiers at such high gains discouraged the use of this tape recorder. The time and expense barred procuring of adequate amplifiers.

11. Oscillograph

A Honeywell Model 1012 Visicorder Recording Oscillograph, with the frequency and sensitivity characteristics of optically recording oscillographs, provided a satisfactory replacement for the tape recorder. It consisted of several (maximum of 36) subminiature, electromagnetically-damped, optical galvanometers. Each of these deflected a small mirror proportional to the electrical signal. The mirrors reflected a light beam proportional to the deflection onto a motor-driven, photosensitive, paper chart. The linear speed of the chart was controlled at various values ranging from 0.1 to 160 in./sec within a tolerance of ±2%. For this work, electromagnetic damped galvanometers were used because of their high sensitivity. These were rated for a flat (±5%) frequency response of 0-24 cps.

Block diagrams of the thermocouple and transducer inputs to the recorder are shown in Fig. 3.6.

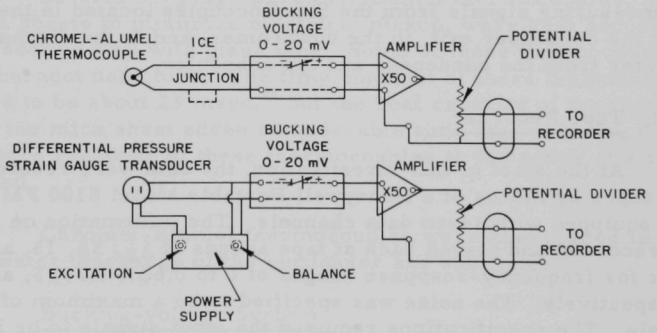

Fig. 3.6. Block Diagrams of Thermocouple and Transducer Signals to Recorder

C. Safety Features

This high-pressure and high-power experimental facility included several safety features, which are described in the following paragraphs.

1. Burnout Detectors

Burnout detectors were used to prevent the "burnout" of the test-section wall whenever the safe power input to the test section was exceeded. Figure 3.7 is a block diagram of the electric circuit. Six thermocouples located at strategic positions on the test-section wall acted as burnout detectors. Each was connected to a bucking-voltage supply, and then to a normally-open relay. Whenever any thermocouple signal exceeded a preassigned value of the bucking voltage (20 mV, equivalent to 910°F), the relay was closed, thus tripping the power to the test section. This safety device prevented damage to the test sections on several occasions.

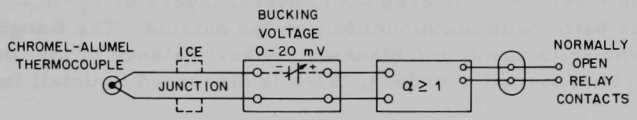

Fig. 3.7. Block Diagram of Burnout-detecting System

2. Test-section Shroud

Though each test section was designed for a bursting pressure of over 3500 psi, additional safety was provided by a metal shroud. It consisted of a piece of thick steel tube whose inside diameter was slightly more than the outside diameter of the test section. This was cut into two semicylindrical pieces, which were put around the test-section wall and held tightly by hose clamps. The shroud was insulated from the test section by 1/64-in.-thick Durable.

3. Rupture Disc and Check Valves

As shown in Fig. 3.1, a 1700-psi rupture disc was located in the steam line to the condenser to prevent damage to the loop due to accidental overpressurization.

In the event of the failure of the cooling tubes, the laboratory water piping system was isolated from a pressure surge by means of 2000-psi check valves. Two check valves were installed in each line upstream of the cooler.

4. General Safety Features

The loop was loosely held in the vertical direction to allow for thermal expansion.

The whole loop was shielded by a 1/4-in.-thick aluminum plate. Two readily-accessible push buttons were provided for power shut-off in case of emergency.

D. Thermal Insulation

After completion, the loop assembly was hydrostatically tested by pressurizing the water-filled loop to 3500 psi. (An appropriate rupture disc was substituted for this test.) This was repeated after installing every new test section/riser assembly. All leaks were stopped, and the electrical insulation of the test section from the rest of the loop was checked.

Except for the test section, riser, and flanges, the loop was thermally insulated with several layers of 85% magnesia lagging. The test section and riser were covered with several layers of $1\frac{1}{2}$-in.-thick spun-fiber-glass batts, with aluminum foil on the outside. The flanges were covered with thick insulation blankets. A heat balance of the loop components indicated normal heat loss. This is discussed in detail in the next chapter.

E. Experimental Procedure

The operational procedure of the loop was simple and is briefly described here. The loop was first filled with demineralized water, which was allowed to overflow through the vent line. The manometer, transducer, and liquid-level gauge lines were bled to expel any air and were put into service. The water overflow was then stopped and the vent valve was closed. The loop was then allowed to drain until the liquid level was a little higher than the value for the test condition. The power was turned on, and the loop was slowly heated. When the loop pressure approached the test condition, air from the loop was vented by keeping the steam vent line open for several minutes. At this point, the loop was allowed to stabilize at the test conditions.

The above procedure required 2 to 3 hr. In the meantime, the recording instruments and other accessories were checked and calibrated. The zero position of each galvanometer signal on the oscillograph chart was corrected, and a calibrated signal was fed to each amplifier in turn. The gain was adjusted to obtain the desired response of the galvanometer on the chart. This calibration procedure of the recorder was repeated at least once more during the operation. When the loop was brought to the test conditions, the switches were selected so that the light traces of the thermocouple and transducer signals were seen on the oscillograph. These were positioned by adjusting the bucking voltages.

The loop required manual control of the flow of the condenser cooling water for maintaining the loop pressure and that of the subcooler or preheaters for the temperature of the water at the test-section inlet. Occasionally the liquid level required adjustment. Whenever required during the operation, the water to the loop was added through the make-up line by means of a high-pressure pump.

Data were recorded at a given power when the system was stabilized at the predetermined values of the system pressure, the liquid level, and the temperature of the water at the test-section inlet. The power was then step-increased for the next set of data. Including the time required to stabilize the loop at the new power input, a new set of data could generally be taken in about 15-20 min. The power was increased to as high a value as possible; some of the general limitations were the power trip by one of the detectors, the limited cooling capacity of the condenser or subcooler, or the limited heating capacity of the preheaters.

IV. EXPERIMENTAL RESULTS AND DISCUSSION

A. Loop Heat Balance

Several runs were made to calculate heat losses at various pressures and heat inputs after the loop assembly was completed and thermally insulated. With an increase in loop pressure, the heat losses increased. Increased heat input to the test section at a given pressure did not result in any significant change in the heat loss. Total heat loss from the loop is plotted against pressure in Fig. 4.1.

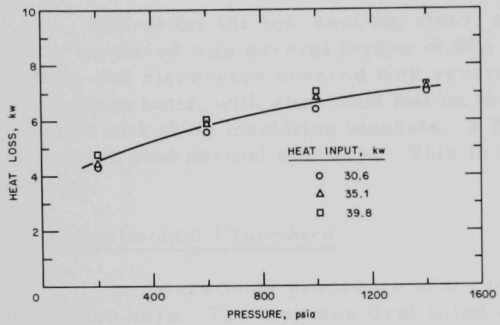

Fig. 4.1. Loop Heat Loss vs Pressure

Heat loss was checked systematically for each component of the loop. The calculations showed that the heat loss from the test-section surface was less than 3% at lowest power input (10 kW), and it decreased with increase in input power

B. Experimental Data

As explained in Chapter III, the data for each run were recorded after the system was permitted to come to a steady condition at the predetermined values of the loop parameters. These parameters were power, pressure, liquid level, and inlet subcooling for each test-section and riser geometry. It was not always possible, however, to bring the loop conditions (pressure, liquid level, and inlet subcooling) to an exact setting. Table II indicates the range within which each parameter was controlled for a given set of runs.

TABLE II. Range of Various Parameters

Geometry	Table No.	Data Point No.	Pressure, psia	Inlet Subcooling, °F	Power, kW
	Test Section:	Length = 96 in.		ID = 0.8125 in.	
	Riser:	Length = 48 in.		ID = 1.0490 in.	
1	V	1-8	199-201	0-3	10-40
		9-16	200-202	8-11	15-48
		17-25	201-204	18-22	20-59
		26-36	598-602	1-3	15-60
		37-49	600-603	8-10	15-70
		50-61	600-603	20-23	25-80
		62-70	998-1000	2-3	25-68
		71-82	1000-1003	7-9	20-70
		83-98	1001-1003	18-20	17-84
		99-112	1400-1403	9-12	25-83
		113-116	1498-1502	1-2	60-76

TABLE II (Contd.)

Geometry	Table No.	Data Point No.	Pressure, psia	Inlet Subcooling, °F	Power, kW
	Test Section: Length = 96 in. ID = 0.3640 in.				
	Riser: Length = 48 in. ID = 0.3125 in.				
2	VI	1-6	200-202	0-3	10-23
		7-13	200-202	7-10	10-25
		14-19	200-202	16-18	12-25
		20-28	601-603	0-3	10-30
		29-38	601-604	10-11	10-30
		39-46	601-603	17-20	12-30
		47-54	1001-1003	0-3	10-30
		55-63	1001-1003	9-11	10-32
		64-72	1002-1003	20-22	12-33
	Test Section: Length = 96 in. ID = 0.625 in.				
	Riser: Length = 48 in. ID = 0.625 in.				
3	VII	1-8	201-204	27-29	24-60
		9-18	200-203	35-38	30-70
		19-30	201-204	43-46	24-80
		31-36	602-603	26-30	24-51
		37-42	601-603	35-37	39-66
		43-50	602-604	45-47	34-70
		51-59	1000-1003	45-49	44-85
	Test Section: Length = 72 in. ID = 0.625 in.				
	Riser: Length = 48 in. ID = 0.625 in.				
4	VIII	1-11	200-204	19-22	14-50
		12-27	200-203	28-31	20-65
		28-44	200-204	38-42	20-70
		45-53	600-603	29-32	25-70
		54-64	599-603	39-42	20-70
		65-74	600-603	49-51	29-73
		75-81	601-604	61-64	34-70
	Test Section: Length = 48 in. ID = 0.625 in.				
	Riser: Length = 48 in. ID = 0.625 in.				
5	IX	1-10	201-203	8-11	10-40
		11-19	200-203	17-19	15-42
		20-29	202-203	29-31	20-45
		30-35	601-603	49-52	35-60
	Test Section: Length = 96 in. ID = 0.625 in.				
	Riser: Length = 60 in. ID = 0.625 in.				
6	X	1-12	201-203	24-26	10-43

For each range, the inlet pressure was adjusted to within ±4 psi of the desired pressure by regulating coolant flow through the condenser, while the inlet subcooling was kept as close to the desired value as possible. The range of deviations in pressure and inlet subcooling is shown with the other data in Tables V to X, contained in Appendix C. The liquid level was maintained within a range of 10-10.5 in. below the condenser. Table II shows the values of each of the variables of the loop for different sets of runs.

The output variables, as well as some of the parameters of the system, were recorded on an oscillograph as described in the previous chapter. An error analysis of the variables is presented in Appendix A. Appendix B shows a sample calculation procedure, and the calculated values of the readings from the oscillograph charts are tabulated in Appendix C.

C. Flow Rates at Inlet to Test Section

1. Calculation of Flow Rates

The inlet flow rates were calculated from the readings of a differential pressure transducer measuring the pressure drop across a venturi located in the downcomer. A venturi is considered to be a satisfactory device for measuring steady flow rates, but under oscillatory flow condition the effects of acceleration and deceleration may become significant,[35,36] so that the venturi may give erroneous flow rates unless these effects can be corrected. A mathematical expression for estimating the flow rates from the data of the pressure drop across the venturi under oscillatory conditions is obtained below.

Consider a control volume enclosed by a venturi between two pressure taps. For an incompressible fluid, the one-dimensional momentum equation may be written, neglecting frictional and body forces and radial momentum transport, as

$$\frac{\partial u}{\partial t} + u \frac{\partial u}{\partial z} = -\frac{1}{\rho} \frac{\partial P}{\partial z}. \tag{4.1}$$

Integrating this equation with respect to z yields

$$\frac{1}{2} \int_1^2 \frac{\partial (u^2)}{\partial z} \, dz = -\frac{1}{\rho} \int_1^2 \frac{\partial P}{\partial z} \, dz - \int_1^2 \frac{\partial u}{\partial t} \, dz, \tag{4.2}$$

where the numerals 1 and 2 signify the cross sections at the high- and low-pressure taps, respectively. Since

$$uA = u_2 A_2, \tag{4.3}$$

Eq. (4.2) becomes

$$\frac{u_2^2 - u_1^2}{2} = -\frac{P_2 - P_1}{\rho} - \frac{du_2}{dt} \int_1^2 \left(\frac{A_2}{A} \right) dz, \tag{4.4}$$

or

$$u_2^2\left[1 - \left(\frac{A_2}{A_1}\right)^2\right] = \frac{\Delta P}{\rho} - C\,\frac{du_2}{dt}, \tag{4.5}$$

or

$$u_2^2 = \frac{1}{\beta}\left[\frac{\Delta P}{\rho} - C\,\frac{du_2}{dt}\right], \tag{4.6}$$

where

$$C = \int_1^2 \left(\frac{A_2}{A}\right) dz, \tag{4.7}$$

$$\beta = 1 - \left(\frac{A_2}{A_1}\right)^2, \tag{4.8}$$

u_2 = Fluid velocity at the venturi throat,

ΔP = Pressure drop due to velocity head between two taps, $P_1 - P_2$,

and

ρ = Fluid density.

A numerical integration of Eq. (4.6) for several cases of flow oscillations showed that the correction for acceleration effect was negligible at the peak values of the velocity.

An experimental verification of this calculation was made by installing a turbine meter (3/4-in. Pottermeter, Potter Aeronautical Corporation) for measuring flow rates upstream of the test section. A comparison of the flow rates measured simultaneously with the venturi and turbine meter showed that under oscillatory flow conditions the maximum flow rates matched quite well. Figure 4.2 shows typical traces recorded simultaneously from the two measuring devices.

The most important feature that these tests revealed was the existence of flow reversal. Cases (A) and (B) of Fig. 4.2 show the existence of two minima in each oscillation period of the flow traces. In the turbine meter traces, both minima occur near zero flow, whereas, in the venturi traces, only one minimum shows zero flow. Under the conditions of flow reversal, both measuring devices are incapable of showing negative flow.

The pressure drop due to velocity head in a venturi remains positive because the flow velocity in the venturi throat (pressure tap 2) is always greater than the velocity in the connecting pipe (pressure tap 1). In the turbine meter, the volumetric flow rate is proportional to the rotational speed of the turbine. The magnetic sensing device that measures these rotations is not designed to sense the direction of the flow.

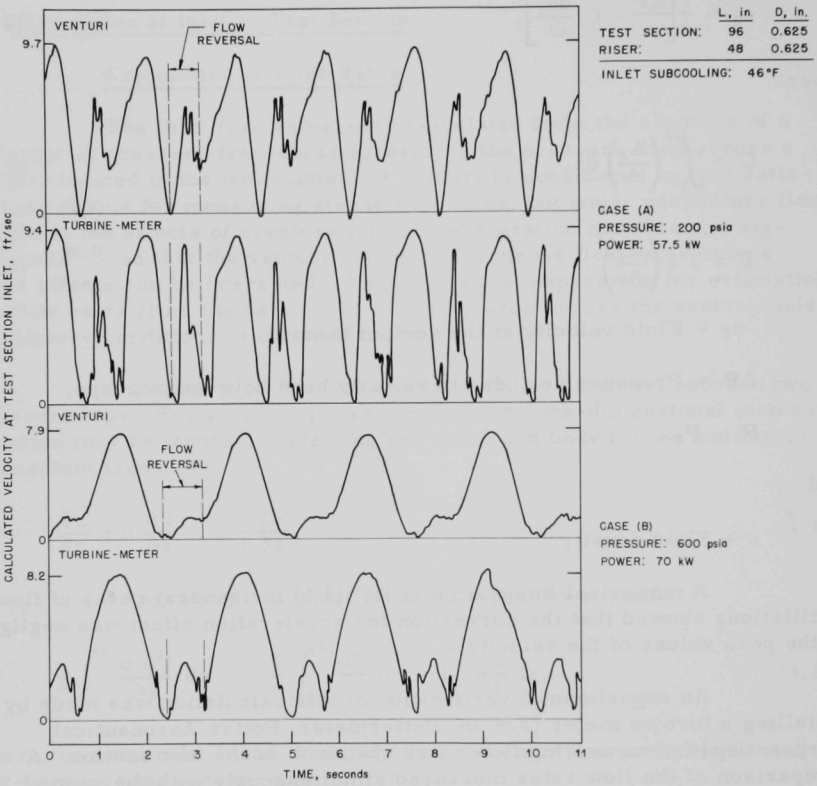

Fig. 4.2. Flow-rate Traces from Venturi and Turbine Meter

A pitot tube was therefore installed upstream of the test section to confirm whether flow reversal existed. The tip of the pitot tube was faced towards the test-section inlet, so that it would record a pressure drop in case of flow reversal. A strain-gauge differential-pressure transducer was connected across the pitot tube, and the signals were recorded on the oscillograph. Some typical record traces for two conditions of the loop are shown in Fig. 4.3. The observations from these tests confirmed that, as in the interpretation of the venturi and the Pottermeter traces, a flow reversal existed.

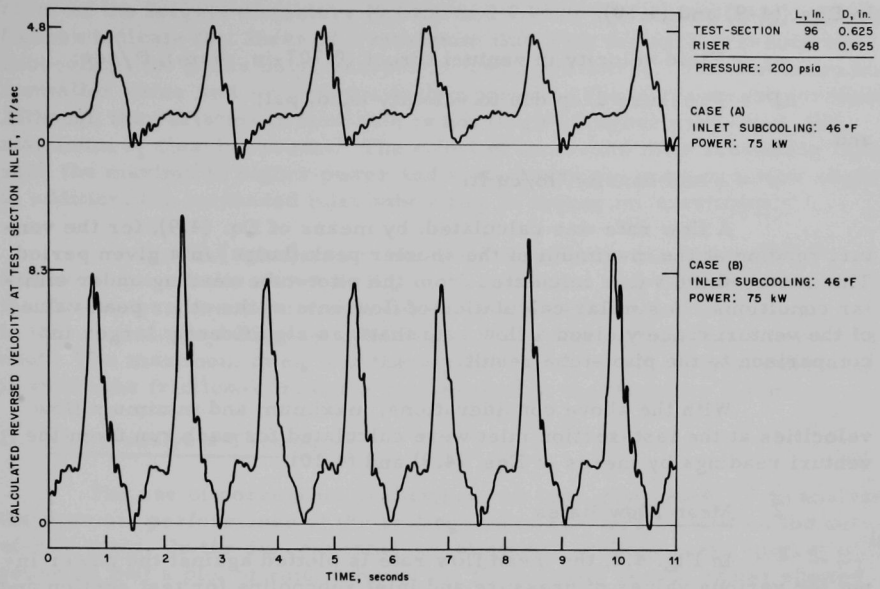

Fig. 4.3. Flow Reversal as Indicated by Pitot Tube

The following considerations led to the belief that in a given oscillation period the higher peak was due to flow in the normal direction, and a shorter bulge (in case of venturi traces) was due to flow reversal:

1. The peak flow rates matched for the venturi and the turbine meter, when calculated on the assumption that the larger peak was due to direct flow.

2. The profiles of the traces of venturi and turbine meter signals, when recorded on the same time scale, were similar in the region of the large peak, whereas it was not so in the remaining part.

3. A calibration of the venturi in the reversed flow direction gave the following relationship:

$$u_2 = 123.1 \left(\frac{\Delta P}{\rho}\right)^{0.465} . \tag{4.9}$$

A similar calibration of venturi in the direction of the normal flow yielded

$$u_2 = 96.5 \left(\frac{\Delta P}{\rho}\right)^{0.5} . \tag{4.10}$$

In Eqs. (4-9) and (4.10),

u_2 = Fluid velocity in venturi throat (0.707-in. diam), ft/sec;

ΔP = Pressure drop due to velocity head, psi;

and

ρ = Fluid density, lb/cu ft.

A flow rate was calculated, by means of Eq. (4.9), for the venturi reading at the maximum of the shorter peak (bulge) in a given period. This matched the value calculated from the pitot-tube reading under similar conditions. A similar calculation of flow rate at the other peak value of the venturi trace yielded a flow rate that was significantly larger in comparison to the pitot-tube result.

With the above considerations, maximum and minimum flow velocities at the test-section inlet were calculated for each run from the venturi readings by means of Eqs. (4.9) and (4.10).

2. Mean Flow Rates

In Fig. 4.4, the mean flow rate is plotted against the power input for various values of pressure and inlet subcooling for test section and

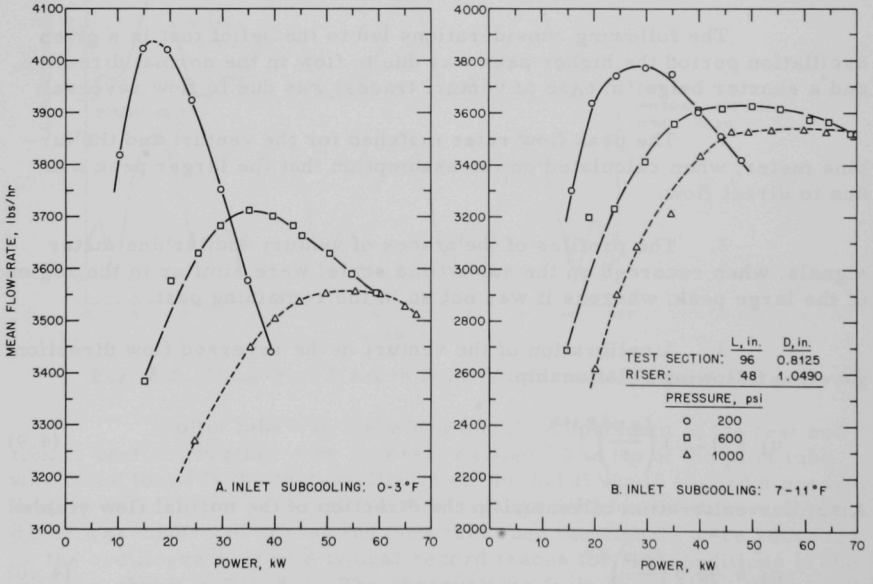

Fig. 4.4. Mean Flow Rate vs Power

riser of the largest diameters (0.8125 and 1.0490 in., respectively). These figures indicate that there is a maximum flow rate for each pressure and subcooling, the peaks being sharper at lower pressures. The maximum has a smaller value and occurs at a higher power as the pressure is increased. Although the variation in flow rate is not large at higher pressures, the maximum is clearly present. The effect of increased inlet subcooling is to shift the maxima to higher power and to decrease the maximum flow slightly. In addition, the increased inlet subcooling broadens the maximum.

Similar trends were observed by other researchers.[11,15,17] However, the results shown in Fig. 4.4 are for the loop conditions when the flow rates were quite steady (very little oscillation or none at all). In this region, the buoyancy and frictional-pressure-drop effects are prominent. The maximum in each of these plots is indicative of the phenomena in which the frictional pressure drop overtakes the buoyancy force.

D. Noise-analysis Techniques

The use of correlation techniques has been suggested[37,38] to analyze the dynamic performance of the boiling-water reactors as well as the out-of-pile tests. In the experimental investigations at Eindhoven, Spigt, et al.[11] reported that a plot of rms value of the fluctuations versus power showed a change in the slope, which, while marked, did not take place at a single point. Also, this change in slope depended on the loop variables, such as pressure and inlet subcooling. They obtained the autocorrelation function and the corresponding power-density spectrum of the pressure-drop signal at the inlet to the test section. The autocorrelation function $[\phi(\tau)]$ and the power-density spectrum $[\Phi(\omega)]$ for a signal f(t) are given by

$$\phi(\tau) = \int_{-\infty}^{\infty} f(t)\, f(t+\tau)\, dt, \tag{4.11}$$

and

$$\Phi(\omega) = \frac{1}{2\pi} \int_{-\infty}^{\infty} \phi(\tau)\, e^{-i\omega\tau}\, d\tau. \tag{4.12}$$

Spigt and co-workers obtained the rms values of the fluctuating part of the recorded signals from the peaks in the power-density curves and plotted this as a function of heating power. These plots, especially when the point of inception of oscillations (or instability) is not well-defined, provide a means of comparing the effects of different parameters of the loop.

A similar plot is given in Fig. 4.5., where the normalized (with respect to the mean value) standard deviations of the inlet flow rate, the pressure drop across venturi, and the pressure drop across the test section are

plotted against the heat flux. The general characteristics of the oscillations in each of these three measured quantities are similar in that the slopes become steep at about the same heat flux. The inception point of the oscillations is not sharply defined, however. Greater than 20% fluctuations in the value of pressure drop across the venturi were not obtained in this geometry, because of the limitations of the heat removal in the condenser.

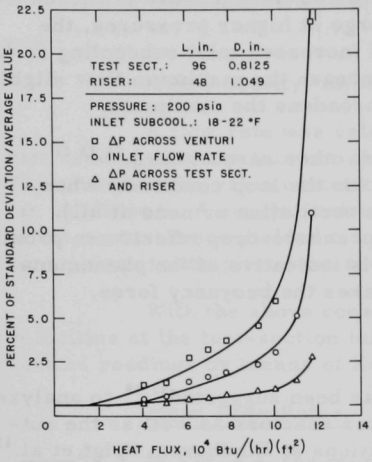

Fig. 4.5. Normalized Standard Deviation vs Heat Flux

E. Oscillation Envelopes

An interesting result of the study comes from the examination of the envelopes of the oscillations. Here the maximum and minimum flow velocities and pressure drop across the test section are plotted against power. Figure 4.6 shows that the fluctuations are indistinguishable until the power is greater than 25 kW for the conditions shown. First a slow and then a large divergence of maximum and minimum flow velocities are evident. At about 30 kW, the minimum inlet-flow velocity becomes zero and then negative. The inception point is quite sharply defined.

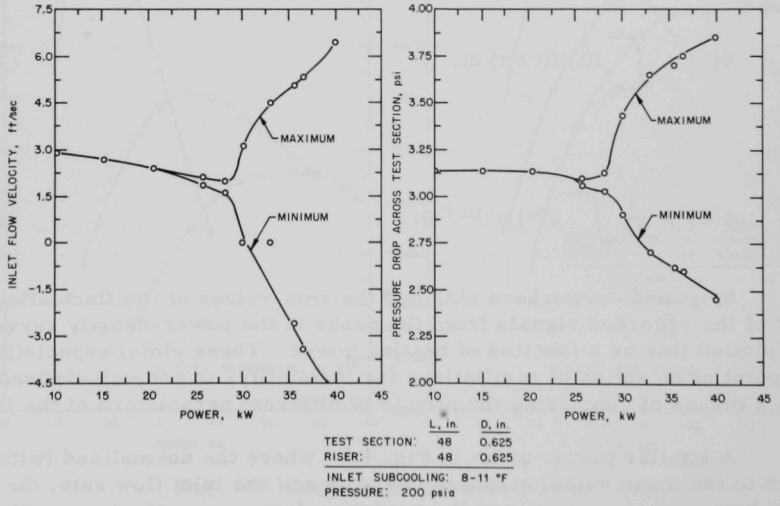

Fig. 4.6. Some Flow-oscillation Envelopes at 200 psia for Inlet Subcooling of 8-11°F

The sharp rise in the amplitude of oscillation may be attributed to storage of energy in the channel wall and an associated superheated-liquid boundary layer. Figure 4.6 shows that the mean flow rate in this power range appears to have a negative slope, which is most likely due to increased frictional loss. These large frictional losses and reduced net flow rates result in an increased choking effect with increased power as the rate of transport of energy out of the channel becomes less and less, as compared to the heat input. The energy probably has a threshold point, which depends upon the nucleation characteristics of the heating surface over the leading edge of the two-phase region.

Once vaporization of the superheated liquid begins, the stored energy is suddenly released into the system in the form of an internal burst of vapor. Depending upon the magnitude of the vapor burst, the inlet velocity decreases, or even becomes negative. From the sharp peaks in the flow-reversal trace, shown in Fig. 4.3, it may be said that this is a relaxation phenomenon, and the system quickly returns to the normal flow direction. The excess vapor passes out of the heated section, and the build-up of a superheated-liquid boundary layer begins again.

This appears to be the most plausible explanation of the self-sustained oscillations, and the subsequent discussion contains brief repeated remarks explaining the effect of various parameters on the system behavior in the light of the suggested flow mechanism.

The behavior of the system with respect to the pressure drop across the test section (also shown in Fig. 4.6) is similar, except that the pressure drop does not become negative.

The symmetry of maximum and minimum velocities about the steady-state conditions in Fig. 4.6 can be explained by the effect of frictional forces on the earlier-described flow mechanism. This explanation considers the behavior of a manometer when a sudden impulse is applied at its one end. In a similar way, the liquid in the downcomer, after minimization or reversal of the flow velocity, tries to return with a peak of equal amplitude relative to the mean flow rate. The two legs of the manometer in this case are, however, asymmetric because of the presence of two-phase mixture in the channel. Depending upon the channel geometry, there can be large dissipation of energy due to the frictional losses in the two-phase region, and the maximum flow velocity may be damped. For the larger-diameter riser and test sections, this effect of frictional damping is much less marked.

Figure 4.7 is for a longer test section and a higher pressure and inlet subcooling. In this case, the sharp fluctuations begin at a higher power (about 45 kW), which is most probably related to the fact that the system is at a much higher pressure, and thus more stable. In terms of

the suggested mechanism, the vapor bursts are smaller at higher pressure, because of the increased vapor density and the smaller liquid superheat that can be sustained.

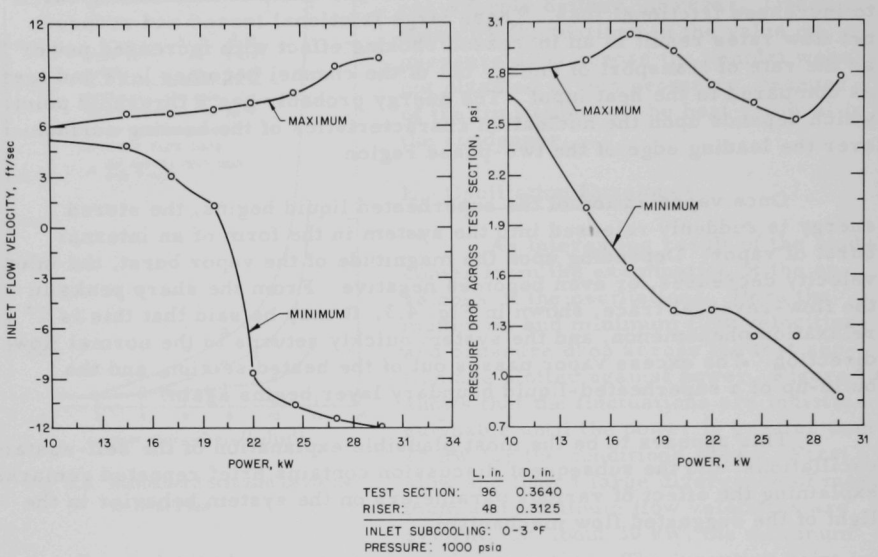

Fig. 4.7. Some Flow-oscillation Envelopes at 1000 psia for Inlet Subcooling of 0-3°F

The envelope of the oscillation in this case shows a tendency to become bounded towards the end. At the same time, the frequency increases from 0.40 to 0.50 cps. This indicates that the stored energy threshold for a vapor burst tends to level off with increased heat flux.

Figure 4.8 (smaller-diameter test section and riser and longer test section) indicates that the maximum and minimum flow velocities are distinguishably different at 10 kW. One noticeable difference is that there is a lack of symmetry in the maximum and minimum in that the maximum does not change as much as the minimum does. Probably, in this case, the system is behaving like a highly damped asymmetric manometer because the flow area of the test section and riser is reduced by a factor of three. The buoyancy forces which, in general, should contribute to the maximum flow rate are nullified by the increased frictional forces, as explained earlier.

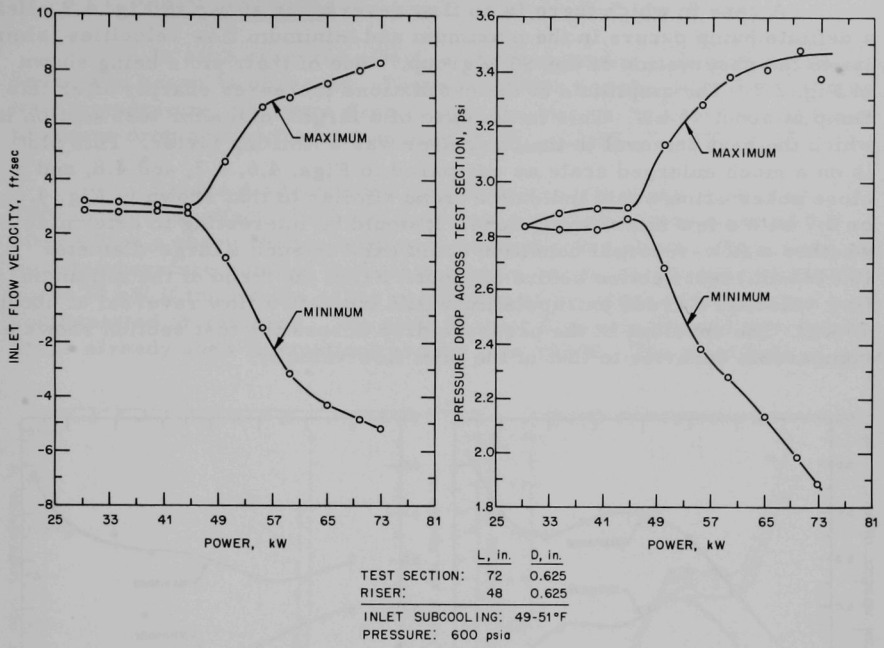

Fig. 4.8. Some Flow-oscillation Envelopes at 600 psia for Inlet Subcooling of 49-51°F

The peak velocities in this case are much larger than would be expected for steady-state flow in the system. Both 9 ft/sec and a negative 12 ft/sec are large for a natural-circulation system, indicating sizable pressure surges.

Similar examination of the pressure drop across the test section shows a comparable asymmetry, but the curves are not similar. It is evident that the two plots in this figure (the inlet flow velocities and the pressure drops across the test section) are not closely correlated. The pressure drop across the test section is indicative of the difference between local pressures at the inlet and the exit of the test section. After the inception of self-sustained oscillations, the pressure wave travels in both directions from within the test section by the earlier-described mechanism. Under such conditions, the pressure drop is not likely to have any direct correlation with the flow rate. This also explains the nonmonotonic character of the envelope of the oscillation of the pressure drop across the test section.

A case in which there is no flow reversal is shown in Fig. 4.9. Here a definite hump occurs in the maximum and minimum flow velocities, similar to the observation of the STL group,[14] one of their plots being shown in Fig. 2.2. The amplitude of the oscillations increases sharply after this hump at about 45 kW. This is the case of a larger-diameter test section in which the heat removal in the condenser was a limiting factor. This plot is on a much enlarged scale as compared to Figs. 4.6, 4.7, and 4.8, and a close observation would indicate a trend similar to that shown in Fig. 4.6 or 4.7 with a few minor exceptions. It would be interesting to determine whether a flow-reversal condition could exist in such a large-diameter (0.8125-in.) test section before burnout. From the trend of the minimum flow velocity, a crude extrapolation would indicate a flow reversal at about 75 kW. The envelope of the pressure drop across the test section shows a comparable behavior to that of the inlet flow velocity.

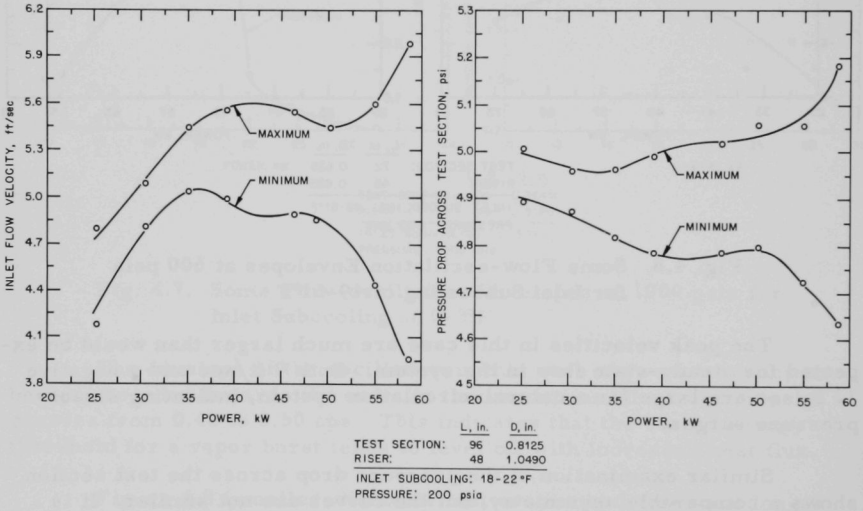

Fig. 4.9. Some Flow-oscillation Envelopes at 200 psia for Inlet Subcooling of 18-22°F

F. Effects of Various Parameters

Since the behavior of the oscillations was harmonic, the effort of obtaining the results in statistical terms (see Section IV-D) was eliminated, and peak-to-peak amplitudes were plotted. In the following discussion, the effects of various parameters of the system are analyzed. All the amplitudes are peak-to-peak values.

1. Inlet Subcooling

In each case, the effect on the amplitudes of four variables with respect to power is observed. These variables are the inlet flow velocity, wall temperature, pressure drop across the test section, and normalized pressure drop across the test section $[(\Delta P_{max} - \Delta P_{min})/\Delta P_{mean}]$.

Figure 4.10 provides the above-described set of plots at 1000 psia. The effect of subcooling is not significant up to about 28 kW, after which a sharp change leading to burnout takes place. Thus, from the wall-temperature point of view, this system can be safely operated up to about 28 kW if the effects of the oscillation of the other variables can be compensated or removed. The plots of inlet flow velocity and pressure drops already show fluctuations at less than 15 kW. The amplitude of inlet

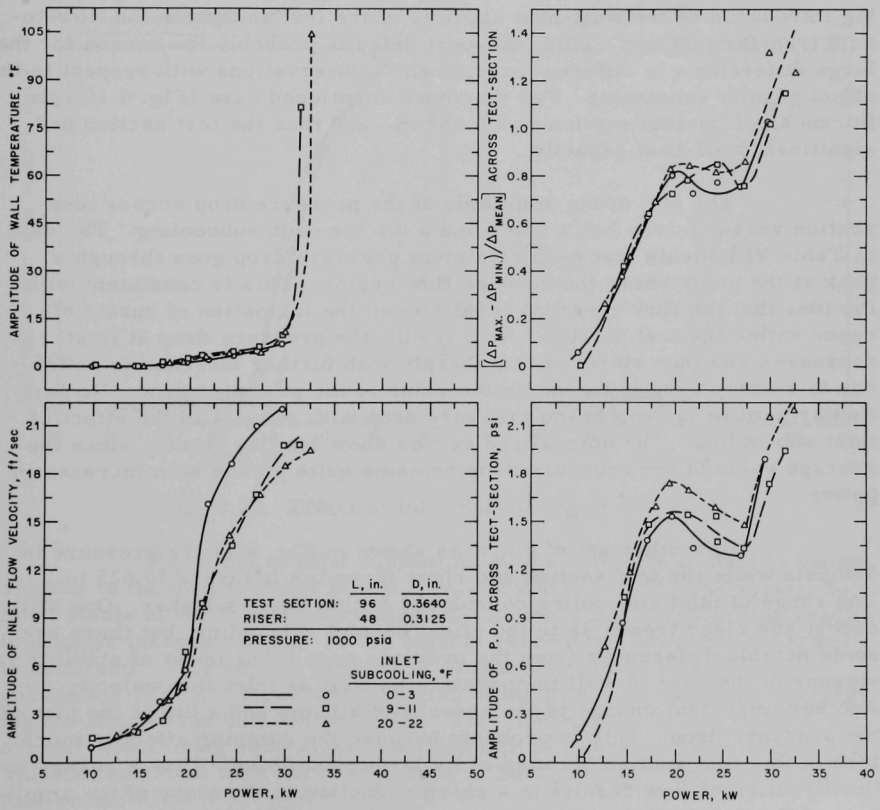

Fig. 4.10. Effect of Inlet Subcooling at 1000 psia

flow velocity is insensitive to the inlet subcooling up to about 20 kW, after which the amplitudes of the inlet flow velocities are larger, for small subcooling. Significantly, the inception point is not defined sharply.

The insensitivity to inlet subcooling, as compared to the results of Levy and Beckjord[8] and Becker et al.[15] at the same pressure (1000 psia), may be, in part, due to the smaller test section and riser flow area in the present work. In effect, this corresponds to a downstream constriction, which has been shown to have a destabilizing effect, and which may nearly obscure the effect of inlet subcooling. These investigations reported only the 10% inception point for oscillations, which could not be measured in the present geometry because of excessive heat losses at low powers.

Neal and Zivi[27] made an interesting point concerning the phase lag introduced by the wall-heat capacity of the test section in the flow-to-void transfer function. This transport delay is probably the reason for the large differences in different experimental observations with respect to the effect of inlet subcooling. For the above-mentioned case (Fig. 4.10), the thickness of the test section was 0.088 in., and thus the test section had significant wall-heat capacity.

The plot of the amplitude of the pressure drop across test section versus power has a hump and a dip for each subcooling. The data in Table VI indicate that each maximum pressure drop goes through a peak at the point where the reverse flow begins. This is consistent with the idea that the flow reversal results from the formation of bursts of vapor within the test section. As a result, the pressure drop at first decreases and then starts rising sharply with further increase in power due to a sharp drop in the minimum value of the pressure drop. No particular pattern is seen in the pressure drop with respect to the effect of inlet subcooling. The normalized curves show similar trends, since the average value of the pressure drop remains quite steady with increase in power.

In another set of plots, as shown in Fig. 4.11 the pressure is 600 psia while the test section and riser diameter is larger (0.625 in.). The range of inlet subcooling considered in this case is higher. One still cannot see clear trends as to the effect of inlet subcooling, but there are some notable differences from the previous case. The onset of stability is steeper in the case of wall temperature as well as inlet flow velocity. Another important change is the absence of a hump and a dip in the plot of the pressure drop. This is probably because the damping effect is much less in this test section because of its larger diameter. Thus a change in the direction of flow results in a sharp reduction in the slope of the amplitude of the pressure drop, but it does not change sign.

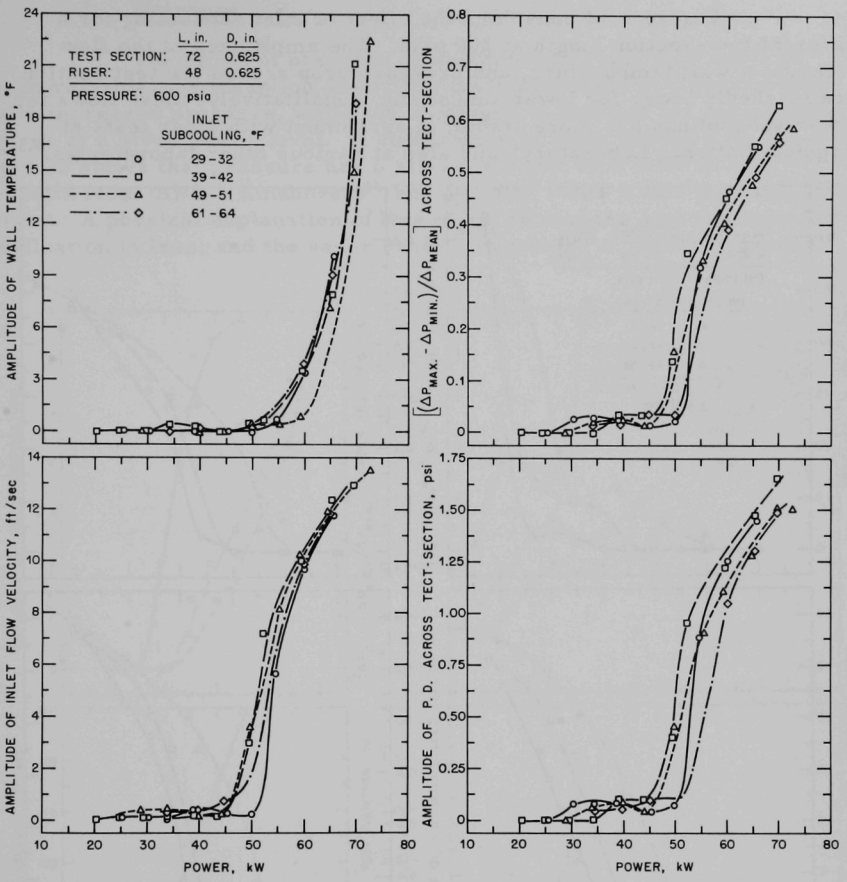

Fig. 4.11. Effect of Inlet Subcooling at 600 psia

The effect of inlet subcooling on the inception of oscillation is similar to the observations in other experiments.[8,11,15,17] The system is most stable at the lowest subcooling, and an increase in subcooling results in a lower inception point. At the highest subcooling, however, the trend is reversed. This change in trend is probably because, at such a high subcooling (60°F), a significant fraction of the power is absorbed in bringing the fluid to the bulk boiling point. This decreases the exit quality, the overall effect being equivalent to a reduction in power at lower subcooling. This is consistent with the observation of Becker et al.[15] and Gouse and Andrysiak.[49]

Figure 4.12 considers the effect of inlet subcooling for a different test-section length at 200 psia. The amplitudes of the flow velocities, wall temperature, and pressure drop across the test section are markedly lower for lower subcooling. Qualitatively, these flows for lower subcoolings are more stable, in agreement with other tests at Argonne National Laboratory[1] and also at various other laboratories.[8,11,15,17]

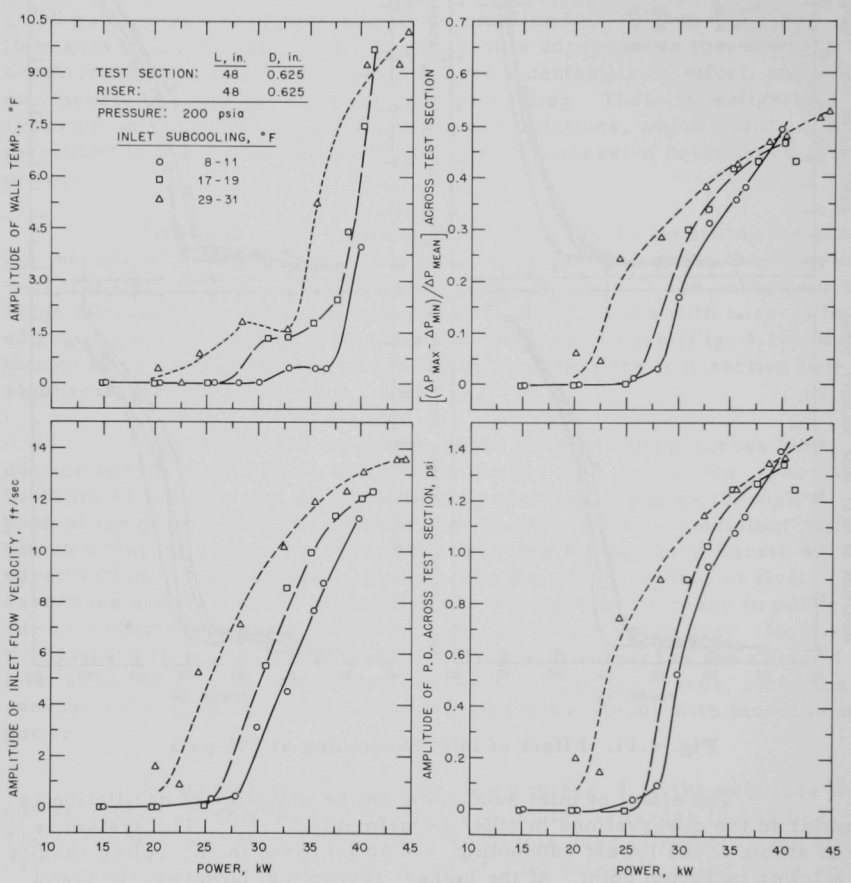

Fig. 4.12. Effect of Inlet Subcooling at 200 psia

This clear trend as to the effect of inlet subcooling at this pressure might be due to an increase in the nucleation effect at lower pressures. An increase in inlet subcooling lengthens the subcooled boiling region, and hence increases the volume of the vapor bursts. At higher pressures, the nucleation effects are much less marked.

2. Pressure

The effect of pressure is examined in Figs. 4.13 and 4.14. For each variable, the inception of oscillations takes place at higher powers with increased pressure, while the amplitude is smaller for higher pressures at a given power level. A comparison of these curves with Figs. 4.10 to 4.12 shows that pressure has a stronger effect than inlet subcooling. The results from ANL,[1] Eindhoven,[11] and Sweden[15] show a similar qualitative trend. A physical explanation of this might be that the superheat needed for nucleation is less, and the vapor density is greater at higher pressure.

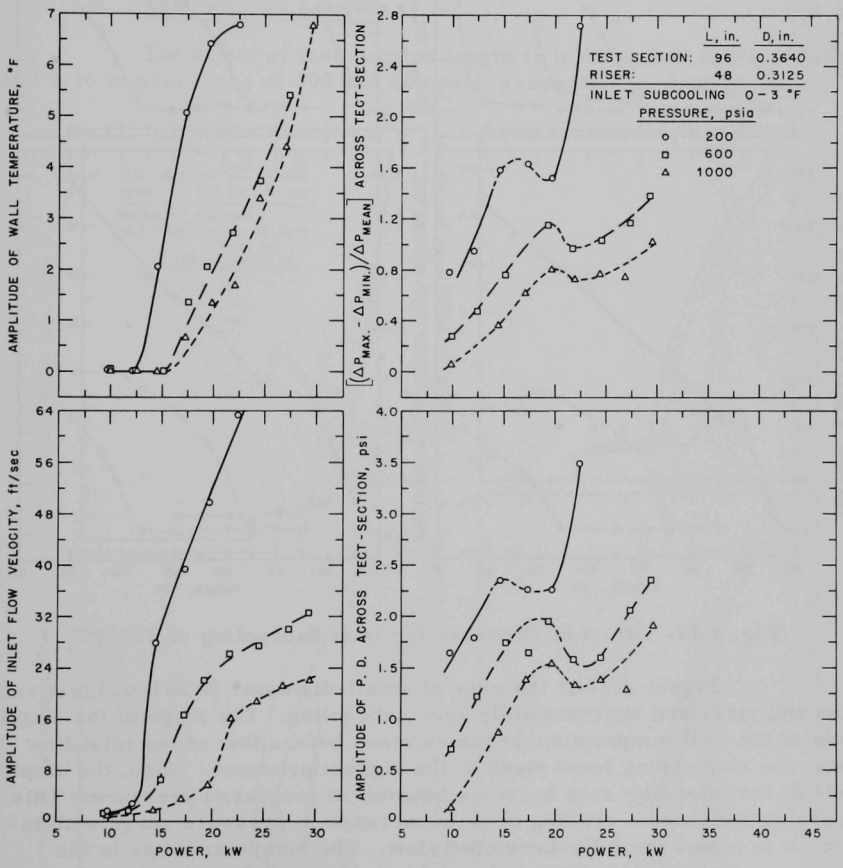

Fig. 4.13. Effect of Pressure for Inlet Subcooling of 0-3°F

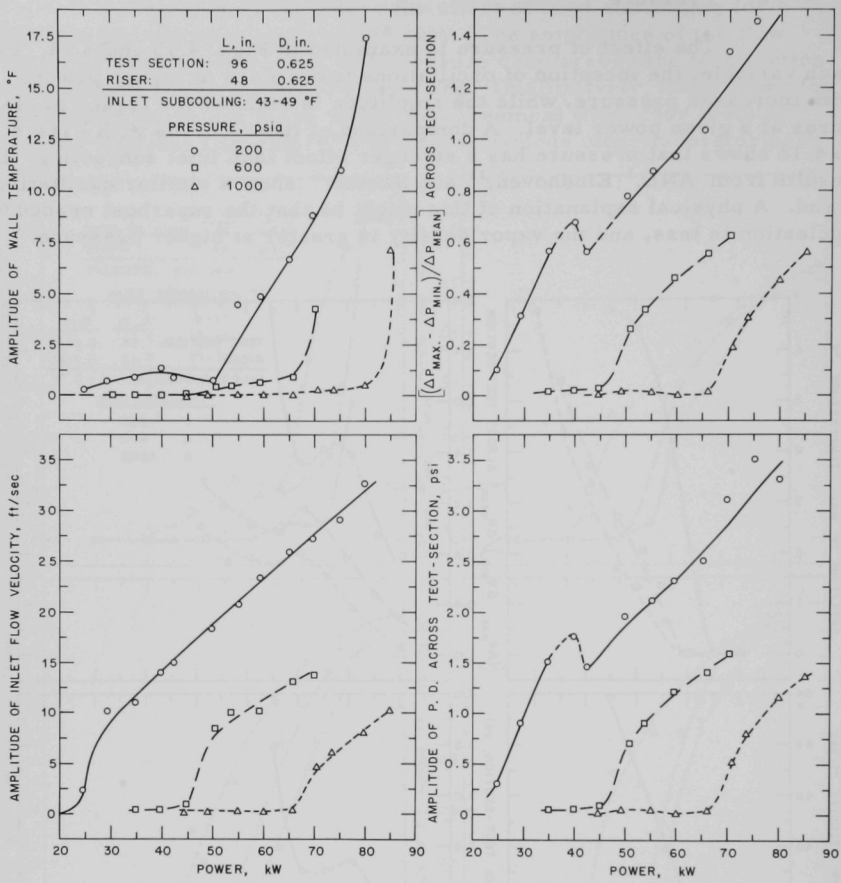

Fig. 4.14. Effect of Pressure for Inlet Subcooling of 43-49°F

Figure 4.13 is the case of small-diameter (0.364-in.) test section and riser and approximately zero subcooling. The slope of the amplitude of the wall temperature becomes steep before that of the inlet flow rate, the slope being least steep at the highest pressure. Also, the amplitude of the inlet flow rate becomes bounded at increased pressure. This probably indicates a slowing down in increase in pressure surge with increase in power for fully-developed flow. The humps and dips in the pressure-drop curves seem to be characteristic of the test section and riser geometry, as this trend is seen at all pressures. The temporary decrease in pressure drop is associated with the commencement of flow reversal. This is seen from the oscillation envelope plotted in Fig. 4.8.

Figure 4.14 shows the effect of pressure for a larger-diameter (0.625-in.) test section and large-inlet subcooling. The wall temperature is relatively stable as compared to the other two variables. The system shows a sharper inception of flow oscillation. The power at which this occurs is approximately three times as large at 1000 psia, and twice as large at 600 psia, than at 200 psia. In the previous case, this change was not as well-defined, nor was the contrast as well-marked. The difference in the two cases appears to be due to the smaller frictional pressure drop in the larger-diameter test section. A hump and a dip in the pressure-drop curve occur only at 200 psia in this case.

3. Test-section Length

The effect of test-section length is investigated in Figs. 4.15 and 4.16 at pressures of 600 and 200 psia, respectively. In both cases, the

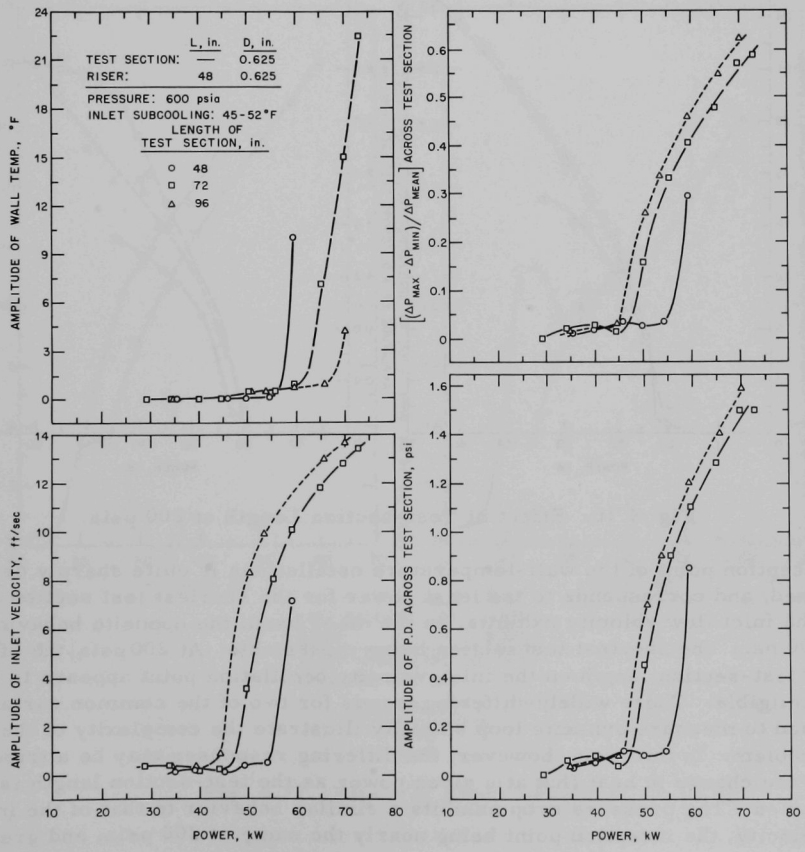

Fig. 4.15. Effect of Test-section Length at 600 psia

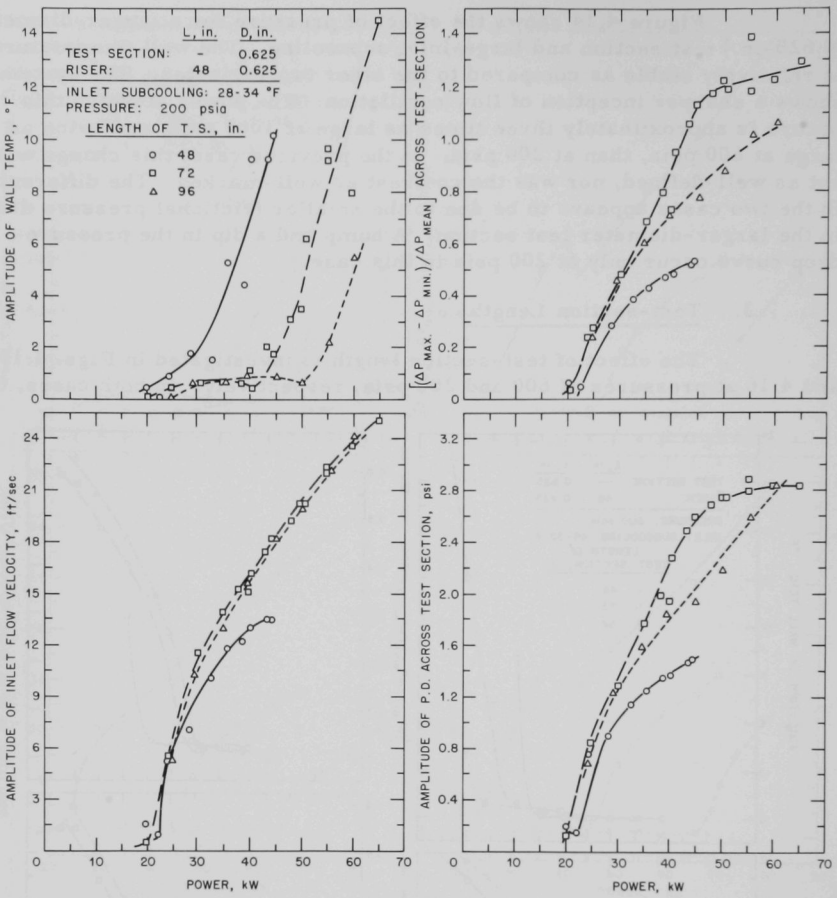

Fig. 4.16. Effect of Test-section Length at 200 psia

inception point of the wall-temperature oscillations is quite sharply defined, and corresponds to the least power for the shortest test section. The inlet flow velocity exhibits, on the other hand, the opposite behavior at 600 psia, the shortest test section being most stable. At 200 psia, the effect of test-section length on the inlet-velocity oscillation point appears to be negligible. These widely-differing trends for two of the common variables used to measure dynamic loop stability illustrate the complexity of the problem. In this case, however, the differing responses may be attributed to the change in heat flux at a given power as the test-section length is varied. The pressure drop exhibits a similar behavior to that of the inlet velocity, the inception point being nearly the same at 200 psia, and greatest

for the shortest test section at 600 psia. At both pressures, the longer test sections appear to be less stable, presumably because of the increased downstream frictional effect, which has a destabilizing influence. In addition, the longer two-phase region corresponds to a softer spring, and hence results in a greater amplitude in response to a given vapor burst.

4. Riser Length

The effect of riser length on flow characteristics of the loop is important since this determines the pumping effect of the density difference generated in the boiling process. This effect is examined in Fig. 4.17. Here, the pressure is maintained at 200 psia and the inlet subcooling at 24-29°F. The comparison is limited to riser lengths of 48 and 60 in.

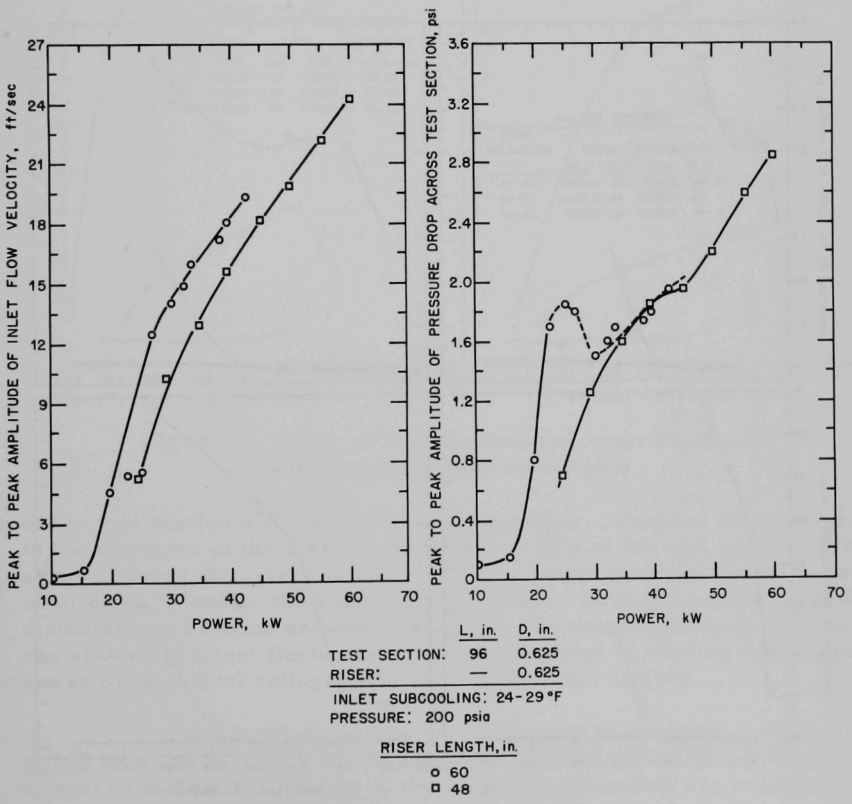

Fig. 4.17. Effect of Riser Length

The oscillations in the inlet flow velocities are larger for the longer riser. As explained earlier by an analogy to a spring, this effect is most likely due to additional compressible volume. The oscillations in the pressure drop across the test section are larger for the longer riser at lower power and show a pronounced hump. At higher powers, the two risers seem to show approximately the same pressure drops.

5. Test-section and Riser Diameters

Test-section and riser diameters appear to be the most significant variable. In Fig. 4.18 the pressure is held constant at 600 psia and the inlet subcooling approximately near 20°F. In Fig. 4.19, the pressure is maintained at 200 psia, inlet subcooling again being near 20°F. In both cases, the test-section and riser lengths are held constant, and the diameters

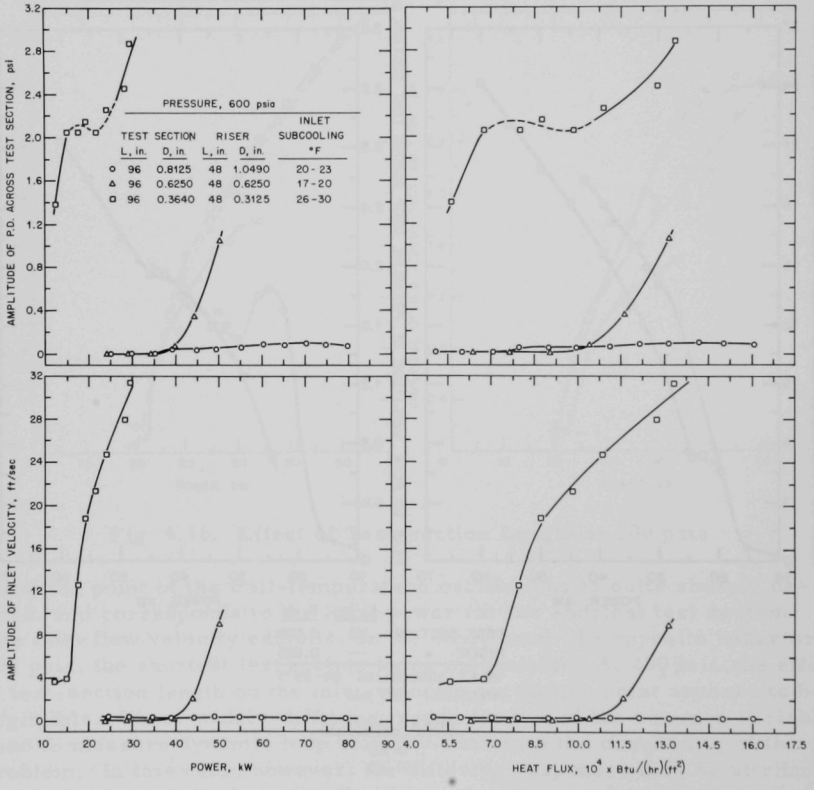

Fig. 4.18. Effect of Test-section and Riser Diameters with Pressure Held at 600 psia

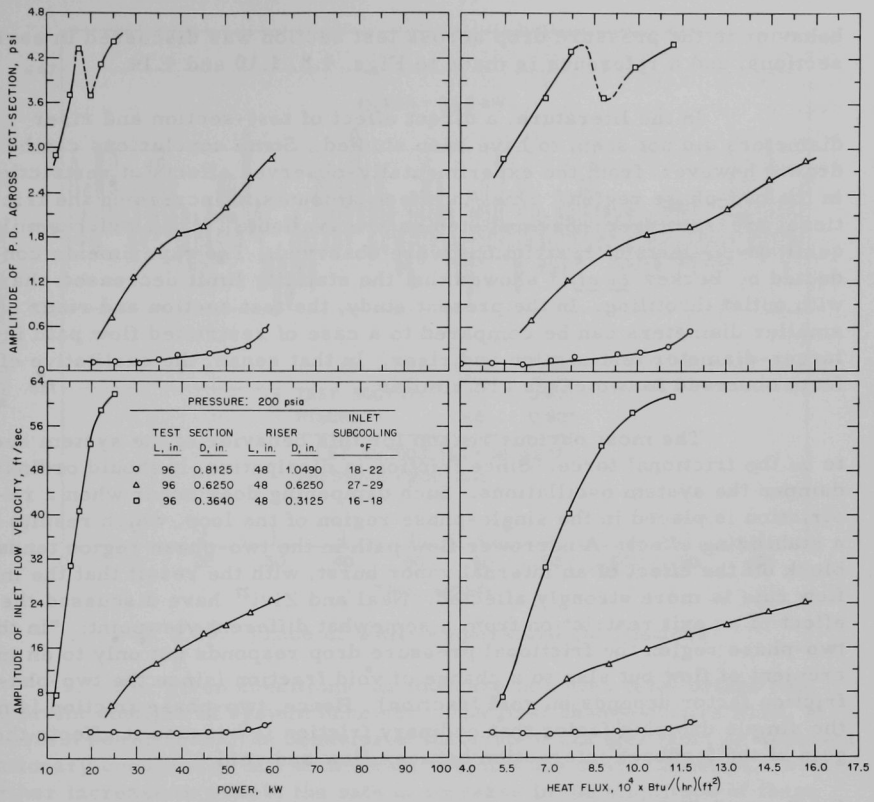

Fig. 4.19. Effect of Test-section and Riser Diameters with Pressure Held at 200 psia

of the test section and riser are varied together. There is no sharp change in the diameter of the riser as compared to that of the test section. The effect of these diameters is compared on a power and heat flux basis in an attempt to isolate the significant variables. In all cases, the largest-diameter combination showed a negligible fluctuation, whereas the smallest one showed greatest fluctuations. Neither method of plotting (i.e., against power or heat flux) collapsed the curves onto one another.

The amplitude of flow velocities can be as much as 30 ft/sec at 600 psia and 60 ft/sec at 200 psia for the smallest-diameter combination, whereas the flow oscillations in the largest combination are negligible. In both cases, a hump and a dip may be noted in the curves of the pressure-drop amplitudes for the smallest diameters, whereas in the in-between combination, a negligible effect is seen only at 200 psia. This type of

behavior in the pressure drop across test section was discussed in earlier sections, and a reference is made to Figs. 4.8, 4.10 and 4.14.

In the literature, a direct effect of test-section and riser diameters did not seem to have been studied. Some conclusions can be drawn, however, from the experimentally-observed effects of restrictions in the two-phase region. This, in effect, amounts to increasing the frictional pressure drop. Several studies are available[1,8,15] in which similar qualitative effects of restrictions were observed. The experiments conducted by Becker et al.[15] showed that the stability limit decreased sharply with outlet throttling. In the present study, the test section and riser of smaller diameters can be compared to a case of restricted flow path in a larger-diameter test section and riser. In that sense, the qualitative effects observed in two cases are similar.

The most obvious reason for this behavior of the system seems to be the frictional force. Since friction is dissipative, it should ordinarily dampen the system oscillations. Such dampening does occur when a restriction is placed in the single-phase region of the loop, which results in a stabilizing effect. A narrower flow path in the two-phase region tends to block off the effect of an internal vapor burst, with the result that the inlet flow rate is more strongly affected. Neal and Zivi[27] have discussed the effect of an exit restriction from a somewhat different viewpoint: "In the two-phase region the frictional pressure drop responds not only to an increment of flow but also to a change of void fraction (since the two-phase friction factor depends on void fraction). Hence, two-phase friction is not the simple damping factor that ordinary friction is because it affects the gain of the feedback interaction between flow and void."

G. General Observations

1. In the present study, the variables of the system showed self-sustained bounded oscillations in certain power ranges, depending on the operating conditions. It is belived that a complete mathematical formulation should not only predict the oscillation thresholds, but should also predict correctly the basic features of the data. With this point of view, the data presented in Appendix C provide adequate information as to the amplitude and frequency of the important variables such as inlet flow rates, pressure drops across the test section, and wall temperature for a wide range of parameters.

2. The fluctuations in wall temperature, as shown in Fig. 4.20 and by the data in Appendix C, indicate that a correct mathematical formulation should take wall-heat capacity into consideration. This seems to be an important factor in the behavior of the boiling systems, particularly under oscillatory conditions. For the case shown, the high-frequency peak-to-peak fluctuations in the wall temperature are roughly equivalent to a 4-kW change in the 55.2-kW steady power. This estimation is probably low, since the thermocouple was insulated from the outside wall by a thin mica sheet.

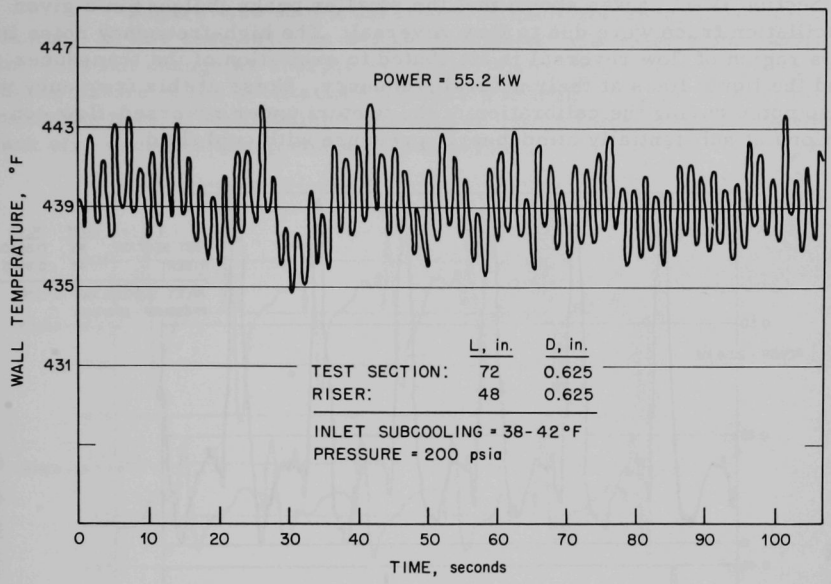

Fig. 4.20. Trace of Wall-temperature Oscillations

3. For given conditions, an increase in power level brings two important changes in system behavior. The first change occurs when, at a certain power level, the behavior of the system changes from an apparent stationary condition to one with clearly oscillatory characteristics. With further increase in power, the rate of increase in the amplitude of these oscillations is at first slow, and then is followed by a second change when the magnitude of these oscillations quite rapidly increases with increase in power. For engineering convenience, this point of sharp rise in amplitude can be taken as the threshold of instability. However, this is not an instability in the mathematical sense. It will be appropriate to indicate that, in spite of the oscillatory behavior, such conditions could permit a safe and useful operation of the equipment. A common example of the system in which fluctuations are very large compared to the mean value is that of fluid flow in a coffee percolator. This example should emphasize the fact that no arbitrary criterion of instability that will be suitable to all systems can be chosen.

4. Figure 4.21 shows some typical traces of the pressure drop across the venturi. With an increase in power, the amplitude of the oscillation of the venturi pressure drop, and hence the flow rate, increases sharply.

In Section IV-C, it was shown that the smaller peaks (bulges) in a given oscillation trace were due to flow reversal. The high-frequency noise in this region of flow reversal is attributed to excitation of the transducer and the liquid lines at their natural frequency. Noise at this frequency was also noted during the calibration of the venturi under reversed-flow conditions at substantially atmospheric pressure with cold fluid.

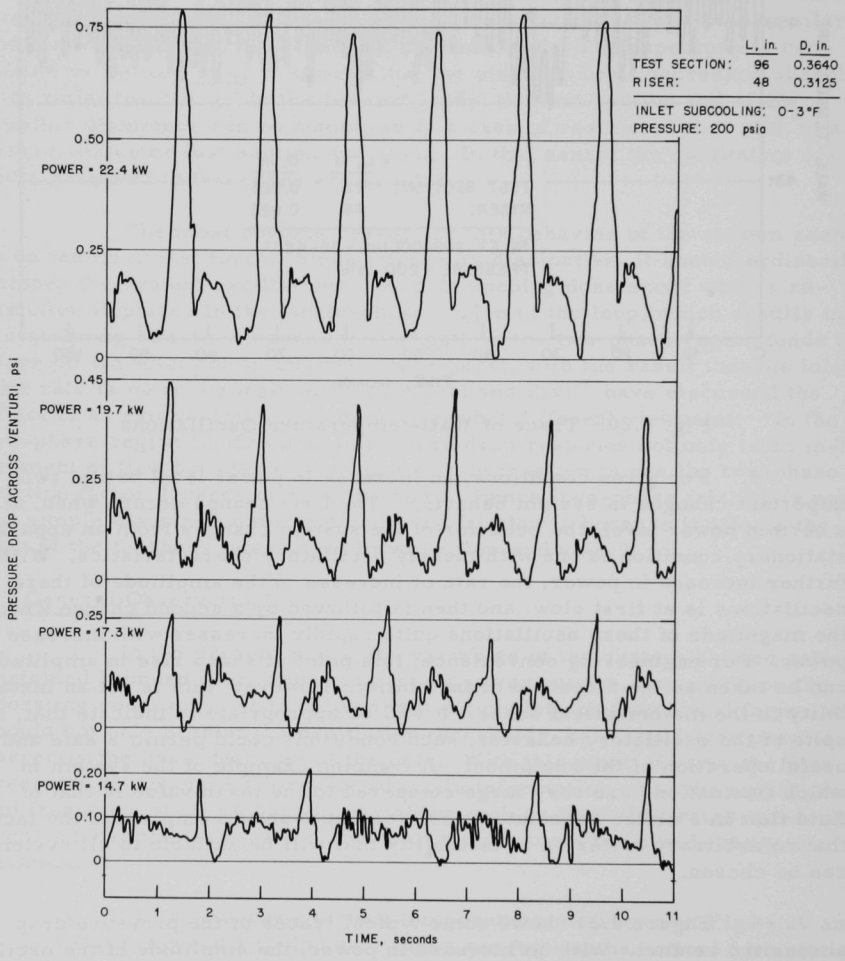

Fig. 4.21. Traces of Pressure Drop across Venturi

Figure 4.22 shows the traces of pressure drop across the test section. In this case, with an increase in power, the amplitude of oscillation does not change as sharply as in the case of the venturi pressure drop, but the nature of the oscillations changes markedly. At low power, the maximum peak is well-defined, but with increasing power, the minimum peak also becomes sharp and well-defined.

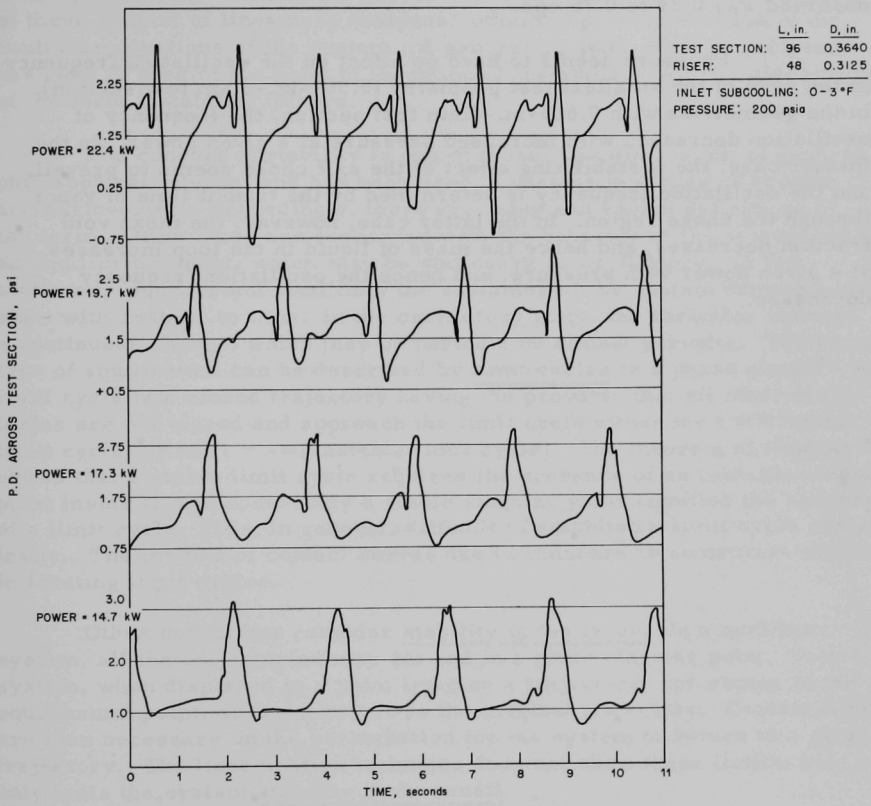

Fig. 4.22. Traces of Pressure Drop across Test Section

5. From the oscillations in the present experiment it is observed that these are "almost-periodic oscillations." (See Appendix D.) Such oscillations have been previously reported,[1,18] but the presence of almost-periodic characteristics with appreciable harmonics and subharmonics have never been stressed. It may be noted, however, from Figs. 4.20 and 4.21 that the amplitude of oscillations is continuously varying for each case and that it remains within certain bounds for a given case. The period is also varying but to a lesser extent. All of these point to an almost-periodic characteristic of the system oscillations.

6. The frequencies of oscillation in each case are presented in Tables VI to X. For the largest test geometry, this information is not presented because oscillations in the power range shown are not well-defined. For other geometries, the frequency of oscillation definitely appears to be a function of power, an increase in power, in general, resulting in an increase in oscillation frequency. The range of frequency observed was 0.24 to 0.76 cps.

Pressure seems to have no effect on the oscillation frequency in the case of the smallest test geometry (0.364-in.-diam test section). In the geometries with 0.625-in.-diam test section, the frequency of oscillation decreases with increased pressure at a given power. In the former case, the destabilizing effect of the exit choke seems to prevail, and the oscillation frequency is determined by the transit time of vapor through the choke region. In the latter case, however, the mean void fraction decreases, and hence the mass of liquid in the loop increases, at a given power with pressure, and hence the oscillation frequency decreases.

V. THEORETICAL CONSIDERATIONS

A. General

Studies of physical systems having oscillations and of the mathematical descriptions representing these systems have yielded analytical techniques for the study of the properties of the systems described. Many of these consist of linearized analyses; others represent solution of the nonlinear equations of the system. A general purpose of these analyses has been to predict the point of inception of instability. A brief discussion of the term instability follows.

The concept of stability is one of those, like dimension, of general philosophical interest and has been used in various branches of science and engineering. Accordingly, there are many and varied definitions of the term. Often these are concerned with the behavior of the system near an equilibrium point, which may be stationary or oscillatory. In the stationary-equilibrium condition, the variables of the system remain constant with respect to time; in the oscillatory state, the variables undergo a continuous change, which may be periodic or almost periodic. The latter type of equilibrium can be described by limit cycles in a phase plane.[39] A limit cycle is a closed trajectory having the property that all other trajectories are not closed and approach the limit cycle either for $t \to \infty$ (stable limit cycle) or for $t \to -\infty$ (unstable limit cycle). The theorem of Poincaré[37,38] shows that a stable limit cycle requires the presence of an unstable singular point inside it, and conversely a stable singular point signifies the absence of a limit cycle. It is, in general, difficult to establish a limit cycle analytically. The method of contact curves due to Poincaré is sometimes helpful in locating limit cycles.

Other definitions consider stability in the large. In a nonlinear system, all the trajectories may not end in a given singular point. Such a system, when displaced to a point lying on a trajectory not ending in the equilibrium point, does not return to the original trajectory. Certain limits are then necessary on the perturbation for the system to return to a given trajectory. The linearization technique does not show these limits, but only tests the system stability in the small.

In general, physical systems can be represented by means of a set of nonlinear partial differential equations and their boundary conditions. The technique of linearization is a convenient method for studying the effect of a small perturbation to such a system at equilibrium. For the analysis, the coefficients of the linearized differential equations are formed into a matrix. The eigenvectors of this matrix define the directions along which the trajectories may approach the singular point; the eigenvalues give information as to the stable or unstable behavior of the singular point. It is stable when the real parts of these eigenvalues are negative; a positive

real part in one of the eigenvalues means an unstable condition. The contribution of the higher-order terms in the system equations becomes important when the real part is zero. In such a case, the linearized technique becomes unsatisfactory.

Alternately, transfer-function analysis[45] may provide a satisfactory technique of predicting the stability in the small. An analysis based on this technique due to Jones[23] was used to make predictions of instability in this study. A detailed discussion is presented in the next chapter.

An important analytical contribution to the study of the stability of a singular point in the large is due to Liapounov, as stated in his second method.[39] The first method, applicable only to some analytical systems, consisted of finding explicit power-series solutions, convergent near the singular point, and deducing the stability in the small from the behavior of these series. In contrast to this, the second method requires no explicit solutions, and can be used to determine stability in the large. The method allows for functions with discontinuities, but it provides no information as to the actual behavior of the solutions. The great merit of Liapounov's work is to have given these precise definitions and then to have introduced certain functional properties guaranteeing stability, and whose behavior has now been proved to constitute necessary and sufficient conditions. The main difficulty in using this method lies in finding a suitable family of the Liapounov functions for the given system.

Logical extension of these concepts indicates that a linearized solution is satisfactory only before the inception of oscillations in the physical system. Beyond this point, linearized analysis should predict instability. To provide additional understanding, the nonlinear terms cannot be neglected, and the equations require consideration of stability in the large. As previously mentioned, the second method of Liapounov is theoretically satisfactory but construction of an appropriate Liapounov function for this system presents great difficulties. With high-speed digital computers, however, it is possible to solve the nonlinear equations numerically for extended values of time. If the system is correctly formulated mathematically, this analysis should lead to limit cycles for the reasons given in Chapter IV. An impulse can be then induced such that the resulting trajectory lies outside the limit cycle. If the trajectory then approaches the limit cycle with increase in time, the system is orbitally stable; that is, it follows the path of the limit cycle.

A solution[32] consisting of numerical integration of the nonlinear differential equations is provided in Chapter VII.

B. Mathematical Formulation

Two analyses, one linear and the other nonlinear, are given in the next two chapters. Some common features of the two analyses are described here.

1. Assumptions

a. One-dimensional spatial dependency of the variables is considered. It is assumed that the fluid over any cross section of the channel is homogeneous, though the liquid and vapor phases in the boiling region may be moving at different velocities.

b. The contribution of kinetic and potential energy terms is considered to be negligible as compared to the enthalpy terms.

c. The empirical correlations for two-phase slip ratio, as well as for two-phase frictional pressure gradient based on the experimental data, may be used in dynamic analyses.

d. The pressure drop along the test section is assumed to be small. Thus, variations in the physical properties of fluid (density, viscosity, specific heat) are considered to be negligible.

2. Conservation Equations

Consider a fixed control volume of differential length, dz. The laws of conservation of mass, momentum, and energy may then be expressed for a vertical test section as follows (all terms are defined in the Nomenclature, and the bar denotes averaged properties with respect to the cross-sectional area at a given axial position):

Mass

$$\frac{\partial \bar{\rho}}{\partial t} + \frac{\partial \overline{\rho u}}{\partial z} = 0. \tag{5.1}$$

Momentum

$$\frac{\partial \overline{\rho u}}{\partial t} + \frac{\partial \overline{\rho u^2}}{\partial z} = -\frac{\partial P}{\partial z} - \bar{\rho} g - \frac{\partial P_f}{\partial z}. \tag{5.2}$$

Energy

$$\frac{\partial \overline{\rho E}}{\partial t} + \frac{\partial \overline{\rho u H}}{\partial z} = \frac{Q'}{A_c}. \tag{5.3}$$

Equation (5.1) signifies that the rate of change of mass is equal to net change in mass of the volume element $A_c dz$, where A_c is the cross-sectional area of the channel. The next equation implies that the sum of the rate of change of momentum and the net change in the momentum of the control volume is equal to the sum of the forces working on it. The terms to the right are the contributions due to pressure, gravitational, and frictional forces, respectively. Similarly, the law of conservation of energy, as represented by Eq. (5.3), states that the sum of the rate of change of energy of the fluid in the control volume and the net change in its energy is equal to the heat added to it. In a two-phase flow region, the averaged quantities are defined as

$$\overline{\rho} = \rho_\ell(1 - \alpha) + \rho_g\alpha, \tag{5.4}$$

$$\overline{\rho u} = \rho_\ell u_\ell(1 - \alpha) + \rho_g u_g\alpha, \tag{5.5}$$

$$\overline{\rho u^2} = \rho_\ell u_\ell^2(1 - \alpha) + \rho_g u_g^2\alpha, \tag{5.6}$$

$$\overline{\rho E} = \rho_\ell E_\ell(1 - \alpha) + \rho_g E_g\alpha, \tag{5.7}$$

and

$$\overline{\rho uH} = \rho_\ell u_\ell H_\ell(1 - \alpha) + \rho_g u_g H_g\alpha. \tag{5.8}$$

3. Empirical Correlations

In the two-phase flow region, there are five unknowns represented by the above three equations of conservation. These are the gas and liquid velocities, void fraction, pressure, and the frictional force. Thus, two more equations are necessary for a mathematical solution.

The analyses considered in this study use empirical or semi-empirical correlations for the two-phase friction term and for the slip ratio between the gas and liquid velocities (u_g/u_ℓ). These, being different in the two cases, are given with the descriptions of the analyses.

VI. LINEAR ANALYSIS

As discussed in the previous chapter, there may be several viewpoints in the dynamic analysis of a system and thereby in the prediction of the system stability. Design of some boiling systems requires that flow oscillations of negligible magnitude be present at the maximum heat input. An example of such a system is the boiling-water (nuclear) reactor. If a linear analysis can predict the oscillation thresholds of such systems, the design purpose is served and the more elaborate, nonlinear model becomes unnecessary. Jones[23] made a linear analysis in the frequency domain, the predictions from which checked quite well with other experimental data.[26,27] The important steps in the derivation of this model are briefly presented here for completeness.

The basic approach to the problem is to obtain a set of linearized differential equations from which an open-loop system-transfer function is derived. System stability is then examined by means of the Nyquist criterion.[45] The basic equations are those of conservation of mass, momentum, and energy in the bulk-boiling and subcooled regions of the test section. Boundary conditions are stated at the interface between the two regions, and at the test-section inlet and exit.

A. Bulk-boiling Region

The variables in the conservation equations for mass, momentum, and energy shown in Eqs. (5.1) to (5.3) are written in dimensionless form. The equations are then linearized, and the Laplace transform is taken.

1. Conservation of Mass

In the bulk-boiling region, Eq. (5.1) may be expressed as

$$\frac{\partial}{\partial t}\left[\rho_\ell(1-\alpha)+\rho_g\alpha\right]+\frac{1}{A_c}\frac{\partial W}{\partial z}=0, \tag{6.1}$$

or

$$\left(1-\frac{\rho_g}{\rho_\ell}\right)\frac{\partial \alpha}{\partial t}=u_{in}\frac{\partial W^*}{\partial z}, \tag{6.2}$$

or

$$\frac{\partial \alpha}{\partial t}=\frac{u_{in}}{\eta}\frac{\partial W^*}{\partial z}, \tag{6.3}$$

where

$$\eta = (1 - \rho_g/\rho_\ell),$$

$$W^* = \frac{W}{W_{in}} = u^* \left[1 - \alpha \left(1 - \frac{\rho_g}{\rho_\ell} S \right) \right], \tag{6.4}$$

and

$$S = \frac{u_g}{u_\ell},$$

which is the slip ratio between the gas and liquid velocities.

The variable-density single-fluid model derived by Bankoff[24] was used for the slip ratio in this analysis with some modifications, as shown below. Bankoff assumed that the gas and liquid have the same velocity at any radial position, and that the average velocity of the gaseous phase is greater than that of the liquid phase, only because the gas is concentrated in the regions of higher velocity. He then assumed a power-law distribution for both the velocity and the void fraction and obtained a mathematical expression by integrating over the tube cross section. Thus, his original equation for the slip ratio can be written as

$$S = \frac{1 - \alpha}{K - \alpha}, \tag{6.5}$$

where K is the flow parameter dependent upon the constants of the power-law-profile relations. The following empirical relation for K as a function of pressure was recommended by Bankoff:

$$K = 0.71 + 0.0001P,$$

where P is the pressure, in psia. Jones modified this correlation to

$$K = 0.71 + \left(\frac{0.29}{0.32062} \right) 0.0001P, \tag{6.6}$$

so that K = 1 at the critical pressure of steam-water. Furthermore, the singularity in Eq. (6.5) at α = K was eliminated by adding a term to the denominator:

$$S = \frac{1 - \alpha}{K - \alpha + (1 - K)\alpha^r}, \tag{6.7}$$

where values of r were determined by Jones and Dight[40] by using Eq. (6.7) to satisfy the boundary conditions: x = 0 at α = 0, and x = 1 at α = 1. The following polynomial in pressure was found to be satisfactory:

$$r = 3.33 + 0.18\left(\frac{P}{1000}\right) + 0.46\left(\frac{P}{1000}\right)^2. \tag{6.8}$$

2. Conservation of Momentum

Equation (5.2) may be rewritten as

$$-\frac{\partial P}{\partial z} = \frac{1}{gA_c}\frac{\partial W}{\partial t} + \frac{1}{gA_c}\frac{\partial (Wu)}{\partial z} + [\rho_\ell (1-\alpha) + \rho_g \alpha] + \frac{\partial P_f}{\partial z}, \tag{6.9}$$

or

$$-\frac{1}{\rho_\ell}\frac{\partial P}{\partial z} = \frac{u_{in}}{g}\frac{\partial W^*}{\partial t} + \frac{u_{in}^2}{g}\frac{\partial (BW^{*2})}{\partial z} + (1-\eta\alpha) + \frac{1}{\rho_\ell}\frac{\partial P_f}{\partial z}, \tag{6.10}$$

where

$$B = \frac{1 - \alpha(1 - \rho_g/\rho_\ell S^2)}{[1 - \alpha(1 - \rho_g/\rho_\ell S)]^2}; \tag{6.11}$$

$\partial P_f/\partial z$, the frictional pressure gradient for single-phase turbulent flow, may be given by

$$\left.\frac{\partial P_f}{\partial z}\right|_{\text{single-phase}} = \frac{f\rho_\ell u^2}{2gd_c} = \frac{fW^2}{2g\rho_\ell d_c A_c^2}. \tag{6.12}$$

A corresponding term for two-phase flow is obtained by using a modification of the Martinelli-Nelson correlation,[25] yielding

$$\left.\frac{\partial f}{\partial z}\right|_{\text{two-phase}} = \frac{fW^2}{2g\rho_\ell d_c A_c^2}\phi^2\Omega. \tag{6.13}$$

The parameters ϕ^2 and Ω are correction factors to the single-phase relationship. The parameter ϕ^2 is a function of the steam quality and static pressure and is expressed in a polynomial form as follows:

$$\ln \phi^2 = \sum_{k=1}^{4} a'_k [\ln(100X+1)], \tag{6.14}$$

where

$$a'_k = \sum_{j=0}^{7} C_{kj} \left(\frac{P}{1000}\right)^j, \tag{6.15}$$

P is static pressure in psia, and X is the steam quality. The coefficients C_{kj} are given in Reference 40.

In the dimensionless form, Eq. (6.13) may be expressed as

$$\left.\frac{\partial P_f}{\partial z}\right|_{\text{two-phase}} = \frac{f_0 u_{in}^2 \rho_\ell}{2gd_c} W^{*(2-a_2)} \phi^2 \Omega, \tag{6.16}$$

where the friction factor, f, may be analytically expressed by a function of the form

$$f = a_1 \left(\frac{W d_c}{\mu_\ell A_c}\right)^{-a_2}, \tag{6.17}$$

and f_0 is the friction factor associated with the steady-state mass flow rate of the subcooled liquid.

Inserting Eq. (6.16) into Eq. (6.12) gives

$$-\frac{1}{\rho_\ell}\frac{\partial P}{\partial z} = \frac{u_{in}}{g}\frac{\partial W^*}{\partial t} + \frac{u_{in}^2}{g}\frac{\partial (BW^{*2})}{\partial z} + (1-\eta\alpha) + \frac{f_0 u_{in}^2}{2gd_c} W^{*(2-a_2)} \phi^2 \Omega. \tag{6.18a}$$

Substituting

$$P^* = \frac{P}{\rho_\ell L_c},$$

$$\tau_1 = \frac{u_{in}}{g},$$

and

$$F = \frac{f_0 u_{in}^2}{2gd_c}, \tag{6.18b}$$

into Eq. (6.18a) yields

$$-L_c \frac{\partial P^*}{\partial z} = \tau_1 \frac{\partial W^*}{\partial t} + u_{in}\tau_1 \frac{\partial (BW^{*2})}{\partial z} + (1 - \eta\alpha) + FW^{*(2-a_2)} \phi^2 \Omega. \tag{6.19}$$

3. Conservation of Energy

Equation (5.3) for the bulk-boiling region may be stated as

$$\frac{\partial}{\partial t}[\rho_\ell E_\ell (1 - \alpha) + \rho_g E_g \alpha] + \frac{\partial}{\partial z}[\rho_\ell u_\ell H_\ell (1 - \alpha) + \rho_g u_g H_g \alpha] = \frac{Q'}{A_c}. \tag{6.20}$$

Now

$$E_\ell = H_\ell - \frac{Pv_\ell}{J}, \tag{6.21}$$

and

$$E_g = H_g - \frac{Pv_g}{J}. \tag{6.22}$$

The term Pv_ℓ/J is negligible in comparison with H_ℓ; however, the term Pv_g/J is not negligible. Further,

$$H_g = H_\ell + H_{fg}. \tag{6.23}$$

Thus, Eq. (6.20) becomes

$$H_\ell \left\{\frac{\partial}{\partial t}\left[\rho_\ell (1 - \alpha) + \rho_g \alpha\right]\right\} + \frac{\partial}{\partial t}\left[\rho_g \alpha \left(H_{fg} - \frac{Pv_g}{J}\right)\right]$$

$$+ H_\ell \left\{\frac{\partial}{\partial z}\left[\rho_\ell u_\ell (1 - \alpha) + \rho_g u_g \alpha\right]\right\} + \frac{\partial}{\partial z}\left[\rho_g u_g H_{fg} \alpha\right] = \frac{Q'}{A_c}. \tag{6.24}$$

The law of conservation of mass simplifies the above equation to give

$$\rho_g H_{fg}(1 - \xi) \frac{\partial \alpha}{\partial t} + \rho_g H_{fg} \frac{\partial(\alpha u_g)}{\partial z} = \frac{Q'}{A_c}, \tag{6.25}$$

where

$$\xi = \frac{P v_g}{J H_{fg}}. \tag{6.26}$$

Substitution of Eq. (6.3) into Eq. (6.25) yields

$$\frac{(1 - \xi)\, u_{in}}{\eta} \frac{\partial W^*}{\partial z} + u_{in} \frac{\partial(\alpha S u^*)}{\partial z} = \frac{Q_0 Q^{*\prime}}{A_c \rho_g H_{fg}}. \tag{6.27}$$

Equation (6.4) gives

$$u^* = \frac{W^*}{1 - \alpha(1 - S\rho_g/\rho_\ell)}.$$

Thus, Eq. (6.27) becomes

$$\frac{\partial}{\partial z}\left[\left(1 - \xi + \frac{\eta \alpha S}{1 - \alpha(1 - S\rho_g/\rho_\ell)}\right) W^*\right] = \frac{\rho_\ell \eta Q_0}{W_{in} H_{fg} \rho_g} Q^{*\prime},$$

or

$$\frac{\partial}{\partial z}(\nu W^*) = \frac{\eta Q_0}{(1 - \eta)\, W_{in} H_{fg}} Q^{*\prime}, \tag{6.28}$$

where

$$\nu = 1 - \xi + \frac{\eta \alpha S}{1 - \alpha(1 - S\rho_g/\rho_\ell)}. \tag{6.29}$$

4. Energy Balance on the Wall

The energy balance on a differential length of the wall may be written as

$$Q = Q' + (\rho_w A_w C_w) \frac{\partial T_w}{\partial t}. \tag{6.30}$$

Equation (6.30) states that the heat input is equal to the sum of the heat transferred to the fluid and the heat stored in the test section wall. Thus,

$$Q' = h_b P_c (T_w - T_{sat}). \tag{6.31}$$

The Jens-Lottes correlation[46] was used to obtain the temperature difference:

$$T_w - T_{sat} = 60(q/10^6)^{1/4} e^{-P/900}. \tag{6.32}$$

In the above equation, q is the heat flux in Btu/hr-ft^2, P is the pressure in psia, and the temperatures are in degrees Fahrenheit. It is assumed that at a given axial position the wall temperature is uniform over the cross section.

5. Linearization and Laplace Transform

The final equations of continuity, momentum, and energy were obtained by linearization and the Laplace transformation of Eqs. (6.3), (6.19), (6.28), and (6.30). In these equations, the notations represent the following:

δ represents the first-order perturbation in the variable;

a bar represents the Laplace transform of the variable;

subscript 1 denotes a variable in the inlet end of a node;

subscript 2 denotes a variable at the outlet end of a node;

subscript a denotes the average value of a perturbed variable within a node. Thus, Eq. (6.3) yields

$$s\tau_a \delta\bar{\alpha}\Big|_a = \delta\overline{W^*}\Big|_a - \delta\overline{W^*}\Big|_1. \tag{6.33}$$

Equation (6.19) becomes

$$\delta\overline{P^*}\Big|_1 - \delta\overline{P^*}\Big|_2 = (s\tau_1' + C_{13})\,\delta\overline{W^*}\Big|_a - C_{15}\,\delta\overline{W^*}\Big|_1 + C_{14}\delta\bar{\alpha}\Big|_a - C_{16}\delta\bar{\alpha}\Big|_1, \tag{6.34}$$

and Eq. (6.28), along with Eqs. (6.30) to (6.32), gives

$$\delta\overline{W^*}\Big|_a = C_1\delta\overline{W^*}\Big|_1 + C_2\delta\bar{\alpha}\Big|_1 - C_3\delta\bar{\alpha}\Big|_a + \frac{C_0}{1 + s\tau_{fb}}\,\delta\overline{Q^*}, \tag{6.35}$$

where

$$\tau_{fb} = \frac{\rho_w A_w C_w}{h_{b0} P_c} . \tag{6.36}$$

The coefficients in Eqs. (6.33) to (6.35) are defined as

$$\tau_1' = \frac{\tau_1 \Delta z}{L_c} = \frac{u_{in} \Delta z}{g L_c} ,$$

$$C_0 = \frac{\eta \Delta z Q_0}{2\nu_{02}(1-\eta) H_{fg} W_{in}} = \frac{\nu_{02} - \nu_{01}}{2\nu_{02}} ,$$

$$C_1 = \frac{\nu_{0a}}{\nu_{02}} ,$$

$$C_2 = \frac{1}{\nu_{02}} \left.\frac{\partial \nu}{\partial \alpha}\right|_{0a} ,$$

$$C_3 = \frac{1}{\nu_{02}} \left.\frac{\partial \nu}{\partial \alpha}\right|_{02} ,$$

$$C_4 = \frac{\eta \Delta z}{L_c} ,$$

$$C_5 = \frac{4 u_{in} \tau_1 B_{02}}{L_c} ,$$

$$C_6 = \frac{4 u_{in} \tau_1 B_{0a}}{L_c} ,$$

$$C_7 = \frac{2 u_{in} \tau_1}{L_c} \left.\frac{\partial B}{\partial \alpha}\right|_{02} ,$$

$$C_8 = \frac{2 u_{in} \tau_1}{L_c} \left.\frac{\partial B}{\partial \alpha}\right|_{0a} ,$$

$$C_9 = \frac{F \Delta z}{3 L_c} (\phi_{01}^2 + 2\phi_{02}^2) \left[(2 - a_2) \Omega_0 + \left.\frac{\partial \Omega}{\partial W^*}\right|_0 \right] K_{fba} ,$$

$$C_{10} = \frac{F\Delta z}{6L_c}(\phi_{02}^2 - \phi_{01}^2)\left[(2 - a_2)\,\Omega_0 + \left.\frac{d\Omega}{dW^*}\right|_0\right] K_{fba},$$

$$C_{11} = \frac{F\Delta z\,\Omega_0}{L_c}\left[\frac{1}{3}\left.\frac{\partial\phi^2}{\partial\alpha}\right|_{01} + \frac{2}{3}\left.\frac{\partial\phi^2}{\partial\alpha}\right|_{02} - \frac{1}{6}\left(\sqrt{\left.\frac{\partial\phi^2}{\partial\alpha}\right|_{02}} - \sqrt{\left.\frac{\partial\phi^2}{\partial\alpha}\right|_{01}}\right)^2\right] K_{fba},$$

$$C_{12} = \frac{F\Delta z\,\Omega_0}{6L_c}\left[\left.\frac{\partial\phi^2}{\partial\alpha}\right|_{02} - \left.\frac{\partial\phi^2}{\partial\alpha}\right|_{01}\right] K_{fba},$$

$$C_{13} = C_5 + C_9,$$

$$C_{14} = -C_4 + C_7 + C_{11},$$

$$C_{15} = C_6 + C_{10},$$

and

$$C_{16} = C_8 + C_{12}.$$

B. Boiling Boundary

The temperature of the subcooled fluid is assumed to be uniform over any channel cross section. An energy balance is written on the fluid at the boiling-boundary position z_1, if it is assumed that water (either superheated or subcooled) approaches it, and a saturated water-steam mixture leaves it:

$$H_{z_1} = X_{z_1}H_g + (1 - X_{z_1})\,H_\ell = X_{z_1}H_{fg} + H_\ell.$$

Therefore,

$$X_{z_1} = \frac{H_{z_1} - H_\ell}{H_{fg}}, \tag{6.37}$$

and

$$\delta X_{z_1} = \frac{1}{H_{fg}}\,\delta H_{z_1}$$

$$= \frac{1}{H_{fg}}\,C_p\Delta T_{in}\frac{\delta T_{z_1}}{T_{in}}. \tag{6.38}$$

The perturbation in the steam-quality may be expanded as follows:

$$\delta X_{z1} = \frac{\delta W_g\Big|_{z1}}{W_{sc}} = \frac{\delta(\rho_g \alpha S u_\ell)\Big|_{z1}}{\rho_\ell u_{sc}}$$

$$= \frac{\rho_g}{\rho_\ell}\left[\alpha_{z1}\Big|_0 \frac{\delta(Su_\ell)\Big|_{z1}}{u_{sc}} + \frac{(Su_\ell)_{z1}\Big|_0}{u_{sc}}\ \delta\alpha_{z1}\right]. \qquad (6.39)$$

But

$$\alpha_{z1}\Big|_0 = 0,$$

and

$$(u_\ell)_{z1}\Big|_0 = u_{sc}.$$

Therefore, Eq. (6.39) becomes

$$\delta X_{z1} = (1 - \eta)\, S_{z1}\Big|_0\ \delta\alpha_{z1}. \qquad (6.40)$$

Eliminating δX_{z1} between Eqs. (6.38) and (6.40) gives

$$\delta\overline{\alpha}_{z1} = C_{17}\frac{\delta\overline{T_{z1}}}{\Delta T_{in}}, \qquad (6.41)$$

where

$$C_{17} = \frac{C_p \Delta T_{in}}{H_{fg}(1 - \eta)\, S_{z1}\Big|_0}.$$

Continuity at the boiling boundary requires that

$$\overline{\delta W^*_{sc}} = \overline{\delta W_{z1}}. \qquad (6.42)$$

Equations (6.41) and (6.42) are the required coupling equations between the subcooled and boiling regions of the test section. The temperature

perturbation δT_{z_1} and mass-flow-rate perturbation $\delta W^*_{z_1}$ are obtained by examination of the subcooled region.

C. Subcooled Region

1. Conservation of Momentum

Equation (5.2) may be rewritten as

$$- \frac{\partial P_{sc}}{\partial z} = \frac{1}{gA_c} \frac{\partial W_{sc}}{\partial t} + \frac{1}{gA_c} \frac{\partial (W u_\ell)}{\partial z}\bigg|_{sc} + \rho_{sc} + \frac{\partial P_f}{\partial z}\bigg|_{sc}$$

$$= \frac{1}{gA_c}\left[\frac{\partial W_{sc}}{\partial t} + \frac{W_{sc}^2}{A_c} \frac{\partial}{\partial z}\left(\frac{1}{\rho_{sc}}\right)\right] + \rho_{sc} + \frac{\partial P_f}{\partial z}\bigg|_{sc} \tag{6.43}$$

similar to Eq. (6.16),

$$\frac{\partial P_f}{\partial z}\bigg|_{sc} = \frac{f_0 u_{in}^2 \rho_\ell^2}{2gd_c \rho_{sc}} (W^*_{sc})^{2-a_2}. \tag{6.44}$$

Thus, Eq. (6.43) becomes

$$- \frac{\partial P_{sc}}{\partial z} = \frac{\rho_\ell u_{in}}{g} \frac{\partial W^*_{sc}}{\partial t} + \frac{\rho_\ell^2 u_{in}^2}{g} (W^*_{sc})^2 \frac{\partial}{\partial z}\left(\frac{1}{\rho_{sc}}\right) + \rho_{sc}$$

$$+ F \frac{\rho_\ell^2}{\rho_{sc}} (W^*_{sc})^{2-a_2}, \tag{6.45}$$

or

$$- \frac{\partial P^*_{sc}}{\partial z} = \frac{u_{in}}{gL} \frac{\partial W^*_{sc}}{\partial t} + \frac{u_{in}^2}{gL} (W^*_{sc})^2 \frac{\partial}{\partial z}\left(\frac{\rho_\ell}{\rho_{sc}}\right) + \frac{\rho_{sc}}{\rho_\ell L_c}$$

$$+ \frac{F\rho_\ell}{L_c \rho_{sc}} (W^*_{sc})^{2-a_2}. \tag{6.46}$$

Integrating over the subcooled region from the inlet to the boiling boundary yields

$$P^*_{in} - P^*_{z1} = \frac{u_{in} z_1}{g L_c} \frac{\partial W^*_{sc}}{\partial t} + \frac{u^2_{in}}{g L_c} (W^*_{sc})^2 \left(1 - \frac{\rho_\ell}{\rho_{in}}\right)$$

$$+ \left[\frac{1}{L_c} + \frac{F}{L_c} (W^*_{sc})^{2-a_2}\right] \int_0^{z_1} \left(\frac{\rho_\ell}{\rho_{sc}}\right) dz. \qquad (6.47)$$

In the above equation, subscripts "in" and "z_1" denote the values at the test-section inlet and at the boiling boundary, respectively. If it is assumed that ρ_{sc} is only space-dependent, Eq. (6.47), after Laplace transformation, becomes

$$\overline{\delta P^*_{in}} - \overline{\delta P^*_{z1}} = \frac{u_{in} z_1}{g L_c} s \overline{\delta W^*_{sc}}$$

$$+ \left[\frac{2u^2_{in}}{g L_c} \left(1 - \frac{\rho_\ell}{\rho_{in}}\right) + \frac{K_p F (2 - a_2) z_1}{L_c}\right] \overline{\delta W^*_{sc}} \qquad (6.48)$$

where

$$K_\rho = \frac{1}{z_1} \int_0^{z_1} \left(\frac{\rho_\ell}{\rho_{sc}}\right) dz,$$

or, assuming a linear variation,

$$K_\rho \simeq \frac{1 + \rho_\ell / \rho_{in}}{2}. \qquad (6.49)$$

Thus, if

$$C_{18} = \frac{1}{\frac{2u^2_{in}}{g L_c} \left(1 - \frac{\rho_\ell}{\rho_{in}}\right) + \frac{K_\rho F (2 - a_2) z_1}{L_c}},$$

and

$$\tau_L = C_{18} \frac{u_{in} z_1}{g L_c},$$

then Eq. (6.48) may be rewritten as

$$\overline{\delta W^*_{sc}} = \frac{C_{18}\left(\overline{\delta P^*_{in}} - \overline{\delta P^*_{z1}}\right)}{1 + s\tau_L} . \tag{6.50}$$

2. Energy Balance

The subcooled region is divided into nonboiling and subcooled boiling regions. The boundary between these two regions is determined by using the Jens-Lottes equation (Eq. 6.32). Thus, the dividing line may be located by the use of

$$T = -\frac{q}{h_{nb}} + T_{sat} + 60\left(\frac{q}{10^6}\right)^{1/4} e^{-P/900}, \tag{6.51}$$

where h_{nb} is the heat-transfer coefficient in the nonboiling region, calculated from the Dittus-Boelter equation:

$$h_{nb} = K_h(Re)^{g_1}(Pr)^{g_2}, \tag{6.52}$$

where K_h, g_1, and g_2 are constants.

The heat-transfer coefficient in the subcooled boiling region is obtained from the Jens-Lottes correlation:

$$h_{sc} = \frac{10^6}{15} e^{P/900}(q/10^6)^{3/4} . \tag{6.53}$$

The energy balance in the subcooled region may be written as

$$\frac{\partial}{\partial t}(\rho_{sc}A_cC_pT) + \frac{\rho(W_{sc}C_pT)}{\partial z} = Q', \tag{6.54}$$

or

$$\overline{\rho}_\ell A_c \overline{C}_p \frac{\partial T}{\partial t} + W_{sc}\overline{C}_p \frac{\partial T}{\partial z} = Q', \tag{6.55}$$

where

$$\overline{C}_p = \frac{H_\ell - H_{in}}{\Delta T_{in}},$$

and

$$\overline{\rho}_{\ell} = \rho_{\ell}\left(\frac{1 + \rho_{in}/\rho_{\ell}}{2}\right).$$

Equation (6.55) is linearized, and the Laplace transform is obtained:

$$\overline{\rho}_{\ell} A_c \overline{C}_p s\overline{\delta T} + W_{sc}\overline{C}_p \frac{\partial \overline{\delta T}}{\partial z} + \overline{C}_p \frac{\partial T}{\partial z}\bigg|_0 \overline{\delta W}_{sc} = \overline{\delta Q'}. \tag{6.56}$$

Multiplying both sides by

$$\frac{z_1}{W_{sc}\overline{C}_p \Delta T_{in}} = \frac{z_1}{Q_{sc}}$$

yields

$$\frac{1}{2}\left(1 + \frac{\rho_{in}}{\rho_{\ell}}\right)\frac{z_1 s}{u_{sc}} \frac{\overline{\delta T}}{\Delta T_{in}} + z_1 \frac{\partial}{\partial z}\left(\frac{\overline{\delta T}}{\Delta T_{in}}\right) = \frac{z_1 Q_0}{Q_{sc}}\left[\overline{\delta Q^{*'}} - \overline{\delta W^*_{sc}}\right], \tag{6.57}$$

where

$$Q_0 = W_{sc} C_p \frac{\partial T}{\partial z}\bigg|_0.$$

If Eq. (6.30) is used, it may be shown that

$$\overline{\delta Q^{*'}} = \frac{\overline{\delta Q^*}}{1 + s\tau_{fsc}}, \tag{6.58}$$

where

$$\tau_{fsc} = \frac{\rho_w A_w C_w}{h p_c}. \tag{6.59}$$

Integrating Eq. (6.57) with respect to z yields

$$\frac{\overline{\delta T}_{z1}}{\Delta T_0} = e^{-s\tau'} \frac{\overline{\delta T}\big|_{in}}{\Delta T_0} + H_0(\tau')\left[\frac{\overline{\delta Q^*}}{1 + s\tau_{fsc}} - G(\tau_{fsc})\,\overline{\delta W^*_{sc}}\right], \tag{6.60}$$

where

$$H_0(\tau') = \frac{1 - e^{-s\tau'/m}}{s\tau'/m} \sum_{i=1}^{m} \frac{f_i}{m} e^{-\left(\frac{m-i}{m}\right)s\tau'},$$

$$\tau' = \frac{z_1 \bar{\rho}_\ell}{2u_{in}} \left(1 + \frac{\rho_w A_w C_w}{\bar{\rho}_\ell A_c \bar{C}_p}\right),$$

$$G(\tau_{fsc}) = \frac{1 + s(1 - g_1)\,\tau_{fsc}}{1 + s\tau_{fsc}} \text{ in the nonboiling region}$$

$$= 1 \text{ in the subcooled boiling region,}$$

and

$$m = \text{number of nodes in the subcooled region.}$$

D. Pressure Drop Downstream of the Test-section Exit

An enlargement of the cross-sectional area is assumed to occur at the test-section exit. In the region of the area change, an approximate expression is obtained for the pressure drop by using a spatially-uniform fluid density equal to the average density at the test-section exit. A steady-state energy balance at the point of area change yields

$$P_{n+1} - P_{ex} = \Delta P_{ex} = \frac{\rho_{ex} u_{ex}^2}{g} \sigma_e(1 - \sigma_e), \tag{6.61}$$

where

$$\sigma_e = \frac{A_c}{A_r},$$

and

$$\rho_{ex} = \rho_\ell(1 - \alpha_{ex}) + \rho_g \alpha_{ex} = \rho_\ell(1 - \eta\alpha_{ex}).$$

If

$$2\sigma_e(1 - \sigma_e) = K'_e, \tag{6.62}$$

Equation (6.61) may be expressed in the dimensionless form as

$$\Delta P^*_{ex} = \frac{K'_e u_{in}^2}{2gL_c(1 - \eta\alpha_{ex})} W^{*2}_{ex}. \tag{6.63}$$

Linearizing, and taking the Laplace transform, yields

$$\overline{\delta(\Delta P^*_{ex})} = \frac{K'_e u_{in}^2}{2gL_c}\left[\frac{2\overline{\delta W^*_{ex}}}{1 - \eta\alpha_{ex}\big|_{01}} + \frac{\eta\overline{\delta\alpha_{ex}}}{\left(1 - \eta\alpha_{ex}\big|_{01}\right)^2}\right] \tag{6.64}$$

or

$$(\overline{\delta\Delta P^*_{ex}}) = C_{19}\overline{\delta W^*_{ex}} + C_{20}\overline{\delta\alpha_{ex}}, \tag{6.65}$$

where

$$C_{19} = \frac{K'_e u_{in}^2}{gL_c\left(1 - \eta\alpha_{ex}\big|_{01}\right)},$$

and

$$C_{20} = \frac{K'_e u_{in}^2 \eta}{2gL_c\left(1 - \eta\alpha_{ex}\big|_{01}\right)^2}.$$

E. Solution of the Equations

Jones and Dight[40] solved the differential equations by using a Philco 2000 digital computer. The program computes the open-loop frequency response of the system and uses the Nyquist criterion to determine whether the specified system is stable. Figure (6.1) is a block diagram of the closed-loop transfer function.

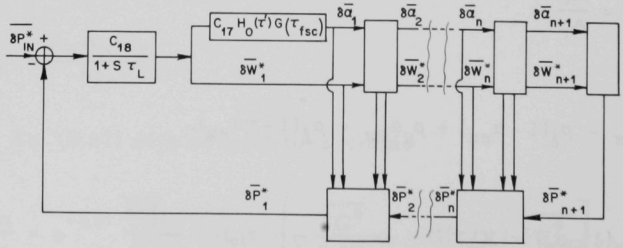

Fig. 6.1. Block Diagram of Closed-loop Transfer Function

The STL group[26,27] translated the above program to a FORTRAN code after modifying it to accommodate the test sections of circular as well as rectangular cross sections. This modified FORTRAN version, STABLE-3, was used in the present study and the results are discussed in Chapter VIII.

VII. NONLINEAR ANALYSIS

This section is of interest for two reasons: (1) to investigate the effect of the disturbances of large magnitude on the system equilibrium; and (2) to study the system behavior beyond the point of inception of oscillations. Beyond this point, flow disturbances are no longer damped out, but instead diverge to self-sustained oscillations. The nonlinear analysis should predict the amplitudes as well as frequency of these bounded oscillations.

A digital-computer code written in FORTRAN at STL based on the numerical integration of the nonlinear equations of conservation and state and the boundary conditions was used with some modifications. The mathematical analysis was that originally proposed by Jahnberg.[32] The important steps of this analysis are presented here.

The basic assumptions and the equations of conservation are the same as those given in Chapter V. The model does not consider the effect of the heat capacity of the test-section wall. The boundary between the subcooled and the bulk-boiling regions is considered to be the same as that obtained by thermodynamic equilibrium. Perfect mixing of the fluid is assumed at each cross section of the test section.

The boundary condition is that the total pressure drop across the test section is the same as that for the nonheated part of the loop. The pressure drops are expressed as functions of the time derivative of the inlet velocity and quantities describing the instantaneous state of the system. An explicit equation is obtained for the time derivative of the inlet velocity from the boundary condition, from which the instantaneous inlet velocity is obtained by a forward numerical integration.

A. Pressure Drops

1. Nonboiling Region

The pressure drop in the nonboiling part of the test section is obtained by solving Eq. (5.2) for single phase. Thus,

$$\Delta P_{nb} = -\int_0^{z_1} \left(\frac{\partial P}{\partial z}\right) dz$$

$$= \rho_\ell g z_1 + \int_0^{z_1} \left(\frac{\partial P_f}{\partial z}\right)_{nb} dz. \qquad (7.1)$$

2. Bulk-boiling Region

Equation (5.2) yields

$$\Delta P_b = -\int_{z_1}^{L_c} \left(\frac{\partial P}{\partial z}\right) dz$$

$$= \int_{z_1}^{L_c} \left(\frac{\partial \overline{\rho u}}{\partial t}\right) dz + \int_{z_1}^{L_c} \left(\frac{\partial \overline{\rho u^2}}{\partial z}\right) dz + g \int_{z_1}^{L_c} \bar{\rho} dz + F_b, \qquad (7.2)$$

where F_b is the total frictional pressure drop in the boiling region given by

$$F_b = \int_{z_1}^{L_c} \left.\frac{\partial P_f}{\partial z}\right|_b dz.$$

If

$$\overline{\rho u} = G_c, \qquad (7.3)$$

and

$$\frac{1}{\rho'} = \frac{1}{\rho_\ell}\left[\frac{(1-X)^2}{1-\alpha} + \frac{\rho_\ell}{\rho_g}\frac{X^2}{\alpha}\right]$$

$$= \frac{1}{G_c^2}\left[\rho_\ell u_\ell^2 (1-\alpha) + \rho_g u_g^2 \alpha\right], \qquad (7.4)$$

then Eq. (7.2) becomes

$$\Delta P_b = \int_{z_1}^{L_c} \left(\frac{\partial G_c}{\partial t}\right) dz + \left.\frac{G_c^2}{\rho'}\right|_{z_1}^{L_c} + g \int_{z_1}^{L_c} \bar{\rho} dz + \int_{z_1}^{L_c} \left(\frac{\partial P_f}{\partial z}\right)_b dz$$

$$= \int_{z_1}^{L_c} \left(\frac{\partial G_c}{\partial t}\right) dz + \left.\frac{G_c^2}{\rho'}\right|_{ex} - \rho_\ell u_{in}^2 + g \int_{z_1}^{L_c} \bar{\rho} dz + \int_{z_1}^{L_c} \left(\frac{\partial P_f}{\partial z}\right)_b dz.$$

(7.5)

Equations (5.1) and (5.3) can be combined to give

$$H_{fg} \frac{\partial}{\partial z}\left[u_\ell(1-\alpha) + u_g\alpha\right] = \frac{Q}{A_c}\left(\frac{1}{\rho_g} - \frac{1}{\rho_\ell}\right), \tag{7.6}$$

or

$$\left[u_\ell(1-\alpha) + u_g\alpha\right]\Bigg|_{z_1}^{z} = \frac{\eta}{\rho_g A_c H_{fg}} \int_{z_1}^{z} Q\, dz,$$

or

$$u_\ell(1-\alpha) + u_g\alpha = u_{in} + \frac{\eta}{\rho_g A_c H_{fg}} \int_{z_1}^{z} Q\, dz. \tag{7.7}$$

Now,

$$u_\ell(1-\alpha) + u_g\alpha = G_c\left[\frac{1-X}{\rho_\ell} + \frac{X}{\rho_g}\right]. \tag{7.8}$$

Substituting Eq. (7.8) into Eq. (7.7) yields

$$\frac{\partial G_c}{\partial t} = \frac{1}{\frac{1-X}{\rho_\ell} + \frac{X}{\rho_g}}\left\{\frac{du_{in}}{dt} + \frac{\eta}{\rho_g A_c H_{fg}}\left[\int_{z_1}^{z} \frac{\partial Q}{\partial t}\, dz - \frac{dz_1}{dt} Q_{z_1}\right] - \frac{1}{\rho_\ell \rho_g} \frac{\partial X}{\partial t}\right\}. \tag{7.9}$$

In Eq. (7.9), the terms dz_1/dt and $\partial X/\partial t$ may be obtained as follows: The heat absorbed by the subcooled liquid volume $A\,dz$ in travelling from inlet to z is given by

$$\left[\int_{t-\tau}^{t} Q(\zeta, t')\, dt'\right] dz = \left[\int_{0}^{z} \frac{Q(\zeta, t-\tau)}{u_{in}(t-\tau)}\, d\zeta\right] dz, \tag{7.10}$$

where $\tau(\zeta, z, t)$ is the time required in travelling from ζ to z. Thus,

$$z - \zeta = \int_{t-\tau}^{t} u_{in}(t')\, dt'. \tag{7.11}$$

At the boiling boundary,

$$\rho_\ell(H_\ell - H_{in}) = \frac{1}{A_c} \int_{0}^{z_1} \frac{Q(\zeta, t-\tau)}{u_{in}(t-\tau)}\, d\zeta, \tag{7.12}$$

and

$$z_1 - \zeta = \int_{t-\tau}^{t} u_{in}(t')\, dt'. \tag{7.13}$$

Differentiation of Eqs. (7.12) and (7.13) with respect to time and elimination of $\partial\tau/\partial t$ give

$$\frac{dz_1}{dt} = \frac{I u_{in}(t)}{I - \dfrac{Q(z_1, t)}{u_{in}(t)}}, \tag{7.14}$$

where

$$I = \int_0^{z_1} \left\{ \frac{1}{u_{in}(t')} \frac{\partial}{\partial t'} \left[\frac{Q(\zeta, t')}{u_{in}(t')} \right] \right\} \Bigg|_{t'=t-\tau} d\zeta; \tag{7.15}$$

$\partial X/\partial t$ may be evaluated from the continuity equation, Eq. (5.1), to give

$$\frac{\partial X}{\partial t} = \frac{dX}{d\alpha} G_c \frac{\partial G_c}{\partial z}. \tag{7.16}$$

Equations (7.1), (7.9), (7.15), and (7.16), when substituted in Eq. (7.5), result in

$$\Delta P_c = c_1 \frac{du_{in}}{dt} + c_2, \tag{7.17}$$

where

$$c_1 = \rho_g \int_{z_1}^{L_c} \frac{dz}{1 - \eta + \eta X}, \tag{7.18}$$

and

$$c_2 = \frac{\eta}{A_c H_{fg}} \int_{z_1}^{L_c} \frac{1}{1 - \eta + \eta X} \left[\int_{z_1}^{z} \frac{\partial Q}{\partial t} dz - \frac{dz_1}{dt} Q(z_1, t) \right] dz - \frac{1}{\rho_\ell} \int_{z_1}^{L_c} \frac{1}{1 - \eta + \eta X} \frac{dX}{d\alpha} G_c \frac{\partial G_c}{\partial z} dz$$

$$+ \frac{G_c^2}{\rho'} \Bigg|_{ex} - \rho_\ell u_{in}^2 + \int_0^{L_c} \left\{ g \left[\rho_\ell (1 - \alpha) + \rho_g \alpha \right] + \frac{\partial P_f}{\partial z} \right\} dz. \tag{7.19}$$

In Eqs. (7.17) to (7.19), $\partial P_f/\partial z$ and α are calculated from empirical correlations, described in Section C below.

3. Nonheated Part

In a natural-circulation boiling system, the nonheated part generally consists of a riser, a steam separator, a condenser, a downcomer, and a subcooler. The riser has a two-phase mixture, and the pressure drop across it may be calculated in a way similar to that for the test section. The pressure losses at the test-section inlet and exit and at the riser exit are given below (the inlet pressure drop includes the frictional losses in the single-phase region of the nonheated part):

$$\Delta P_{in} = \frac{1}{2} k_{in} \rho_\ell u_{in}^2, \tag{7.20}$$

$$\Delta P_{ex} = \frac{1}{2} k_{ex} \left(\frac{G^2}{\rho'}\right)_{ex}, \tag{7.21}$$

and

$$\Delta P_{re} = \frac{1}{2} k_{re} \left(\frac{G^2}{\rho'}\right)_{re}. \tag{7.22}$$

The downcomer is represented by a driving height $\bar{L}_d$ and an equivalent length L_d. The pressure-drop contribution is

$$\Delta P_d = g\rho_\ell \bar{L}_d - \rho_\ell L_d \frac{du_{in}}{dt}. \tag{7.23}$$

The total pressure drop in the nonheated part can be then added to become

$$\Delta P = \Delta P_d - \Delta P_r - \Delta P_{in} - \Delta P_{ex} - \Delta P_{re}$$

$$= c_1' \frac{du_{in}}{dt} + c_2', \tag{7.24}$$

where

$$c_1' = -\rho_\ell L_d - \frac{A_c}{A_r} \rho g \int_{L_c}^{L_c+L_r} \frac{dz}{1 - \eta + \eta X}, \tag{7.25}$$

and

$$c_2' = \rho_\ell g \bar{L}_d - \frac{\eta}{A_r H_{fg}} \int_{L_c}^{L_c+L_r} \frac{1}{1 - \eta + \eta X} \left[\int_{z_1}^{L_c} \frac{\partial Q}{\partial t} dz - \frac{dz_1}{dt} Q z_1 \right] dz$$

$$+ \frac{1}{\rho_\ell} \int_{L_c}^{L_c+L_r} \frac{1}{1 - \eta + \eta X} \frac{dX}{d\alpha} G_r \frac{\partial W_r}{\partial z} dz$$

$$- \int_{L_c}^{L_c+L_r} \left\{ g[\rho_\ell (1 - \alpha) + \rho_g \alpha] + \frac{\partial P_f}{\partial z} \right\} dz - \left(\frac{G^2}{\rho'} \right)_{re} + \left(\frac{G_c^2}{\rho'} \right)_{ex}$$

$$- \frac{1}{2} k_{in} \rho_\ell u_{in}^2 - \frac{1}{2} k_{ex} \left(\frac{G^2}{\rho'} \right)_{ex} - \frac{1}{2} k_{re} \left(\frac{G^2}{\rho'} \right)_{re}. \tag{7.26}$$

B. Method of Solution

Equations (7.17) and (7.24), when substituted in the boundary condition, yield

$$\frac{du_{in}}{dt} = \frac{c_2' - c_2}{c_1 - c_1'}, \tag{7.27}$$

where c_1, c_2, c_1', and c_2' are defined by Eqs. (7.18), (7.19), (7.25), and (7.26), respectively. The initial conditions for u_{in} and α are obtained from the steady-state solution. The test section and riser are divided into a finite number of sections. The spatial integrals are evaluated by Simpsons' rule. Equation (7.27) is then approximated to give

$$u_{in}(t + \Delta t) = u_{in}(t) + \Delta t \frac{c_2'(t) - c_2(t)}{c_1(t) - c_1'(t)}. \tag{7.28}$$

Similarly, the steam-void fraction is approximated by solving the continuity equation, Eq. (5.1). Thus,

$$\frac{\partial \alpha}{\partial t} = \frac{1}{\rho_\ell - \rho_g} \frac{\partial G}{\partial z}, \tag{7.29}$$

or

$$\alpha(t + \Delta t, i\Delta z) = \alpha(t, i\Delta z) + \frac{\Delta t}{\Delta z} \frac{1}{\rho_\ell - \rho_g} \{G(t, i\Delta z) - G[t, (i - 1)\Delta z]\}, \tag{7.30}$$

where Δz and Δt are space and time steps, respectively, and $i\Delta z$ represents the axial position.

The steady-state values of α and u_{in} are evaluated by setting all time derivatives to zero in Eq. (7.27), which gives

$$c_2 = c_2'. \tag{7.31}$$

Equation (7.31) and the boundary conditions,

$$\alpha_{z1} = 0 \tag{7.32}$$

and

$$X_{ex} = X_r, \tag{7.33}$$

are iterated to yield the steady-state values. The dynamic solution is then obtained by setting the power input to a new value and calculating all the variables at each interval of Δt.

C. Empirical Correlations

The original version of the digital-computer program uses models developed in Sweden for the slip-ratio and two-phase frictional pressure gradient. It was modified to allow the use of any of the several empirical correlations available in the literature. The Swedish models are described here.

1. Slip Ratio

The slip ratio is given by

$$S = (1 + C_3 X^{3/4})(0.795 + 0.410\rho_\ell / G), \tag{7.34}$$

where C_3 is the parameter given as input data. The void fraction is then obtained by using the mass balance equation in the form,

$$\alpha = \frac{X}{X + S(\rho_g/\rho_\ell)(1 - X)}. \tag{7.35}$$

2. Frictional Pressure Gradient

The single-phase pressure gradient is given by

$$\left.\frac{\partial P_f}{\partial z}\right|_{nb} = \frac{f G_\ell^2}{2\rho_\ell d_c}, \tag{7.36}$$

where

$$f = 0.013 + \frac{1.8}{Re^{1/2}}. \tag{7.37}$$

The analysis assumes that the surface boiling in the subcooled region starts when

$$T = T_{sat} - T', \tag{7.38}$$

where

$$T' = \frac{Q}{h_{nb} P_c} \tag{7.39}$$

and h_{nb} is given by the Dittus-Boelter equation:

$$h_{nb} = 0.023 \frac{\lambda}{d_c} Re^{0.8} Pr^{0.4}. \tag{7.40}$$

In the part below the boiling boundary, the frictional pressure gradient is given by

$$\left.\frac{\partial P_f}{\partial z}\right|_{sc} = \left.\frac{\partial P_f}{\partial z}\right|_{nb} + \frac{0.2 h p_c G_c}{A_c \rho_\ell H_{fg}} (T + T' - T_{sat}). \tag{7.41}$$

For two-phase flow,

$$\left.\frac{\partial P_f}{\partial z}\right|_{b} = \left.\frac{\partial P_f}{\partial z}\right|_{nb} (1 + aX^b), \tag{7.42}$$

where

$$a = \frac{3.9 \cdot 10^8 - 1.96P}{6.75 \cdot 10^5 + 0.1P}, \tag{7.43}$$

and

$$b = 1.025 - 1.74 \cdot 10^{-8} P. \tag{7.44}$$

Pressure, P, is expressed in dynes/cm^2. In the heated section, a correction similar to that in Eq. (7.41) for surface boiling is added. Thus, in the

bulk-boiling region of the test section, the correlation for the frictional pressure gradient becomes

$$\left.\frac{\partial P_f}{\partial z}\right|_b = \left.\frac{\partial P_f}{\partial z}\right|_{nb} (1 + aX^b) + \frac{0.2Q(1-\alpha)\, G_c}{A_c \rho_\ell H_{fg}}. \tag{7.45}$$

VIII. COMPARISON OF PREDICTIONS FROM THEORETICAL MODELS WITH EXPERIMENTAL RESULTS

The basic features of two theoretical models, one linear and the other nonlinear, are given in Chapters VI and VII. Predictions from these models are compared with the experimental data from the natural-circulation boiling system used in the present study. These are discussed below under the appropriate headings.

A. Jones's Transfer-function Model

As described in Chapter VI, in this model an open-loop transfer function for a boiling system is obtained by taking the Laplace transform of the linearized equations of conservation and state, and the boundary conditions. When the Nyquist criterion is used, the gain of the feedback loop at 180° phase lag (see Fig. 6.1) indicates whether a system is stable or not. For a minimum phase system (no zero in the right-hand plane), a magnitude ratio of less than one indicates stability, while a magnitude ratio equal to or greater than one indicates instability.

In this linearized model, the steady-state inlet flow rate is supplied separately. The zeroth-order (steady-state) perturbation equations are not considered and, in general, may not be satisfied. Only the first-order (linear) equations are used. This allows a greater degree of freedom in choosing the steady-state flow rate, which may be determined experimentally or from a separate calculation. On the other hand, there is a loss of physical consistency.

Another drawback of this model (and other linear models) is that it considers the stability in the small, as discussed in Chapter V. Thus, it can only predict whether a system perturbed by a small disturbance would return to the original stationary condition or not. As a consequence, the capability of this model is limited to the prediction of the point of inception of self-sustained oscillations in the present case.

Table III shows, for various combinations of geometry, pressure, and inlet subcooling, the power and frequency at which the magnitude ratio of the feedback loop is expected to become unity at a phase lag of 180°. The table also shows the power at which inception of oscillations was observed experimentally. The two bases shown for the choice of threshold power for these need additional explanation.

The flow velocity at the test-section inlet was used as a dependent variable for determining the threshold points. The peak-to-peak amplitudes of the inlet velocities were plotted against power for a given set of conditions.

As discussed in Chapter IV, this plot, in general, showed three regions:

1. stationary flow rates; zero amplitude;
2. small-amplitude oscillations;
3. large-amplitude oscillations.

TABLE III. Comparison of Predictions from Jones Model with Experimental Data

Geometry	Table No.	Pressure, psia	Inlet Subcooling, °F	Experimental Threshold Power, kW (a)	Experimental Threshold Power, kW (b)	Experimental Threshold Freq, cps	Jones-model Threshold Power, kW (c)	Jones-model Threshold Freq, cps
1	V	200	1	>39	>39	-	39	0.60
			10	42	>48	-	38	0.68
			20	38	58	0.49	54	0.47
3	VII	200	28	<25	<25	0.30	25	0.30
			36	<30	<30	0.24	<30	0.28
			45	<25	<25	0.29	24	0.34
		600	28	41	42	0.45	43	0.51
			36	39	45	0.38	45	0.43
			46	40	45	0.35	45	0.38
		1000	47	64	67	0.41	65	0.44
4	VIII	200	20	18	21	0.43	17	0.45
			30	20	21	0.39	17	0.36
			40	20	22	0.35	20	0.36
		600	30	51	52	0.51	44	0.57
			40	45	48	0.49	43	0.52
			50	47	48	0.40	50	0.46
			62	51	54	0.37	51	0.40
5	IX	200	10	24	29	0.76	14	0.70
			18	25	27	0.68	14	0.61
			30	<20	23	0.44	<20	0.48
		600	50	47	56	0.51	43	0.58
6	X	200	25	10	18	0.29	16	0.31

All values of power are rounded off to the nearest integer.

NOTES:

(a) Represents the power at which flow oscillations of 10% peak-to-peak amplitude with respect to the mean occurred.

(b) Represents the power at which the slope of the amplitude versus power was 45° (see text).

(c) Represents the power at which the calculated magnitude ratio of the closed-loop transfer function was unity at 180° phase lag. These values were interpolated or extrapolated from the computed results.

In the region of the small-amplitude oscillations, the change in the amplitude was not well-defined with respect to change in power; an increase in power could result in a decrease or in no change in amplitude. For this reason, it was of interest to compare the inception points of the flow oscillations arbitrarily defined in two different ways. For both criteria, described below, a smoothed plot of the peak-to-peak amplitude of the flow oscillations versus power was obtained for each combination of the test parameters.

A variation of 10% (peak-to-peak) from the mean inlet flow velocity was taken as the first criterion for the threshold power.

The transition from small-amplitude oscillations to large-amplitude oscillations was, in general, fairly sharply defined. The second criterion was, therefore, taken to be the point at which the slope of the amplitude of flow oscillations versus power was 45°, with a standard scale of 2 ft/sec/in. along the Y-axis and 5 kW/in. along the X-axis.

The frequency shown with the experimental data is the frequency of oscillations at the lowest power after the onset of oscillations. Other notations in Table III are explained at the end of the table.

Comparison between the predictions from the Jones model and the experimental values for the oscillation thresholds shows good agreement. The experimental and the theoretically-determined frequencies of oscillations show similar trends with respect to change in the inlet subcooling, pressure, and geometry. Prediction of the threshold power is correct within ±5% for more than 60%, and within ±10% for more than 80%, of the tested cases.

Neal and Zivi[26,27] also found the Jones model to be quite satisfactory. In their study, the predictions from this model for other experimental studies (see Reference 27) showed good agreement with 70% of the experimental values. Thus, this model appears to be quite satisfactory for predicting the oscillation thresholds in a natural-circulation boiling-water loop within the range of parameters of this and other experimental studies.

Results from this model were also obtained at higher pressures (600-1500 psia) for the geometry shown in Table V. The model predicted a stable system within the power range of the tests, which is in agreement with the experimental observations. Predictions from this model were not obtained for the test geometry of Table VI because, in this case, the tests showed large-amplitude oscillations at the lowest heat inputs.

B. Jahnberg's Nonlinear Model

Jahnberg's nonlinear model solves the equations of conservation and state along with the boundary conditions for a given boiling system in the time domain. Since the nonlinear terms are not neglected in this analysis, the behavior of a system, when the disturbances become large in amplitude, should be predicted. Another advantage of this model over Jones's linear model is that it does not require a prior knowledge of the steady-state flow rate at the test-section inlet. An approximate value of the inlet flow rate is put as input to the program, which then iterates the steady-state equations of the system to estimate the best value within the required accuracy. In the STL version of the digital-computer program, for the Jahnberg model, the dynamic calculations are calculated by making a step change in power and solving the equations at each increment of time at the new power. The following changes were made in this program:

1. All the integrals were estimated by Simpson's rule instead of the trapezoidal rule.
2. Suitable modifications were made so that the computations are also continued at negative values of the instantaneous flow rates.

The basic features of the Jahnberg model were retained in the computations, and the test data obtained from the STL[47] were reproduced to check that there was no error in the computation procedure.

The results for the steady-state inlet flow velocities for one of the test geometries are shown in Fig. 8.1. In this figure, the predictions from the Jahnberg model, using the originally suggested empirical slip-ratio and frictional pressure-gradient correlations (Swedish models), are shown by solid continuous lines for various conditions. A comparison with the experimental data, also plotted in Fig. 8.1, shows that there is a large difference between the two results. The predictions for the steady-state inlet flow velocities similarly did not check with the experimentally determined values for the other test geometries.

The predictions of inception of oscillations were also obtained, despite the large discrepancies in the steady-state values of the inlet flow velocities. Table IV compares the Jahnberg predictions with the experimental values. The method for obtaining the experimental threshold of oscillations was described in Section A. The frequency of oscillation was not obtained for the Jahnberg model since it was noted that, in most cases, the inlet velocity either converged to a stationary value or diverged to a value outside the range of the computer within two periods of oscillations. The threshold power was taken to be the minimum power at which the inlet velocity diverged with respect to time.

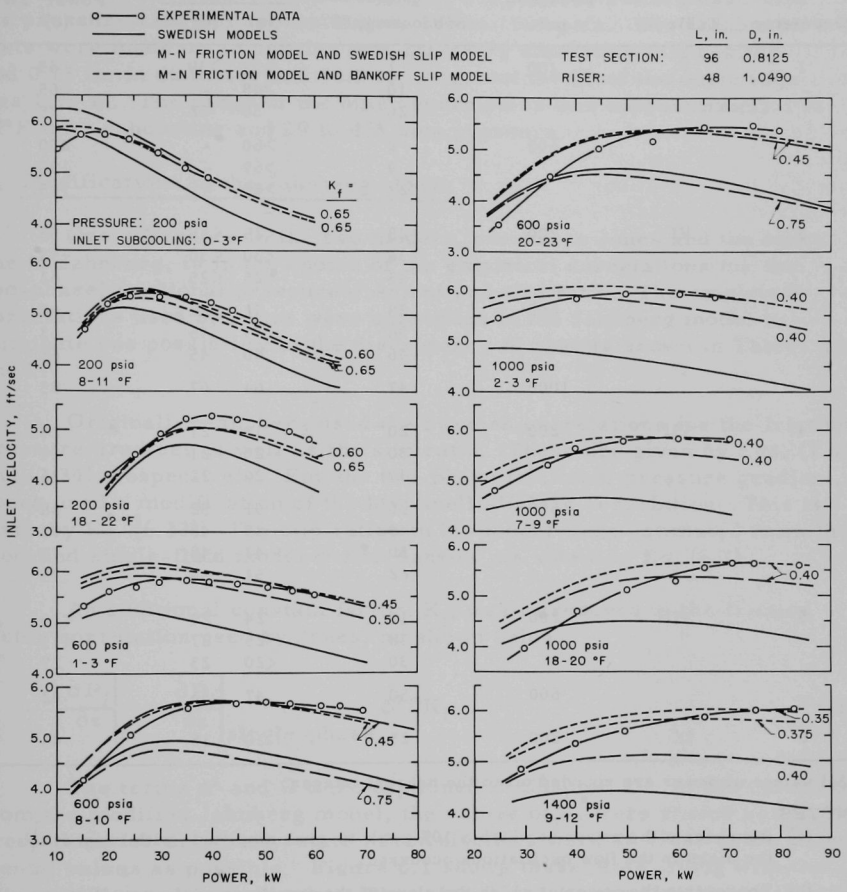

Fig. 8.1. Comparison of Data with Steady-state Predictions

TABLE IV. Comparison of Predictions from Jahnberg Model with Experimental Data

Geometry	Table No.	Pressure, psia	Inlet Subcooling, °F	Experimental Instability Power, kW (a)	Experimental Instability Power, kW (b)	Jahnberg Model Power, kW (c)
1	V	200	1	>39	>39	55
			10	>48	-	>65
			20	38	58	75
		600	2	>60	-	200
			9	>69	-	190
			21	>80	-	165
3	VI	200	28	<25	<25	53
			36	<30	<30	53
			45	<25	<25	62
		600	28	41	42	60
			36	39	45	63
			46	40	45	68
		1000	47	64	67	83
4	VII	200	20	18	21	29
			30	20	21	34
			40	20	22	36
		600	30	51	52	68
			40	45	48	72
			50	47	48	73
			62	51	54	75
5	VIII	200	10	24	29	<10
			18	25	27	<15
			30	<20	23	27
		600	50	47	56	42
6	IX	200	25	10	18	46

All values of power are rounded off to the nearest integer.

NOTES:

(a) Represents the power at which a 10% peak-to-peak amplitude with respect to the mean in the flow oscillations occurred.

(b) Represents the power at which the slope of the amplitude of flow oscillations versus power was 45°.

(c) Represents the minimum power at which the inlet velocity became divergent with respect to time.

It may be noted from Table IV that Jahnberg's model generally predicts higher oscillation threshold values than the experimental values. Neal and Zivi,[27] in their calculations to check this model with experimental studies at Sweden[16] and Eindhoven,[11] found a discrepancy of 30 to 35% in every case. In their case, however, the model predicted lower values than the experimental thresholds. This may be due to the difference in the

test conditions. For the Swedish experiments, two test sections were used: (1) 0.787-in. diam, 196 in. long; (2) 0.394-in. diam, 196 in. long. In the first test geometry, the range of subcooling was 3.6 to 28.8°F; in the second case, two values of subcooling of 295 and 439°F were used with the pressure range of approximately 150 to 1000 psia. The Eindhoven tests were made on an annular test geometry consisting of a heating rod 0.75 in. in diameter and 94.5 in. long, and the ID of the outer tube was 1.98 in. The range of the other parameters was approximately 3 to 27°F inlet subcooling and 29 to 435 psia pressure.

C. Modifications in the Jahnberg Model

One difference in the two models, one due to Jones and the other due to Jahnberg, is in the choice of the empirical correlations for the two-phase, frictional pressure gradient and slip ratio. The empirical correlations used by Jones were substitued in the Jahnberg model to eliminate one possibility of the discrepancy in results shown in Tables III and IV.

Originally, Jahnberg used the Swedish correlations for the frictional pressure gradient as well as the slip ratio. These are given by Eqs. (7.45) and (7.34), respectively. For the two-phase frictional pressure gradient, Jones used a modification of the Martinelli-Nelson correlation. This is given by Eq. (6.13). The slip ratios in his model were estimated from the modified single-fluid model due to Bankoff, as shown in Eq. (6.7).

An additional constant factor, K_f, was introduced in the friction factor correlation used by Jones, as shown below:

$$\left.\frac{\partial P_f}{\partial z}\right|_b = \left.\frac{\partial P_f}{\partial z}\right|_{\text{single-phase}} \phi^2 \Omega K_f. \tag{8.1}$$

The terms ϕ^2 and Ω were explained in Chapter VI. In the calculations from the modified Jahnberg model, the values of K_f were varied so that the predictions for the steady-state inlet velocities were as close to the experimental values as possible. Figure 6.1 shows these plots, along with the values of K_f used in each case. Thus, for the test geometry shown in Fig. 6.1, approximate values of K_f for the best fits were found to be 0.65, 0.45, 0.40, and 0.375 for pressures of 200, 600, 1000, and 1400 psia, respectively. Similar calculations for other test geometries required different values of K_f. Thus, for example, for the test geometries shown in Tables VII and VIII the appropriate values of K_f were roughly 1.25, 1.0, and 0.85 for 200, 600, and 1000 psia, respectively. These results show that the modified Martinelli-Nelson fit predicts too high frictional pressure drop for the larger-diameter test geometry (0.8125-in.-diam test section) used in the first case, and too low (at 200 psia) for the smaller-diameter

test geometry (0.625-in.-diam test section) used in the second case. Significantly, it may be pointed out that the original Martinelli-Nelson correlation was obtained from the data of air-water tests in a horizontal test section and was later extended to the steam-water case. The modification to this correlation was based on the experiments at Westinghouse,[48] where the test channel was of rectangular geometry. The effect of the shape factor has not yet been established in two-phase flow systems. Another possibility is that the cumulative error in the computation of the single-phase pressure drop around the loop may be significant.

The digital program of Jones and Dight and the modified STL version also use a factor K_{fb} similar to K_f used here. K_{fb} is assumed to be independent of the void-fraction and mass flow rate and is assumed to be dependent on the axial position. If K_f in the modified Jahnberg model was also made space-dependent, similar to K_{fb}, the curve fit of the predicted inlet velocity could be further improved.

The effect of the slip-ratio correlations is also shown in Fig. 6.1. The change in the steady-state inlet velocity due to change in the slip models does not seem to be as marked as that due to the frictional pressure gradient.

The dynamic results from the modified Jahnberg model were still not very encouraging. The model failed to predict bounded oscillations after the inception of oscillation, and the inlet velocity diverged to infinity instead. Also, the oscillation thresholds had a large discrepancy between the experimental and predicted values. From these predictions, a clear trend with respect to the prediction of the original Jahnberg model could not be established.

Additional studies were made on duration and shape of changes with time in power and inlet subcooling. Small sinusoidal changes in inlet subcooling had negligible effect. The effect of sinusoidal oscillations and periodic pulses in power was studied. The model seemed to behave as a linear system when the time derivative of power in Eq. (7.15) was neglected. What were most likely numerical instabilities appeared when the terms involving the rate of change of the power were included, which were not eliminated by changing the size of the time increment.

D. Discussion

The Jahnberg model errs in predicting the inception point of the oscillations, whereas the Jones model gives surprisingly good agreement. Since both are based on the conservation laws, with empirical functions for frictional losses and slip ratios, the superior performance of the Jones model might be superficially attributed to the use of more accurate empirical correlations. In the small perturbation range, which is implied

in studying the linearized stability point, both methods (numerical integration and Nyquist procedure) are mathematically equivalent. The Jahnberg model, however, is subjected to an additional constraint, in that not only the first-order (linear), but also the zeroth-order (steady-state) perturbation equations must be satisfied. In contrast, the Jones model may have the steady-state inlet velocity determined experimentally, so that the zeroth-order equations may not be satisfied. The Jones model thus achieves a greater accuracy in predicting local instability, at the expense of a possible loss in physical consistency. However, the Jahnberg model, once the origin becomes unstable, predicts very rapidly diverging oscillations, which exceed the machine capacity in only a few cycles. This is a serious inadequacy, since the experimental observations show bounded periodic (or almost-periodic) oscillations over a considerable range of powers. It seems unlikely that errors in the empirical correlations could account for such behavior; more likely, the one-dimensional formulation of the conservation equations is inadequate. As noted previously, bounded oscillations can be simulated on the computer, if the heat input into the system is assumed to have a periodic component. Physically, this would correspond to storage of energy in the channel wall and an associated superheated-liquid boundary layer, which is periodically released into the system when nucleation and vaporization of the superheated liquid occurs. This is a two-dimensional effect, which cannot be simulated in a one-dimensional formulation except by assuming a periodic forcing function. The system therefore behaves as a stable dissipative system, which is maintained in a steady orbit in the phase hyperplane by a periodic energy input, or forcing function. To this extent, the behavior is similar to that of a clock.

IX. CONCLUSIONS

A. General

The effect of increase in power on the inlet flow velocities can be divided into three broad classifications: (1) stationary flow conditions, (2) flow oscillations of small amplitudes, and (3) large-amplitude flow oscillations. The boundaries between these are, in general, not defined sharply, and the oscillation thresholds can be determined only by using some arbitrary criterion. The traces of the oscillations appeared to be the almost-periodic functions. In the large-amplitude oscillation ranges, reverse flow velocities were noted at the test-section inlet, which were of magnitudes comparable to the maximum flow velocities. Physically, these oscillations are probably associated with vapor bursts within the test section, caused by the periodic release of energy stored in the test-section wall and in the associated superheated-liquid boundary layer.

B. Experimental

The effect of inlet subcooling on the inception of oscillations was similar to that observed by Levy and Beckjord,[8] Becker et al.,[15] and Gouse and Andrysiak,[49] except in the case of the test geometry with smallest-diameter test section (0.364 in.) and riser (0.3125 in.). In this case, the frictional losses seemed to obscure the effect of inlet subcooling. Otherwise, in general, the increased inlet subcooling resulted in higher-amplitude oscillations at a given power. At sufficiently high inlet subcooling, this trend was reversed.

The effect of pressure was quite strong, increased pressure resulting in a more stable system. Similar results were reported previously, but only for the oscillation thresholds.

When the test-section length was varied, it was noted that at 200 psia there was negligible effect on the oscillation threshold, but at 600 psia the shortest test section was most stable. At both pressures, the longer test sections showed a higher amplitude of oscillations for a given power. A similar effect was observed when the riser length was changed. According to the proposed physical model, the increased downstream frictional effect in the longer channels results in an increased void-inlet flow response. Similarly, the smallest-diameter test sections and risers were least stable. In fact, the cross-sectional area of the two-phase region was found to be the most significant parameter in this study.

In the present study, the frequencies of oscillation ranged between 0.24 to 0.76 cps. In general, these frequencies increased with increases in power. For the larger-diameter test sections and risers (0.625-in.-diam),

increased pressure seemed to result in a decrease in the oscillation frequency at a given power. Such a clear effect was not observed when the other parameters were varied.

In general, the thresholds and amplitude of oscillations in the wall temperature did not necessarily follow the pattern of the oscillations of the hydrodynamic variables.

C. Theoretical

In the theoretical investigation, the Jones transfer-function model predicted the frequencies of oscillation well. The power at the oscillation thresholds was predicted correctly within ±5% for more than 60% of the cases, and within ±10% for more than 80% of the cases tested.

The nonlinear model due to Jahnberg failed to predict the steady-state inlet flow rates, as well as the oscillation threshold, within a reasonable accuracy.

The steady-state predictions from the Jahnberg model were improved by substituting the modified Martinelli-Nelson correlation for frictional pressure drop after a suitable multiplier was introduced. It was noted, however, that this modification did not improve the predictions for the oscillation threshold.

The Jahnberg model, in both cases, failed to predict the amplitude of oscillations.

It was concluded that the limitation of the nonlinear analysis of Jahnberg was not due to the inadequate knowledge of the two-phase frictional losses and the slip ratios for dynamic conditions. Probably the one-dimensional formulation of the conservation equations failed to simulate the two-dimensional effect of the energy stored in the channel wall and the associated superheated-liquid boundary layer. The Jones linear analysis was less sensitive to this effect in that it does not require that the zeroth-order (steady-state) equations be satisfied. This effect can be simulated as a periodic heat release, which gives periodic bounded oscillations with the modified Jahnberg model that are roughly similar to those observed experimentally.

APPENDIX A

Experimental Calculations

The power to the test section, in kilowatts, was calculated from the following expression:

$$\text{Power input} = EI/1000, \tag{A.1}$$

where E is the voltage across the test section, and I is the current through the test section. The test section was considered to be a pure resistance, and a unit power factor was taken.

The flow rates were calculated from the reading of the pressure drop across the venturi, as measured from a differential pressure transducer. The pressure-drop readings were corrected for the hydrostatic head between the pressure taps located 7 in. apart on a vertical flow path. If ΔP_{corr} denotes the corrected pressure drop, and ΔP_{meas} the measured pressure drop in psi, then

$$\Delta P_{corr} = \Delta P_{meas} - \frac{7(\rho_h - \rho_c)}{1728}, \tag{A.2}$$

where ρ_h and ρ_c are the densities in lb/cu ft of the fluid in the venturi and the connecting tubes, respectively.

The flow rates at the test-section inlet were then evaluated as

$$u_{in} = K\left(\frac{\Delta P_{corr}}{\rho_h}\right)^n \left(\frac{\rho_h}{\rho_{in}}\right), \tag{A.3}$$

where K and n were estimated from the venturi calibrations; their numerical values are given in Eqs. (4.9) and (4.10).

The pressure drop across the test section measured from a differential pressure transducer was corrected for the hydrostatic head of the fluid in the connecting tubes. The corrected pressure drop, in psi, is given by

$$\Delta P_{corr} = \Delta P_{meas} + \frac{L_{tap}\,\rho_c}{1728}, \tag{A.4}$$

where L_{tap} is the distance in inches between the pressure taps located at the test-section inlet and exit.

The wall temperatures were calculated from the reading of the thermocouple located outside the test-section wall 2 in. below the upper bus bar. The readings in millivolts were converted to degrees Fahrenheit by means of a standard calibration chart.

APPENDIX B

Error Analysis

The power was calculated from the readings of the voltmeter and the ammeter. The full-scale error was estimated to be less than 1%, whereas the error at the lowest power (10 kW) was estimated to be about 2.7%. The power input to the test section was also read from a wattmeter. The uncertainty in these readings was estimated to be ±0.7 kW, which is equivalent to 7% error at the lowest reading and approximately 1% error at full scale.

The heat loss from the test section was estimated to be a maximum of 3% at the lowest power input (10 kW) and less than 0.5% at the highest power (85 kW). Total estimated error of the power, based on the sum of the contributions from errors in power input and heat loss, is ±7.5% at 10 kW and ±1.5% at 85 kW.

The errors in the readings of the pressure drops were considered to be the accumulation of the errors due to each of the electronic components in the circuit and the observation error. A maximum error of ±1% full scale was estimated for the pressure drops across the venturi as well as the test section. Based on this, the uncertainty in the flow rate at the test section inlet was estimated to be of the order of ±0.1 ft/sec. This estimation does not include the reading error of the maximum and minimum readings of the flow rates. Since, in a given run, the peaks of the flow oscillations varied in amplitude, though remaining almost periodic, the maximum and minimum values represent an average of several peaks (individual maxima and minima) in a given run.

The thermocouples for measuring fluid and wall temperatures were carefully calibrated so that the principal error would be due to recording and reading uncertainties. These were estimated to be less than ±0.25°F. An additional uncertainty in the measurement of the wall temperature was caused by the presence of a mica sheet between the wall and the thermocouple.

The chart speed of the oscillograph was calibrated at two different speeds used in the experiments (1 and 4 in./sec) and for three different loads of the chart paper. A maximum error of 1.5% was estimated in the time scale. The uncertainty in the frequency of oscillation was estimated to be ±0.01 cps.

APPENDIX C

Tables of Data

TABLE V. Data for Geometry 1

Test Section: Length = 96 in. ID = 0.8125 in.
Riser: Length = 48 in. ID = 1.0490 in.
Liquid level = 10-10.5 in. below condenser

Data Point No.	Power, kW	Inlet Velocity, ft/sec		Pressure Drop across Test Section, psi		
		Max	Min	Max	Min	Mean
	Pressure = 199-201 psia		Inlet Subcooling = 0-3°F			
1	10.2	5.5	5.5	4.86	4.86	4.86
2	14.8	5.8	5.7	4.82	4.82	4.82
3	19.5	5.8	5.6	4.80	4.80	4.80
4	24.1	5.8	5.5	4.85	4.75	4.80
5	29.7	5.5	5.2	4.88	4.78	4.83
6	29.7	5.5	5.2	4.95	4.80	4.90
7	35.0	5.3	4.9	5.00	4.80	4.92
8	39.3	5.1	4.7	5.05	4.81	4.91
	Pressure = 200-202 psia		Inlet Subcooling = 8-11°F			
9	15.5	4.9	4.5	4.96	4.88	4.93
10	19.9	5.5	4.9	4.94	4.83	4.89
11	24.3	5.6	5.1	4.94	4.81	4.88
12	30.0	5.7	5.0	4.96	4.76	4.86
13	35.0	5.6	5.1	4.94	4.79	4.87
14	39.7	5.4	5.2	5.00	4.78	4.89
15	44.4	5.5	4.6	5.06	4.71	4.88
16	48.1	5.3	4.5	5.06	4.76	4.88
	Pressure = 201-204 psia		Inlet Subcooling = 18-22°F			
17	20.0	4.5	3.8	5.03	4.92	4.97
18	25.2	4.8	4.2	5.01	4.89	4.94
19	30.4	5.1	4.8	4.96	4.87	4.91
20	35.0	5.4	5.0	4.96	4.82	4.89
21	39.1	5.6	5.0	4.99	4.78	4.89
22	46.3	5.6	4.9	5.02	4.78	4.89
23	50.2	5.4	4.8	5.06	4.80	4.91
24	55.0	5.6	4.4	5.05	4.72	4.89
25	58.7	6.0	4.0	5.18	4.63	4.91
	Pressure = 598-602 psia		Inlet Subcooling = 1-3°F			
26	15.1	5.3	5.3	4.42	4.42	4.42
27	20.2	5.6	5.6	4.39	4.39	4.39

TABLE V (Contd.)

Data Point No.	Power, kW	Inlet Velocity, ft/sec		Pressure Drop across Test Section, psi		
		Max	Min	Max	Min	Mean
Pressure = 598-602 psia Inlet Subcooling = 1-3°F (Contd.)						
28	25.4	5.7	5.6	4.38	4.38	4.38
29	29.9	5.8	5.7	4.37	4.37	4.37
30	35.1	5.9	5.8	4.36	4.36	4.36
31	39.5	5.8	5.7	4.38	4.38	4.38
32	45.2	5.8	5.7	4.38	4.38	4.38
33	43.8	5.8	5.7	4.38	4.38	4.38
34	50.9	5.8	5.6	4.38	4.38	4.38
35	55.6	5.7	5.5	4.44	4.36	4.38
36	59.7	5.6	5.5	4.46	4.36	4.41
Pressure = 600-603 psia Inlet Subcooling = 8-10°F						
37	14.9	4.3	4.1	4.54	4.46	4.49
38	19.3	5.1	5.0	4.46	4.41	4.45
39	24.1	5.1	5.0	4.60	4.55	4.58
40	29.6	5.4	5.4	4.44	4.39	4.41
41	35.2	5.6	5.5	4.41	4.37	4.39
42	40.3	5.7	5.5	4.41	4.36	4.38
43	44.5	5.8	5.6	4.42	4.35	4.38
44	50.2	5.8	5.6	4.43	4.37	4.40
45	50.3	5.8	5.6	4.46	4.38	4.41
46	55.3	5.8	5.6	4.47	4.38	4.42
47	61.3	5.8	5.5	4.52	4.42	4.47
48	64.8	5.8	5.5	4.53	4.42	4.47
49	69.2	5.7	5.4	4.53	4.42	4.47
Pressure = 600-603 psia Inlet Subcooling = 20-23°F						
50	24.8	3.8	3.3	4.57	4.57	4.57
51	29.5	4.2	3.8	4.52	4.52	4.52
52	35.0	4.6	4.3	4.50	4.50	4.50
53	39.3	5.0	4.7	4.52	4.47	4.50
54	44.6	5.2	4.9	4.49	4.45	4.47
55	49.3	5.4	4.9	4.47	4.43	4.45
56	55.1	5.4	5.0	4.48	4.42	4.45
57	60.1	5.5	5.1	4.48	4.40	4.44
58	65.2	5.6	5.2	4.46	4.38	4.42
59	70.2	5.7	5.2	4.47	4.38	4.42
60	74.6	5.6	5.3	4.46	4.38	4.42
61	79.8	5.6	5.2	4.47	4.40	4.43

TABLE V (Contd.)

Data Point No.	Power, kW	Inlet Velocity, ft/sec		Pressure Drop across Test Section, psi		
		Max	Min	Max	Min	Mean
Pressure = 998-1000 psia Inlet Subcooling = 2-3°F						
62	24.8	5.5	5.5	4.10	4.10	4.10
63	35.0	5.8	5.8	4.07	4.07	4.07
64	40.1	5.9	5.8	4.07	4.07	4.07
65	44.6	5.9	5.9	4.07	4.07	4.07
66	49.8	6.0	5.9	4.05	4.05	4.05
67	55.5	6.0	5.9	4.06	4.06	4.06
68	60.5	6.0	5.9	4.07	4.07	4.07
69	64.4	6.0	5.9	4.08	4.08	4.08
70	67.4	5.9	5.8	4.06	4.06	4.06
Pressure = 1000-1003 psia Inlet Subcooling = 7-9°F						
71	20.4	4.3	4.3	4.20	4.20	4.20
72	24.2	4.8	4.8	4.16	4.16	4.16
73	28.2	5.1	5.1	4.14	4.14	4.14
74	34.6	5.4	5.3	4.13	4.13	4.13
75	40.1	6.1	6.0	4.11	4.11	4.11
76	40.1	5.7	5.6	4.10	4.10	4.10
77	46.2	5.8	5.8	4.11	4.08	4.09
78	49.4	5.8	5.8	4.11	4.08	4.09
79	54.0	5.9	5.8	4.26	4.22	4.24
80	60.1	5.9	5.8	4.10	4.06	4.08
81	64.4	5.9	5.8	4.10	4.06	4.08
82	70.2	5.9	5.8	4.11	4.06	4.08
Pressure = 1001-1003 psia Inlet Subcooling = 18-20°F						
83	17.8	3.9	3.7	4.23	4.23	4.23
84	29.6	4.1	3.9	4.21	4.21	4.21
85	34.7	4.5	4.3	4.20	4.20	4.20
86	40.2	4.9	4.6	3.84	3.84	3.84
87	44.7	5.2	4.9	3.82	3.82	3.82
88	50.0	5.3	5.0	4.13	4.13	4.13
89	55.3	5.2	4.9	4.14	4.14	4.14
90	59.5	5.4	5.2	4.13	4.13	4.13
91	46.2	5.2	5.1	4.20	4.14	4.16
92	54.7	5.4	5.2	4.18	4.12	4.15
93	59.3	5.5	5.3	4.19	4.10	4.14
94	65.3	5.7	5.4	4.19	4.08	4.13

TABLE V (Contd.)

Data Point No.	Power, kW	Inlet Velocity, ft/sec		Pressure Drop across Test Section, psi		
		Max	Min	Max	Min	Mean
Pressure = 1001-1003 psia Inlet Subcooling = 18-20°F (Contd.)						
95	70.6	5.7	5.6	4.18	4.09	4.13
96	75.0	5.7	5.5	4.19	4.07	4.13
97	79.1	5.8	5.5	4.19	4.05	4.13
98	83.7	5.7	5.5	4.18	4.06	4.12
Pressure = 1400-1403 psia Inlet Subcooling = 9-12°F						
99	25.6	4.6	4.6	3.90	3.90	3.90
100	29.3	4.9	4.9	3.87	3.87	3.87
101	34.5	5.1	5.0	3.86	3.86	3.86
102	39.9	5.4	5.3	3.83	3.83	3.83
103	44.3	5.6	5.5	3.83	3.79	3.82
104	49.6	5.6	5.5	3.84	3.80	3.81
105	55.4	5.8	5.7	3.83	3.80	3.81
106	60.0	5.9	5.7	3.81	3.79	3.80
107	60.5	5.8	5.7	3.81	3.78	3.79
108	65.2	6.0	5.8	3.81	3.77	3.79
109	71.2	6.0	5.9	3.81	3.76	3.78
110	75.2	6.1	5.9	3.80	3.76	3.78
111	79.1	6.1	6.0	3.80	3.76	3.78
112	82.6	6.1	6.0	3.80	3.76	3.78
Pressure = 1498-1502 psia Inlet Subcooling = 1-2°F						
113	59.7	5.5	5.5	3.76	3.76	3.76
114	64.8	5.6	5.5	3.76	3.76	3.76
115	70.8	5.6	5.5	3.76	3.76	3.76
116	75.9	5.6	5.5	3.75	3.75	3.75

TABLE VI. Data for Geometry 2

Test Section: Length = 96 in. ID = 0.3640 in.
Riser: Length = 48 in. ID = 0.3125 in.
Liquid level = 10-10.5 in. below condenser

Data Point No.	Power, kW	Inlet Velocity, ft/sec		Pressure Drop across Test Section, psi			Wall Temperature, °F			Freq, cps
		Max	Min	Max	Min	Mean	Max	Min	Mean	
	Pressure = 200-202 psia Inlet Subcooling = 0-3°F									
1	9.8	6.9	5.7	2.93	1.28	2.10	400.5	400.5	400.5	0.50
2	12.1	8.4	6.9	3.08	1.28	1.90	403.4	403.4	403.4	0.52
3	14.7	14.8	-12.9	3.34	0.97	1.49	412.5	410.5	411.2	0.46
4	17.3	18.8	-20.4	3.03	0.77	1.39	434.0	429.0	431.0	0.49
5	19.7	24.1	-25.5	2.72	0.46	1.49	459.1	452.7	455.4	0.55
6	22.4	32.4	-31.0	2.72	-0.77	1.28	465.1	458.3	461.7	0.61
	Pressure = 200-202 psia Inlet Subcooling = 7-10°F									
7	10.0	5.3	0.5	3.30	1.87	2.21	399.7	399.7	399.7	0.51
8	11.6	5.3	0.0	3.64	1.39	2.10	403.9	403.2	403.6	0.54
9	14.8	14.6	-16.7	3.76	1.09	1.72	415.8	412.4	413.7	0.48
10	17.6	24.2	-24.8	3.29	0.31	1.50	431.7	427.6	429.3	0.49
11	19.6	29.9	-26.3	2.88	0.41	1.37	452.6	446.9	449.6	0.52
12	21.7	32.3	-28.6	2.93	-0.36	1.19	466.2	458.8	462.5	0.61
13	25.1	33.6	-32.8	2.41	-0.57	1.04	681.2	601.2	640.5	0.65
	Pressure = 200-202 psia Inlet Subcooling = 16-18°F									
14	12.1	7.1	0.0	4.16	1.28	2.06	406.4	406.4	406.4	0.51
15	15.3	14.7	-15.8	3.95	0.26	1.69	419.2	417.1	417.8	0.48
16	17.2	21.5	-18.8	3.85	-0.46	1.49	430.2	426.1	428.2	0.47
17	19.6	28.5	-24.1	2.72	-0.98	1.18	447.2	441.8	444.1	0.52
18	21.9	31.2	-27.3	2.57	-1.54	0.98	511.6	506.2	508.9	0.57
19	24.9	32.9	-28.5	2.46	-1.95	0.92	529.3	515.8	522.6	0.67
	Pressure = 601-603 psia Inlet Subcooling = 0-3°F									
20	10.0	6.8	5.4	2.96	2.24	2.55	498.8	498.8	498.8	0.41
21	12.5	7.4	4.6	3.06	1.83	2.60	503.8	503.8	503.8	0.42
22	15.2	8.4	1.9	3.21	1.47	2.29	505.5	505.5	505.5	0.44
23	17.5	8.9	-7.7	3.60	1.96	2.57	512.2	510.9	511.2	0.46
24	19.4	9.8	-12.0	3.13	1.18	1.69	520.4	518.3	519.0	0.50
25	21.8	11.9	-14.0	2.82	1.23	1.64	530.7	528.0	529.4	0.53
26	24.6	13.3	-14.0	2.82	1.23	1.53	545.1	541.4	543.4	0.57
27	27.4	13.9	-16.1	2.82	0.77	1.74	567.7	562.3	564.9	0.60
28	29.4	15.8	-16.6	3.03	0.67	1.71	580.1	574.6	577.4	0.64
	Pressure = 601-604 psia Inlet Subcooling = 10-11°F									
29	10.4	1.8	0.0	3.39	2.31	2.70	501.7	501.7	501.7	0.39
30	12.4	2.5	0.0	3.44	2.00	2.46	506.2	506.2	506.2	0.43
31	15.0	3.7	0.0	3.59	1.69	2.26	510.5	510.5	510.5	0.44
32	17.5	5.5	-6.4	3.64	1.49	2.00	516.9	514.9	515.2	0.46
33	19.7	8.9	-9.2	3.23	1.39	1.85	522.7	520.7	521.7	0.50

TABLE VI (Contd.)

Data Point No.	Power, kW	Inlet Velocity, ft/sec		Pressure Drop across Test Section, psi			Wall Temperature, °F			Freq, cps
		Max	Min	Max	Min	Mean	Max	Min	Mean	
Pressure = 601-604 psia Inlet Subcooling = 10-11°F (Contd.)										
34	22.0	11.5	-11.0	3.18	1.28	1.80	536.2	533.5	534.8	0.53
35	24.7	14.0	-12.7	3.34	1.18	1.76	553.6	546.1	549.9	0.55
36	27.5	14.8	-14.8	3.13	0.62	1.68	583.8	578.4	581.8	0.59
37	29.4	16.6	-16.3	2.93	0.36	1.65	649.7	631.7	640.7	0.63
38	29.8	17.0	-16.6	2.93	0.46	1.65	700.8	680.5	694.0	0.65
Pressure = 601-603 psia Inlet Subcooling = 17-20°F										
39	12.4	3.7	0.0	3.54	2.16	2.46	498.8	498.8	498.8	0.38
40	15.0	4.0	0.0	3.75	1.69	2.57	501.8	501.8	501.8	0.42
41	17.7	6.8	-5.8	3.54	1.49	2.31	509.4	508.4	508.9	0.44
42	19.4	8.8	-10.1	3.44	1.28	2.21	517.7	515.6	517.0	0.48
43	21.8	10.8	-10.5	3.34	1.28	1.85	530.9	527.5	528.8	0.51
44	24.2	12.8	-12.0	3.34	1.08	1.80	545.2	541.1	543.2	0.54
45	28.4	15.1	-12.9	3.13	0.67	1.59	565.7	559.6	562.0	0.57
46	29.6	16.5	-14.9	3.03	0.15	1.55	626.4	610.8	615.9	0.63
Pressure = 1001-1003 psia Inlet Subcooling = 0-3°F										
47	10.0	6.0	5.2	2.82	2.67	2.72	561.0	561.0	561.0	0.00
48	14.6	6.7	4.8	2.87	2.00	2.31	564.1	564.1	564.1	0.41
49	17.2	6.7	3.0	3.03	1.64	2.21	563.7	563.0	563.3	0.41
50	19.8	7.0	1.3	2.93	1.39	1.90	570.8	569.4	570.1	0.44
51	22.0	7.4	-8.7	2.72	1.39	1.84	580.6	578.9	579.2	0.49
52	24.5	8.0	-10.7	2.62	1.23	1.80	585.4	582.0	583.7	0.53
53	27.0	9.5	-11.5	2.52	1.23	1.69	599.8	595.4	597.8	0.60
54	29.6	10.0	-12.1	2.77	0.87	1.85	621.8	615.1	618.4	0.61
Pressure = 1001-1003 psia Inlet Subcooling = 9-11°F										
55	10.3	1.5	0.0	2.67	2.67	2.67	561.0	561.0	561.0	0.00
56	14.8	1.8	0.0	3.13	2.10	2.46	570.5	570.5	570.5	0.41
57	17.3	2.5	0.0	3.29	1.80	2.31	567.1	566.4	566.7	0.42
58	19.8	4.3	-2.5	3.13	1.59	2.12	574.7	571.9	573.3	0.44
59	21.5	6.7	-3.2	2.93	1.39	1.98	584.5	581.1	582.8	0.49
60	24.5	7.8	-5.7	2.82	1.28	1.81	594.5	590.1	592.3	0.52
61	27.2	9.3	-7.4	2.72	1.39	1.76	610.1	604.3	607.2	0.59
62	29.9	9.8	-10.0	2.82	1.08	1.70	662.5	653.0	657.8	0.61
63	31.6	9.8	-10.0	2.93	0.97	1.69	940.4	859.1	896.4	0.62
Pressure = 1002-1003 psia Inlet Subcooling = 20-22°F										
64	12.8	1.6	0.0	3.13	2.41	2.72	554.7	554.7	554.7	0.35
65	15.4	2.8	0.0	3.29	2.10	2.57	559.6	559.6	559.6	0.36
66	18.0	3.8	0.0	3.34	1.74	2.31	562.1	561.5	561.8	0.39
67	19.6	4.6	0.0	3.23	1.49	2.10	568.1	567.1	567.6	0.42
68	21.6	5.9	-3.7	3.13	1.44	2.00	576.5	573.8	575.2	0.45
69	24.3	8.2	-5.9	2.93	1.33	1.94	585.3	582.0	584.0	0.50
70	27.5	9.3	-7.4	2.82	1.33	1.72	604.6	600.6	602.6	0.57
71	30.0	10.2	-8.3	2.93	0.77	1.64	640.8	630.6	635.7	0.61
72	32.7	10.2	-9.3	2.93	0.72	1.80	980.5	876.3	928.4	0.62

TABLE VII. Data for Geometry 3

Test Section: Length = 96 in. ID = 0.6250 in.
Riser: Length = 48 in. ID = 0.6250 in.
Liquid level = 10-10.5 in. below condenser

Data Point No.	Power, kW	Inlet Velocity, ft/sec		Pressure Drop across Test Section, psi			Wall Temperature, °F			Freq, cps
		Max	Min	Max	Min	Mean	Max	Min	Mean	
	Pressure = 201-204 psia Inlet Subcooling = 27-29°F									
1	24.6	6.3	1.0	3.25	2.55	2.90	392.1	392.1	392.1	0.30
2	29.3	8.0	-2.3	3.44	2.19	2.74	396.0	395.4	395.7	0.32
3	34.7	8.1	-4.8	3.35	1.75	2.65	400.6	400.0	400.3	0.39
4	39.5	8.4	-7.2	3.50	1.65	2.60	404.2	403.3	403.7	0.45
5	45.1	9.0	-9.2	3.75	1.80	2.50	409.4	408.6	409.0	0.50
6	50.1	9.1	-10.8	3.95	1.75	2.51	409.9	409.2	409.5	0.54
7	55.5	9.3	-13.0	4.25	1.65	2.55	415.6	413.4	414.5	0.59
8	60.2	9.8	-14.5	4.55	1.70	2.67	424.6	419.1	421.8	0.61
	Pressure = 200-203 psia Inlet Subcooling = 35-38°F									
9	30.3	7.3	-2.3	3.32	2.32	2.82	396.7	395.8	396.2	0.24
10	34.7	8.5	-4.0	3.32	1.72	2.74	400.6	399.8	400.1	0.30
11	34.8	8.3	-4.8	3.37	1.77	2.72	398.9	398.2	398.5	0.32
12	39.4	8.6	-6.3	3.32	1.67	2.66	403.7	402.8	403.2	0.36
13	43.8	8.6	-8.0	3.47	1.82	2.62	408.6	407.2	407.9	0.41
14	49.6	9.2	-9.8	3.72	1.57	2.56	408.1	406.8	407.5	0.49
15	55.3	9.9	-13.0	4.02	1.52	2.47	418.7	414.3	416.5	0.54
16	59.5	10.4	-13.7	4.12	1.57	2.62	424.0	417.8	420.9	0.57
17	65.3	11.5	-15.0	4.39	1.49	2.49	433.2	424.4	428.4	0.61
18	70.3	12.3	-15.9	4.69	1.19	2.49	442.4	430.1	436.2	0.66
	Pressure = 201-204 psia Inlet Subcooling = 43-46°F									
19	24.6	4.1	1.7	3.14	2.84	2.99	394.0	393.8	393.9	0.29
20	29.3	7.0	-3.1	3.39	2.49	2.87	396.7	396.0	396.3	0.26
21	34.7	8.3	-2.7	3.35	1.85	2.67	402.4	401.5	402.0	0.28
22	39.8	8.4	-5.5	3.35	1.60	2.60	406.8	405.5	406.1	0.33
23	42.3	8.2	-6.8	3.25	1.80	2.60	409.9	409.0	409.4	0.37
24	50.0	9.1	-9.2	3.55	1.60	2.51	408.1	407.5	407.8	0.44
25	55.0	9.7	-11.0	3.64	1.54	2.41	416.0	411.6	413.8	0.51
26	59.4	10.2	-13.1	3.82	1.52	2.47	423.1	418.2	420.7	0.55
27	65.1	10.9	-15.0	3.92	1.42	2.42	431.0	424.4	427.9	0.58
28	69.7	11.5	-15.7	4.22	1.12	2.32	442.0	433.2	437.6	0.62
29	75.2	12.5	-16.6	4.35	0.85	2.40	453.0	442.0	447.5	0.67
30	79.9	14.3	-18.3	3.95	0.65	2.32	469.1	451.7	460.6	0.70
	Pressure = 602-603 psia Inlet Subcooling = 26-30°F									
31	24.0	3.3	3.3	2.75	2.75	2.75	489.5	489.5	489.5	0.0
32	29.2	3.5	3.4	2.85	2.85	2.85	493.5	493.5	493.5	0.0
33	34.5	3.4	3.2	2.85	2.85	2.85	497.4	497.4	497.4	0.0
34	39.7	3.5	3.2	2.90	2.83	2.85	500.5	500.5	500.5	0.0
35	44.3	4.3	2.2	3.00	2.65	2.80	504.0	504.0	504.0	0.45
36	50.3	6.6	-2.4	3.22	2.17	2.72	508.0	507.6	507.8	0.44

TABLE VII (Contd.)

Data Point No.	Power, kW	Inlet Velocity, ft/sec		Pressure Drop across Test Section, psi			Wall Temperature, °F			Freq, cps
		Max	Min	Max	Min	Mean	Max	Min	Mean	
Pressure = 601-603 psia Inlet Subcooling = 35-37°F										
37	39.5	3.4	3.0	3.37	3.17	3.27	501.4	501.4	501.4	0.0
38	44.7	3.5	2.8	2.92	2.67	2.75	504.9	504.9	504.9	0.0
39	49.3	6.3	-2.6	3.15	2.37	2.72	503.8	503.8	503.8	0.38
40	54.4	7.5	-3.2	3.24	2.05	2.67	511.3	511.1	511.2	0.41
41	59.7	7.8	-4.2	3.32	1.92	2.52	515.5	515.0	515.3	0.43
42	65.6	8.1	-5.0	3.42	1.77	2.54	519.9	519.0	519.4	0.45
Pressure = 602-604 psia Inlet Subcooling = 45-47°F										
43	34.8	3.2	2.9	2.80	2.76	2.77	500.1	500.1	500.1	0.0
44	39.7	3.4	3.1	2.82	2.77	2.79	504.5	504.5	504.5	0.0
45	44.7	3.6	2.7	2.84	2.76	2.79	507.9	507.9	507.9	0.0
46	50.6	6.1	-2.3	3.07	2.37	2.70	512.4	512.0	512.2	0.35
47	53.6	6.9	-3.1	3.17	2.27	2.67	515.5	515.0	515.2	0.35
48	59.3	6.9	-3.3	3.22	2.02	2.62	519.9	519.2	519.5	0.37
49	65.8	8.8	-4.2	3.25	1.85	2.55	519.0	518.1	518.6	0.39
50	70.1	8.4	-5.3	3.32	1.73	2.55	525.4	521.2	523.3	0.43
Pressure = 1000-1003 psia Inlet Subcooling = 45-49°F										
51	44.5	3.3	3.2	2.67	2.67	2.67	561.0	561.0	561.0	0.0
52	49.0	3.4	3.2	2.72	2.68	2.69	563.9	563.9	563.9	0.0
53	54.8	3.3	3.2	2.70	2.67	2.68	567.8	567.8	567.8	0.0
54	60.0	3.2	3.1	2.69	2.69	2.69	578.6	578.6	578.6	0.0
55	65.8	3.2	2.8	2.71	2.68	2.69	581.5	581.5	581.5	0.0
56	70.6	5.1	0.6	2.89	2.39	2.64	585.4	585.2	585.3	0.41
57	73.6	5.9	0.0	3.04	2.24	2.64	587.6	587.4	587.5	0.42
58	79.8	6.1	-2.0	3.14	1.99	2.54	582.8	582.4	582.6	0.42
59	85.0	7.5	-2.7	3.24	1.89	2.42	594.2	587.2	590.7	0.43

TABLE VIII. Data for Geometry 4

Test Section: Length = 72 in. ID = 0.6250 in.
Riser: Length = 48 in. ID = 0.6250 in.
Liquid level = 10-10.5 in. below condenser

Data Point No.	Power, kW	Inlet Velocity, ft/sec		Pressure Drop across Test Section, psi			Wall Temperature, °F			Freq, cps
		Max	Min	Max	Min	Mean	Max	Min	Mean	
Pressure = 200-204 psia Inlet Subcooling = 19-22°F										
1	14.9	3.6	3.2	3.22	3.07	3.12	391.4	391.4	391.4	0.0
2	20.1	3.5	2.6	3.22	3.02	3.12	396.2	396.2	396.4	0.0
3	25.5	6.8	-3.0	3.45	2.45	2.85	402.8	402.8	402.2	0.43
4	26.7	7.0	-3.6	3.48	2.37	2.85	403.7	403.3	403.4	0.43

TABLE VIII (Contd.)

Data Point No.	Power, kW	Inlet Velocity, ft/sec		Pressure Drop across Test Section, psi			Wall Temperature, °F			Freq, cps
		Max	Min	Max	Min	Mean	Max	Min	Mean	
	Pressure = 200-204 psia			Inlet Subcooling = 19-22°F (Contd.)						
5	30.0	7.5	-5.0	3.45	2.00	2.72	407.2	406.8	407.0	0.47
6	33.5	7.9	-6.1	3.50	1.80	2.63	410.8	410.3	410.5	0.51
7	36.6	8.2	-7.0	3.55	1.60	2.54	413.0	412.3	412.5	0.52
8	40.0	8.6	-8.2	3.70	1.35	2.43	415.6	414.7	415.2	0.56
9	43.7	8.9	-9.1	3.80	1.10	2.36	420.0	418.7	419.1	0.58
10	45.6	9.1	-9.9	3.85	1.05	2.32	424.8	421.3	423.3	0.60
11	49.2	9.5	-10.7	3.95	1.05	2.30	431.9	425.3	428.6	0.62
	Pressure = 200-203 psia			Inlet Subcooling = 28-31°F						
12	20.4	3.2	2.7	3.24	3.12	3.17	397.7	397.7	397.7	0.0
13	24.8	6.4	1.0	3.52	2.67	3.04	402.8	402.4	402.6	0.39
14	30.2	7.3	-4.2	3.37	2.07	2.69	409.4	408.8	409.0	0.41
15	35.0	7.8	-6.1	3.50	1.72	2.61	413.8	413.2	413.6	0.50
16	38.2	8.3	-7.0	3.52	1.52	2.52	410.3	409.7	410.1	0.50
17	40.3	8.4	-7.8	3.62	1.32	2.43	412.5	412.1	412.2	0.53
18	43.1	8.7	-8.7	3.62	1.12	2.37	416.5	414.5	415.6	0.54
19	44.6	8.9	-9.3	3.62	1.02	2.30	416.0	414.3	415.6	0.55
20	47.8	9.2	-10.1	3.67	0.97	2.30	421.8	418.7	421.3	0.55
21	49.9	9.4	-10.9	3.72	0.97	2.25	427.9	424.4	427.5	0.59
22	55.0	10.0	-12.1	3.92	1.02	2.09	442.9	433.6	437.6	0.63
23	39.8	8.2	-7.0	3.55	1.60	2.66	420.0	418.9	419.6	0.47
24	50.7	9.4	-10.9	3.75	1.00	2.30	439.4	433.2	436.7	0.57
25	55.0	10.1	-12.4	3.95	1.15	2.37	451.2	441.6	446.0	0.62
26	59.6	10.5	-13.2	4.05	1.20	2.32	458.3	450.4	453.0	0.63
27	64.7	11.3	-13.9	4.17	1.32	2.19	478.5	464.0	470.6	0.69
	Pressure = 200-204 psia			Inlet Subcooling = 38-42°F						
28	20.8	2.9	2.4	3.22	3.07	3.17	396.5	396.5	396.5	0.0
29	24.4	4.1	1.2	3.17	2.92	3.00	398.7	398.7	398.7	0.35
30	27.1	6.9	0.0	3.37	2.32	2.76	402.4	402.0	402.2	0.31
31	29.9	7.1	-1.5	3.42	2.27	2.73	405.0	404.6	404.8	0.32
32	32.9	7.5	-4.8	3.32	1.97	2.64	406.8	406.4	406.6	0.39
33	34.9	7.8	-5.3	3.37	1.87	2.61	409.9	409.4	409.7	0.39
34	39.4	8.3	-7.1	3.42	1.42	2.44	411.6	411.0	411.3	0.44
35	42.6	8.9	-8.2	3.00	1.05	2.34	417.4	414.5	415.9	0.47
36	46.5	9.1	-9.4	3.54	0.95	2.29	423.1	417.1	420.1	0.49
37	50.3	9.5	-10.3	3.60	0.95	2.25	429.0	424.4	426.8	0.52
38	55.2	10.1	-11.8	3.75	1.00	2.24	443.3	434.7	439.0	0.58
39	58.1	10.5	-12.6	3.82	1.00	2.19	450.8	441.1	446.0	0.60
40	50.4	9.7	-10.4	3.54	0.92	2.29	442.4	434.5	438.5	0.51
41	54.9	10.1	-11.6	3.62	1.02	2.23	450.4	441.6	444.6	0.56
42	60.3	10.8	-13.1	3.77	1.02	2.23	466.6	453.0	459.2	0.61
43	64.9	11.3	-14.1	4.02	1.22	2.22	484.7	466.2	475.5	0.67
44	70.0	11.8	-15.8	3.72	1.02	2.20	535.3	484.7	508.9	0.70

TABLE VIII (Contd.)

Data Point No.	Power, kW	Inlet Velocity, ft/sec		Pressure Drop across Test Section, psi			Wall Temperature, °F			Freq, cps
		Max	Min	Max	Min	Mean	Max	Min	Mean	
Pressure = 600-603 psia Inlet Subcooling = 29-32°F										
45	25.6	3.1	3.1	2.84	2.84	2.84	513.1	513.1	513.1	0.0
46	30.5	3.2	3.1	2.89	2.81	2.84	519.4	519.4	519.4	0.0
47	34.5	3.2	3.1	2.89	2.81	2.86	522.3	522.3	522.3	0.0
48	39.3	3.2	2.8	2.92	2.85	2.89	527.4	527.4	527.4	0.0
49	45.7	3.0	2.8	2.89	2.85	2.87	528.2	528.2	528.2	0.0
50	50.1	2.8	2.6	2.89	2.82	2.84	537.5	537.5	537.5	0.0
51	54.8	5.6	0.0	3.29	2.41	2.76	543.2	542.5	542.9	0.51
52	60.4	6.7	-3.0	3.44	2.19	2.69	535.7	532.2	533.9	0.51
53	65.9	7.5	-4.2	3.49	2.04	2.63	551.6	541.4	546.5	0.51
Pressure = 599-603 psia Inlet Subcooling = 39-42°F										
54	20.5	3.1	3.1	2.81	2.81	2.81	500.5	500.5	500.5	0.0
55	25.3	3.2	3.0	2.82	2.82	2.82	506.2	506.2	506.2	0.0
56	29.8	3.2	3.1	2.85	2.85	2.85	511.6	511.6	511.6	0.0
57	34.4	3.2	3.1	2.87	2.87	2.87	516.8	516.4	516.6	0.0
58	39.4	3.2	3.0	2.92	2.82	2.87	521.0	520.8	520.9	0.0
59	44.0	3.1	3.0	2.92	2.82	2.87	525.6	525.6	525.6	0.0
60	49.6	4.5	1.5	3.07	2.67	2.87	531.8	531.3	531.5	0.49
61	52.4	6.1	-1.1	3.29	2.34	2.74	533.3	532.6	532.9	0.49
62	59.9	6.9	-3.0	3.41	2.19	2.69	536.2	532.6	534.4	0.49
63	65.6	7.7	-4.6	3.51	2.04	2.66	550.7	542.8	546.8	0.50
64	69.8	8.0	-4.8	3.59	1.94	2.62	567.8	546.7	556.7	0.52
Pressure = 600-603 psia Inlet Subcooling = 49-51°F										
65	29.2	3.2	2.9	2.84	2.84	2.84	517.5	517.5	517.5	0.0
66	34.3	3.2	2.8	2.89	2.83	2.84	524.3	524.3	524.3	0.0
67	40.0	3.1	2.8	2.91	2.83	2.89	530.4	530.4	530.4	0.0
68	44.5	3.0	2.8	2.91	2.87	2.89	534.8	534.8	534.8	0.0
69	50.0	4.7	1.1	3.14	2.69	2.86	538.8	538.4	538.6	0.4
70	55.5	6.7	-1.5	3.29	2.39	2.72	527.1	526.7	526.9	0.40
71	59.5	7.0	-3.1	3.39	2.29	2.72	528.7	527.8	528.3	0.41
72	65.0	7.5	-4.3	3.42	2.14	2.68	544.5	537.5	540.5	0.44
73	69.8	8.0	-4.8	3.49	1.99	2.64	560.8	545.8	553.3	0.47
74	72.8	8.3	-5.2	3.39	1.89	2.56	577.5	555.1	566.3	0.50
Pressure = 601-604 psia Inlet Subcooling = 61-64°F										
75	34.4	3.0	2.6	2.89	2.84	2.84	516.8	516.8	516.8	0.0
76	40.0	2.9	2.7	2.84	2.79	2.81	522.1	522.1	522.1	0.0
77	45.2	3.2	2.4	2.89	2.79	2.84	527.4	527.4	527.4	0.0
78	50.2	2.8	2.6	2.89	2.79	2.84	533.1	532.6	532.9	0.0
79	60.4	7.1	-2.8	3.29	2.24	2.69	538.4	534.4	536.4	0.37
80	65.6	7.6	-4.3	3.39	2.09	2.65	550.9	541.9	546.4	0.40
81	70.0	8.0	-4.8	3.47	1.99	2.65	565.2	546.3	555.8	0.42

TABLE IX. Data for Geometry 5

Test Section: Length = 48 in. ID = 0.6250 in.
Riser: Length = 48 in. ID = 0.6250 in.
Liquid level = 10-10.5 in. below condenser

Data Point No.	Power, kW	Inlet Velocity, ft/sec		Pressure Drop across Test Section, psi			Wall Temperature, °F			Freq, cps
		Max	Min	Max	Min	Mean	Max	Min	Mean	
	Pressure = 201-203 psia			Inlet Subcooling = 8-11°F						
1	10.1	2.9	2.9	3.14	3.14	3.14	383.9	383.9	383.9	0.0
2	15.1	2.6	2.6	3.14	3.14	3.14	392.7	392.7	392.7	0.0
3	20.4	2.4	2.4	3.14	3.14	3.14	401.0	401.0	401.0	0.0
4	25.7	2.1	1.8	3.10	3.06	3.08	408.6	408.6	408.6	0.0
5	28.1	2.0	1.6	3.13	3.03	3.09	410.3	410.3	410.3	0.0
6	30.0	3.1	0.0	3.43	2.90	3.07	414.9	414.9	414.9	0.76
7	32.9	4.5	0.0	3.65	2.70	3.00	421.8	421.3	421.5	0.73
8	35.5	5.1	-2.6	3.70	2.62	2.98	423.1	422.6	422.8	0.71
9	36.4	5.3	-3.4	3.75	2.60	2.98	424.4	424.0	424.2	0.71
10	39.8	6.5	-4.8	3.85	2.45	2.83	428.8	424.8	426.2	0.70
	Pressure = 200-203 psia			Inlet Subcooling = 17-19°F						
11	15.0	2.8	2.8	3.20	3.20	3.20	396.2	396.2	396.2	0.0
12	19.9	2.5	2.5	3.15	3.15	3.15	403.7	403.7	403.7	0.0
13	25.0	1.9	1.9	3.14	3.14	3.14	408.1	408.1	408.1	0.0
14	30.9	5.5	0.0	3.61	2.71	2.96	418.9	417.6	418.2	0.68
15	32.9	5.6	-2.9	3.66	2.63	3.01	421.1	419.8	420.4	0.64
16	35.3	5.9	-4.0	3.75	2.50	2.98	424.8	423.1	424.0	0.66
17	37.6	6.6	-4.8	3.77	2.50	2.93	428.4	425.9	427.1	0.65
18	40.2	6.9	-5.1	3.79	2.44	2.89	438.0	430.6	434.3	0.68
19	41.2	7.0	-5.3	3.69	2.44	2.88	442.9	433.2	437.9	0.66
	Pressure = 202-203 psia			Inlet Subcooling = 29-31°F						
20	20.2	3.2	1.6	3.29	3.09	3.19	402.4	402.0	402.2	0.44
21	22.5	2.7	1.8	3.24	3.09	3.19	406.8	406.8	406.8	0.51
22	24.3	5.2	0.0	3.59	2.84	3.07	409.9	409.0	409.4	0.51
23	28.4	5.7	-1.4	3.69	2.79	3.14	415.6	413.8	414.7	0.48
24	32.6	6.4	-3.7	3.70	2.55	2.98	421.5	420.0	420.7	0.53
25	35.6	7.0	-4.9	3.74	2.49	2.92	431.4	426.2	428.8	0.57
26	38.7	7.1	-5.2	3.74	2.39	2.88	433.2	428.8	431.0	0.57
27	40.3	7.4	-5.7	3.71	2.34	2.84	442.4	433.2	437.8	0.59
28	43.6	7.5	-6.0	3.76	2.29	2.83	446.8	437.6	442.2	0.64
29	44.4	7.5	-6.0	3.79	2.29	2.83	454.3	444.2	449.0	0.64
	Pressure = 601-603 psia			Inlet Subcooling = 49-52°F						
30	35.3	2.8	2.7	2.97	2.94	2.95	525.8	525.8	525.8	0.0
31	39.7	2.7	2.5	2.97	2.92	2.97	533.1	533.1	533.1	0.0
32	45.6	2.7	2.5	3.02	2.92	2.97	541.9	541.9	541.9	0.0
33	49.7	2.7	2.3	3.05	2.97	3.02	546.3	546.3	546.3	0.0
34	54.3	2.4	1.9	3.03	2.93	2.97	553.8	553.8	553.8	0.0
35	59.3	5.3	-1.9	3.45	2.60	2.89	562.6	552.6	557.6	0.51

TABLE X. Data for Geometry 6

Test Section: Length = 96 in. ID = 0.6250 in.
Riser: Length = 60 in. ID = 0.6250 in.
Liquid level = 10-10.5 in. below condenser

Data Point No.	Power, kW	Inlet Velocity, ft/sec		Pressure Drop across Test Section, psi			Freq, cps
		Max	Min	Max	Min	Mean	
	Pressure = 201-203 psia			Inlet Subcooling = 24-26°F			
1	10.3	3.0	2.6	2.99	2.89	2.94	0.0
2	15.5	3.5	2.9	2.99	2.84	2.91	0.0
3	19.8	6.5	2.0	3.19	2.39	2.73	0.29
4	22.7	7.6	2.2	3.29	1.59	2.69	0.31
5	25.2	7.8	2.2	3.34	1.49	2.66	0.29
6	26.9	7.7	-4.7	3.29	1.49	2.63	0.37
7	30.2	7.9	-6.1	3.29	1.79	2.57	0.40
8	32.2	8.2	-6.8	3.29	1.69	2.53	0.41
9	33.6	8.3	-7.7	3.34	1.64	2.50	0.43
10	38.3	8.6	-8.6	3.48	1.74	2.45	0.46
11	39.6	8.9	-9.3	3.54	1.74	2.47	0.49
12	42.7	9.3	-10.1	3.59	1.64	2.50	0.51

APPENDIX D

Almost-periodic Functions

A function $f(x)$ is called "almost periodic" if the following conditions are satisfied:

1. For any given $\epsilon > 0$ as small as desired, there exists a set of τ such that

$$\left| f(x+\tau) - f(x) \right| < \epsilon \qquad -\infty < x < +\infty.$$

2. A length $L = L(\epsilon)$ exists such that any interval $\alpha < x < \alpha + L$ contains at least one number τ of the set.

The number τ is called the translation number, and the length L is called the inclusion interval of the set. A general description of almost-periodic oscillations is presented in Reference 50. The theory of almost-periodic functions is described in Reference 51.

ACKNOWLEDGMENTS

Grateful acknowledgment is given Professor S. G. Bankoff for his keen interest, able guidance, suggestions, criticisms, and willingness always to give freely of his time throughout the duration of my graduate work at Northwestern University.

This study was supported under the joint auspices of the Associated Midwest Universities and the Argonne National Laboratory, and was performed at the Heat Engineering Section of Argonne National Laboratory. The author is grateful to Dr. Michael Petrick for his technical assistance and supervision. The valuable help and guidance of Dr. David Miller is also gratefully acknowledged.

This task could not have been completed without direct and indirect assistance of several personnel of the Reactor Engineering and Applied Mathematics Divisions at Argonne National Laboratory. Particularly, the assistance of the following is thankfully acknowledged: Messrs. Edward M. Spleha and Matthew P. Gats for the technical aid in the design, construction, and performance of the experimental facility; Mr. Leonard M. Indykiewicz for operating the loop and assisting with data reduction; Messrs. Joseph R. Kemp and Louis Bova for the instrumentation of the experimental facility; Mrs. Dorothy J. Bingaman and Dr. Mary K. Winter for general assistance in the digital computer programming; Mr. Dean G. Quoss and Mrs. Jane M. Flagg for the graphical work associated with the project.

The digital computer programs for two mathematical models used in this study were obtained from the TRW Space Technology Laboratory, Redondo Beach, California. The author is thankful to Dr. L. G. Neal and other personnel of the Applied Thermodynamics Department of the STL, for their cooperation and assistance.

REFERENCES

1. Anderson, R. P., and P. A. Lottes, Boiling Stability, Progress in Nuclear Energy, Series IV, Vol. 4, Pergamon Press (1961).

2. Gouse, S. W. Jr., Two-phase Gas-Liquid Flow Oscillations: Preliminary Survey, MIT Report No. DSR 8734-5 (July 1964).

3. Efferding, L. E., Static and Dynamic Stability of Steam-Water Systems, Part I, Critical Review of the Literature, General Atomic Report No. GA-5555 (Oct 22, 1964).

4. Ledinegg, M., Instability of Flow During Natural and Forced Circulation, Die Wärme 61, 891-898 (1938).

5. Chilton, H., A Theoretical Study of Stability in Water Flow through Heated Passages, J. Nucl. Energy 5, 273-284 (1957).

6. Wissler, E. H., H. S. Isbin, and N. R. Amundson, Oscillatory Behavior of a Two-phase Natural Circulation Loop, AIChE Journal 2 No. 2, 157-162 (1956).

7. Wissler, E. H., The Transient Behavior of a Two-phase Natural Convection Loop, Ph.D. thesis, University of Minnesota (June 1955).

8. Levy, S., and E. S. Beckjord, Hydraulic Instability in a Natural Circulation Loop with Net Steam Generation at 1000 psia, American Society of Mechanical Engineers, Heat Transfer Conference, Paper No. 60-HT-27, Buffalo, New York (1960).

9. Lottes, P. A., and W. S. Flinn, A Method of Analysis of Natural Circulation Boiling Systems, Nucl. Sci. 1, 461 (1956).

10. Hooker, H. H., and F. G. Popper, A Gamma-ray Attenuation Method for Void Fraction Determination in Steam-Water Mixtures, ANL-5766 (Nov 1958).

11. Spigt, C. L., F. J. M. Dijkman, and M. Bogaardt, The Onset of Hydraulic Instabilities in an Annular Channel, Report WW016-R53, EAES Symposium, Studsvik, Sweden (Sept 1963).

12. Fabrega, S., Experimental Study of Hydraulic Instabilities in Boiling Channel, EAES Symposium, Studsvik, Sweden (Oct 1963).

13. Kinetic Studies of Heterogeneous Water Reactors, Annual Summary Report--1961, Space Technology Laboratories, Inc., No. STL-6112.

14. Kinetic Studies of Heterogeneous Water Reactors, Annual Summary Report--1959, Ramo-Wooldridge Inc., No. RWD-RL-167.

15. Becker, K. M., et al., Measurements of Hydrodynamic Instabilities, Flow Oscillations and Burnout in a Natural Circulation Loop, EAES Symposium, Studsvik, Sweden (Oct 1963).

16. Becker, K. M., et al., Hydrodynamic Instability and Dynamic Burnout in Natural Circulation Two-phase Flow. An Experimental and Theoretical Study, AB Atomenergi, Sweden, Report No. AE-156.

17. Quandt, E. R., Analysis and Measurement of Flow Oscillations, C.E.P., Symp. Series, 57, No. 32 (1961).

18. Garlid, K., N. R. Amundson, and H. S. Isbin, A Theoretical Study of the Transient Operation and Stability of Two-phase Natural Circulation Loops, ANL-6381 (June 1961).

19. Anderson, R. P., et al., Transient Analysis of Two-phase Natural Circulation Systems, ANL-6653 (Dec 1962).

20. Wallis, G. B., and J. H. Heasley, Oscillations in Two-phase Flow Systems, Trans. ASME, J. Heat Transfer, Series C, 83, 363-369 (1961).

21. Boure, J., Theoretical Studies of Hydrodynamic Instability in a Natural Circulation Loop, EAES Symposium, Studsvik, Sweden (Oct 1963).

22. Fleck, J. A., Jr., The Dynamic Behavior of Boiling Water Reactors, J. Nucl. Energy 11, 114-130 (1960).

23. Jones, A. B., Hydrodynamic Stability of a Boiling Channel, KAPL-2170 (Oct 1961).

24. Bankoff, S. G., A Variable Density Single Fluid Model for Two-phase Flow with Particular Reference to Steam Water Flow, Trans. ASME, J. Heat Transfer, Series C, 82, 265-272 (1960).

25. Martinelli, R. C., and D. B. Nelson, Prediction of Pressure Drop During Forced Circulation Boiling of Water, Trans. ASME 70, 695-702 (1948).

26. Neal, L. G., and S. M. Zivi, A Comparative Study of Models Describing Hydrodynamic Instabilities in Boiling Water Reactors and Loops, STL-372-3, Quarterly Progress Report (April 1964).

27. Neal, L. G., and S. M. Zivi, Hydrodynamic Instabilities in Boiling Loops, Conf. on Boiling and Two-phase Flow for Heat Transfer Engineers, Univ. of California, Berkeley (May 1965).

28. Meyer, J. E., and R. P. Rose, Application of a Momentum Integral Model to the Study of Parallel Channel Boiling Flow Oscillations, Trans. ASME, J. Heat Transfer, Series C, 85, No. 1 (1963).

29. Rose, R. P., and R. S. Pyle, XITE-A Digital Program for the Analysis of Two-Dimensional Boiling Flow Transients with Fluid Expansion, WAPD-TM-302 (1963).

30. Blubaugh, A. L., and E. R. Quandt, Analysis and Measurement of Flow Oscillations, WAPD-AD-TH-538 (1960).

31. Meyer, J. E., Hydrodynamic Models for the Treatment of Reactor Thermal Transients, Nucl. Sci. Eng. 10, 269-277 (1961).

32. Jahnberg, S., A One-dimensional Model for Calculation of Non-steady Two-phase Flow, EAES Symposium, Studsvik, Sweden (Oct 1963).

33. Nahavandi, A. N., and R. F. von Hollen, A Space-dependent Dynamic Analysis of Boiling Water Reactor Systems, Nucl. Sci. and Eng. 20, 392-413 (1964).

34. Nahavandi, A. N., and R. F. von Hollen, Flow Stability in Large Vertical Steam Generators, ASME, Winter Annual Meeting, Paper 64-WA/Aut-11, New York (1964).

35. Lindahl, E. J., Pulsation and Its Effect on Flowmeters, Trans. ASME 68, 883-894 (Nov 1946).

36. Grey, J., and F. F. Liu, Methods of Flow Measurement, Rocket Soc., 133-140 (May-June 1953).

37. Thie, J. A., Reactor Noise, Rowman and Littlefield, New York (1963).

38. Noise Analysis in Nuclear Systems, U.S. AEC Symposium Series 4 (Nov 1963).

39. Minorsky, N., Nonlinear Oscillations, Van Nostrand, Princeton, N. J. (1962).

40. Jones, A. B., and D. G. Dight, Hydrodynamic Stability of a Boiling Channel, Part 2, KAPL-2208 (April 1962).

41. Coffin, L. F., Jr., and R. J. Fritz, Thermal Stress and Thermal Stress Fatigue, Liquid Metals Handbook, AEC Report No. TID 5227, pp. 204-235 (July 1955).

42. Hoffman, H. W., and J. J. Keyes, Jr., Heat-transfer Experiments of Significance to Reactor Safety, Nucl. Safety 6, No. 2 (1964-65).

43. Petrick, M., A Study of Vapor Carryunder and Associated Problems, ANL-6581 (July 1962).

44. Green, S. J., and T. W. Hunt, Accuracy and Response of Thermocouples for Surface and Fluid Temperature Measurements, Temperature--Its Measurement and Control In Science and Industry, Vol. 3, Part 2, 695-722 (1962).

45. D'Azzo, J. J., and C. H. Houpis, Feedback Control System Analysis and Synthesis, McGraw Hill Book Company, Inc., (1960).

46. Jens, W.H., and P. A. Lottes, Analysis of Heat Transfer, Burnout, Pressure Drop and Density Data for High Pressure Water, ANL-4627 (1951).

47. Neal, L. G., personal communication (Jan 11, 1965).

48. LeTourneau, B. W., and M. Troy, Heating, Local Boiling, and Two-phase Pressure Drop for Vertical Upflow of Water at Pressures Below 1850 psia: Test Data and Correlations, WAPD-TH-410 (Oct 6, 1958).

49. Gouse, W. S., and Andrysiak, C. D., Flow Oscillations in a Closed Loop with Transparent, Parallel, Vertical, Heated Channels, MIT Report No. 8973-2 (1963).

50. Hayashi, C., Nonlinear Oscillations in Physical Systems, McGraw Hill Book Company, Inc. (1964).

51. Besicovitch, A. S., Almost Periodic Functions, University Press, Cambridge, England (1932).